Enols and Allylic Alcohols as Building Blocks in Synthetic Organic Chemistry

Experimental and Theoretical Studies

Alba Carretero Cerdán

Department of Organic Chemistry

Stockholm University

Enols and Allylic Alcohols as Building Blocks in Synthetic Organic Chemistry
Experimental and Theoretical Studies

Alba Carretero Cerdán

Academic dissertation for the Degree of Doctor of Philosophy in Organic Chemistry at Stockholm University to be publicly defended on Friday 21 October 2022 at 09.00 in Magnélisalen, Kemiska övningslaboratoriet, Svante Arrhenius väg 16B, and online via Zoom, public link is available at the department website.

Abstract
The present thesis describes computational and experimental studies used to drive the reactivity of allylic and enol substrates towards new transformations. These synthetic methods give access to a number of organic molecules that may serve as important moieties in synthetic organic chemistry. Additionally, this thesis describes the synthesis of Metal-Organic Frameworks (MOFs) and their use in catalytic organic reactions.

The introductory chapter (Chapter 1) gives an overview of the concept of catalysis and its typologies, emphasizing those that have been used in the thesis. Moreover, synthetic procedures for the formation of MOFs and their use in catalysis are described. The importance and reactivity of allylic substrates are also presented. The chapter follows with a short introduction to hypervalent iodine and their reactivity. Finally, a brief description of computational studies and those used in this thesis are presented.

In Chapter 2, an umpolung protocol for the cross-nucleophile coupling of silyl enol ethers with heteronucleophiles mediated by an hypervalent iodine reagent has been explored (**Paper I**).

The mechanistic study of the reaction has been carried out employing DFT calculations and kinetic investigations. Together with deuterium labelling studies and kinetic simulations, DFT calculations have been used in Chapter 3 for the examination of the base-catalyzed [1,n]-proton shift in conjugated polyenyl ethers (**Paper II**).

Chapter 4 describes the synthesis of the family MIL-101(Cr) and MIL-101(Cr)-NH2 employing microwave-assisted methods. The method has been compared to the common solvothermal synthetic pathways using common characterization techniques for heterogeneous materials (**Paper III**).

Finally, Chapter 5 of this thesis describes the synthesis of a UiO-67 MOF containing a phosphazene superbase to study the effect of spatial confinement within a MOF on the stereospecific isomerization of allylic alcohols (**Paper IV**).

Keywords: *Base catalysis, Ion-pair, Isomerization, MOFs, Hypervalent Iodine (III), DFT.*

Department of Organic Chemistry

Stockholm University, 106 91 Stockholm

ENOLS AND ALLYLIC ALCOHOLS AS BUILDING BLOCKS IN
SYNTHETIC ORGANIC CHEMISTRY

Alba Carretero Cerdán

Enols and Allylic Alcohols as Building Blocks in Synthetic Organic Chemistry

Experimental and Theoretical Studies

Alba Carretero Cerdán

To my family

"Nothing will work
unless you do"

Maya Angelou

Abstract

The present thesis describes computational and experimental studies used to drive the reactivity of allylic and enol substrates towards new transformations. These synthetic methods give access to a number of organic molecules that may serve as important moieties in synthetic organic chemistry. Additionally, this thesis describes the synthesis of Metal-Organic Frameworks (MOFs) and their use in catalytic organic reactions.

The introductory chapter (Chapter 1) gives an overview of the concept of catalysis and its typologies, emphasizing those that have been used in the thesis. Moreover, synthetic procedures for the formation of MOFs and their use in catalysis are described. The importance and reactivity of allylic substrates are also presented. The chapter follows with a short introduction to hypervalent iodine and their reactivity. Finally, a brief description of computational studies and those used in this thesis are presented.

In Chapter 2, an umpolung protocol for the cross-nucleophile coupling of silyl enol ethers with heteronucleophiles mediated by an hypervalent iodine reagent has been explored. The mechanistic study of the reaction has been carried out employing DFT calculations and kinetic investigations.

Together with deuterium labelling studies and kinetic simulations, DFT calculations have been used in Chapter 3 for the examination of the base-catalyzed [1,n]-proton shift in conjugated polyenyl ethers.

Chapter 4 describes the synthesis of the family MIL-101(Cr) and MIL-101(Cr)-NH$_2$ employing microwave-assisted methods. The method has been compared to the common solvothermal synthetic pathways using common characterization techniques for heterogeneous materials.

Finally, Chapter 5 of this thesis describes the synthesis of a UiO-67 MOF containing a phosphazene superbase to study the effect of spatial confinement within a MOF on the stereospecific isomerization of allylic alcohols.

Populärvetenskaplig sammanfattning

Forskningsarbetet inom fältet för organisk kemi har visat sig ha stor påverkan på samhället. Organiska kemister har bidragit genom att utveckla nya föreningar samt hittat nya tillvägagångssätt för att syntetisera befintliga sådana. Dessa föreningar finns överallt. Många moderna material består av organiska föreningar så som bränsle, läkemedel och plaster. Dessutom kan dessa föreningar designas med datorsimuleringar för att bättre förstå deras struktur och egenskaper. Därför handlar denna avhandling både om beräkningsmässiga och experimentella forskningsstudier på transformationen av allyliska delar och enolderivat till högfunktionaliserade molekyler som kan fungera som byggstenar i läkemedelsindustrin.

En annan del av kemins grenar handlar om att designa och syntetisera material med intressanta strukturer och egenskaper. De potentiella användningsområdena för dessa material är bland annat som katalysatorer, gasförvaring, läkemedelstillförsel och avkänningsoptik. I detta avseende kan en kombination av organisk och oorganisk kemi tillämpas för att syntetisera enastående material som förbättrar resultaten av vissa omvandlingar. I denna avhandling sammanfattas syntesen av porösa material (metall-organiska ramverk) i Kapitel 4 och 5.

Sammanfattningsvis presenterar denna avhandling två nya syntesmetoder som kan vara användbara verktyg för syntes av komplexa organiska molekyler och för syntes av material med många potentiella användningsområden.

List of publications

This doctoral thesis is based on the following publications and manuscripts, which would be referred to in the text with Roman numerals I-IV. The contribution of the author in each publication is presented in Appendix A. Reprints of the publications were made with permission from the publishers.

Paper I
An Expedient Method for the Umpolung Coupling of Enols with Heteronucleophiles.
Víctor García-Vázquez,[‡] <u>Alba Carretero Cerdán</u>,[‡] Amparo Sanz-Marco,[‡] Enrique Gomez-Bengoa and Belén Martín-Matute*
Chem.Eur. J. **2022**, e202201000.

Paper II
Base-Catalyzed [1,n]-Proton Shift in Conjugated Polyenyl Alcohols and Ethers
Samuel Martínez-Erro,[‡] Nagaraju Molleti,[‡] <u>Alba Carretero Cerdán</u>, Amparo Sanz-Marco and Belén Martín-Matute*
ACS Catal. **2019**, 9, 10, 9134–9139.

Paper III
A Novel Microwave-assisted Synthesis of Amino Functionalized Chromium(III) Terephthalate MIL-101-NH$_2$
<u>Alba Carretero Cerdán</u>, Sergio Carrasco,* Amparo Sanz-Marco and Belén Martín-Matute*
Submitted.

Paper IV
Enhancing the Chirality Transfer in the Isomerization of Electron-deficient Allylic Alcohols
<u>Alba Carretero Cerdán</u>, Víctor García Vázquez,[‡] Pablo Martínez Pardo,[‡] Li Man, Gurpreet Kaur, Fahmi Himo and Belén Martín-Matute*
Manuscript.

Previous documents based on this work

This thesis work has been performed at Stockholm University (home university) and at the University of the Basque Country (host university) in Spain, within the multi-partner Marie Skłodowska-Curie (MSCA) Innovative Training Network (ITN) European Joint Doctorate (EJD) "Catalytic Methods for Sustainable Synthesis". A Merged Experimental and Computational Approach (CATMEC). Within this program, the PhD aims to obtain a double PhD degree, from Stockholm University, Sweden and from the University of the Basque Country, Spain.

The content of this thesis is partly based on the author's half-time report presented on September 29th, 2020.

The introduction (Chapter 1) has been revised and updated with the current literature to cover the necessary background.

Chapters 2 and 4 are entirely new.

Chapter 3 was included in the half-time report as a publication; for this thesis, the energy profile has been updated.

Chapter 5 was included in the half-time report as a manuscript in preparation; for this thesis, the project has been slightly modified.

Reprint permissions

Reprint permissions were given by the publishers for each of the following articles:

Paper I
Víctor García-Vázquez,[‡] <u>Alba Carretero Cerdán</u>,[‡] Amparo Sanz-Marco,[‡] Enrique Gomez-Bengoa and Belén Martín-Matute*
Chem.Eur. J. **2022**, e202201000.
Copyright © 2022 Chemistry - A European Journal published by Wiley-VCH GmbH.

Paper II
Base-Catalyzed [1,*n*]-Proton Shift in Conjugated Polyenyl Alcohols and Ethers
Samuel Martínez-Erro,[‡] Nagaraju Molleti,[‡] <u>Alba Carretero Cerdán</u>, Amparo Sanz-Marco and Belén Martín-Matute*
ACS Catal. **2019**, 9, 10, 9134–9139.
Copyright © 2019 American Chemical Society

[‡] Equal contribution.
* Corresponding author

Permissions to reprint figures **1.6a** and **4.1** were obtained from the respective publishers:

Figure 1.6a. Furukawa, H.; Gándara, F.; Zhang, Y. B.; Jiang, J.; Queen, W. L.; Hudson, M. R.; Yaghi, O. M. *J. Am. Chem. Soc.* **2014,** *136*, 4369-81.
Copyright © 2014, American Chemical Society

Figure 4.1. Férey, G.; Mellot-Draznieks, C.; Serre, C.; Millange, F.; Dutour, J.; Surblé, S.; Margiolaki, I. *Science* **2005,** *309*, 2040-2.
Copyright © 2005, The American Association for the Advancement of Science

Abbreviations

Abbreviations and acronyms are in agreement with standard in the field.* Common abbreviations and other non-conventional abbreviations in this report are listed below.

2-ATA	2-Aminoterephthalic acid
S_N2	Bimolecular nucleophilic substitution
c.t.	Chirality transfer
COD	1,5-Cyclooctadiene
DABCO	1,4-Diazabicyclo[2.2.0]octane
DBU	1,8-Diazobicyclo[5.4.0]undec-7-ene
DMF	*N,N*-Dimethylformamide
DFT	Density Functional theory
d.r.	Diastereomeric ratio
4DMAP	4-Dimethylaminopyridine
EDG	Electron-donating group
EWG	Electron-withdrawing group
ee	Enantiomeric excess
HITB	[Hydroxy(tosyloxy)iodo]benzene
HPLC	High performance liquid chromatography
IRC	Intrinsic Reaction Coordinates
KIE	Kinetic Isotope Effect
MTBD	7-Methyl-1,5,7-triazabicyclo(4.4.0)dec-5-ene
MW	Microwave
2-NTA	2-Nitroterephthalic acid
NMR	Nuclear Magnetic Resonance
Phen	1,10-Phenanthroline
PSE	Post-synthetic exchange
PSM	Post-synthetic modification
PXRD	Powder X-Ray Diffraction
RDS	Rate determining step
rt	Room temperature
SBU	Secondary Building Blocks
SEM	Scanning Electron Microscopy
ST	Solvothermal
TBD	1,5,7-triazabicyclo[4.4.0]dec-5-ene
TA	Terephthalic acid
TBS	*Tert*-butyl dimethyl silyl

P$_4$^{t}Bu	(1-*tert*-Butyl-4,4,4-tris(dimethylamino)-2,2-bis[tris(di-methylamino)-phosphoranylidenamino-2λ5,4λ5–catenadi(phosphazene))
TFA	Trifluoroacetic acid
XAS	X-ray Absorption Spectroscopy

*: Petronella, K.M. Abbreviations List, The ACS Guide to Scholarly Communication. 2020 (DOI: 10.1021/acsguide.50308)

Table of Contents

ix

1 Introduction

1.1 Organic chemistry and catalysis

Organic chemistry is the study of the structure, properties and reactivity of carbon-containing compounds. It is a creative branch of chemistry that allows to synthesize new molecules or to develop better methods to access existing molecules.[1] One of the current challenges of the field is the development of more efficient and environmentally friendly synthetic methods.[2, 3] Catalysis may contribute by replacing the use of stoichiometric reagents and enabling reactions under milder reaction conditions, and even new reactions.[4, 5]

A catalyst increases the reaction rate of a chemical reaction by lowering the activation energy barrier, without altering the overall thermodynamics (ΔG) associated to the reaction (**Figure 1.1**). The reaction pathway may follow a completely different mechanism than that followed by the uncatalyzed reaction, as shown in **Figure 1.1** below. The catalyst is regenerated after a turnover, allowing it to be used in substoichiometric amounts.
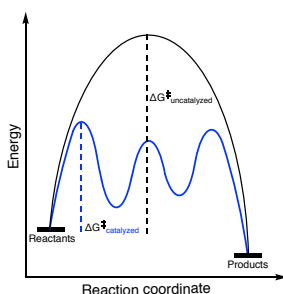
Figure 1.1. An example of the energy profile of an uncatalyzed (black) *versus* a catalyzed (blue) reaction.

According to the nature and the physical state of the catalysts, catalysis can be divided into three main classes: homogeneous, heterogeneous and biocatalysis.[6] Catalysts may contain one or more transition metal centers within their cores (transition metal catalysts). Alternatively, they are referred to as "organocatalysts".[7-10]

1

1.1.1 Organocatalysis

It was during the 90s when the field of organocatalysis was first officially recognised.[7, 11] However, the use of organocatalysts started years before without that recognition. The group of Parrish[12] reported in the 1974 the use of (*S*)-(−)-proline for the asymmetric synthesis of bicyclic intermediates. Later on, a number of research groups contributed significantly to this field. The groups of Shi, Denmark and Yang described the use of enantiomerically pure ketones as catalysts to mediate alkene epoxidations in an enantioselective manner.[13-15] In this period, the group of Jacobsen and Corey reported the first chiral bases for hydrogen-bonding catalysis, and their use in asymmetric Strecker reactions.[16, 17]

Hydrogen-bonding catalysis[18] has proven to be excellent for activating molecules by either enhancing the electrophilicity or the nucleophilicity of the reagents, through intra-[19] or intermolecular[20] H−bond formation (**Scheme 1.1**). This type of organocatalysts has been used for the synthesis of organic molecules of importance in medicinal chemistry.[21, 22]

up to 98% yield
up to 9:1 *d.r.*
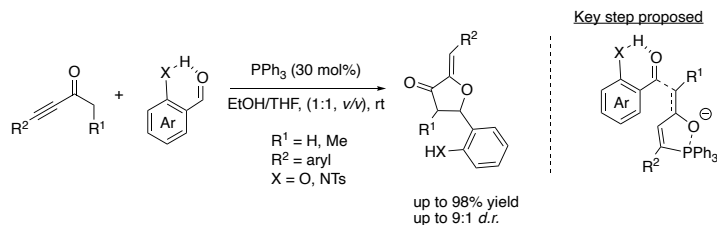
Scheme 1.1. Hydrogen-bonding catalysis for the activation of aldehydes for aldol-type reactions.[23]

N-Heterocyclic carbenes (NHC) have been widely studied as organocatalysts for transformations involving the construction of C−C bonds.[24] An example is the benzoin condensation catalyzed by NHCs that was first investigated in 1943.[25] It was not until 1958 when Breslow[26] proposed a mechanism for this transformation, where the active species is a carbene (thiazolino-2-ylidene), formed *in-situ* after deprotonation of a thiazolium salt (**Scheme 1.2**).
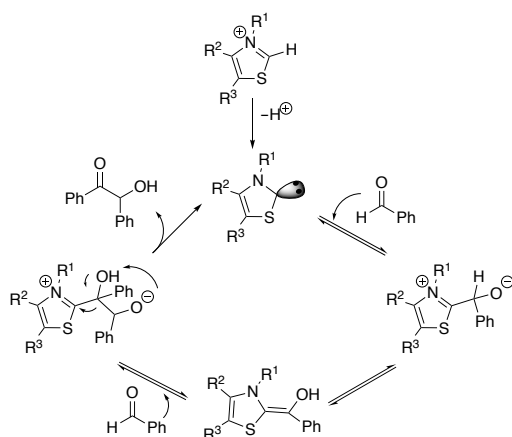
Scheme 1.2. Catalytic cycle of the NHC-catalyzed benzoin condensation reaction.[26]

Two noteworthy publications contributed to the field of organocatalysis by the groups of Benjamin List and of David MacMillan in enamine and iminium catalysis (**Scheme 1.3**). In 2021, the Nobel prize in Chemistry was awarded jointly to both of them for their contribution to the field of asymmetric organocatalysis.[27, 28]
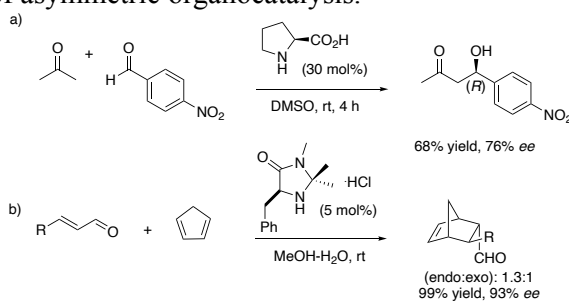
Scheme 1.3. Selected examples for (a) enamine and (b) iminium catalysis.[27, 28]

Brønsted base catalysis has been used as an efficient process due to its excellent results in the formation of C−C or C−X (X = heteroatom) bonds.[29] Brønsted base catalysis is the process by which a species capable of accepting protons increases the rate of a given chemical reaction by enhancing the nucleophilicity of the bonding species.[30] Especially, chiral Brønsted bases can be excellent catalysts for enantioselective transformations.[29] During the 70s the use of Brønsted bases was broadly developed as a result of a better mechanistic understanding.[31]

Cinchona alkaloids are one of the first Brønsted base catalysts that can act as bifunctional organocatalysts showing high activity in important asymmetric reactions such as Mannich reactions (**Scheme 1.4**).[32]
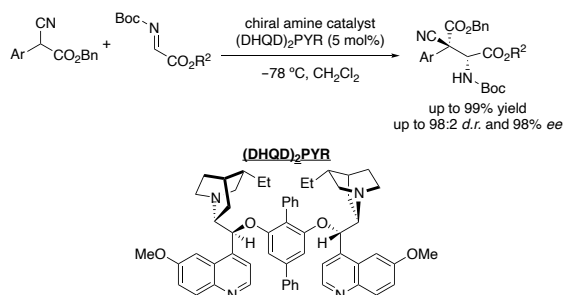
Scheme 1.4. Cinchona alkaloid-based organocatalysts for Mannich reaction.[32]

Organic superbases have also been explored as catalysts in asymmetric reactions. They have better solubility in organic media and lower pK_a compared to inorganic bases. An organic molecule is considered as a superbase when the pK_{BH^+} value is higher than the one of Proton sponge® ($pK_{BH^+} = 18.6$ in MeCN; **Figure 1.2**).[33] Amidines,[34] guanidines[35] and phosphazenes[36] are the functional groups most commonly present in organic molecules showing super basicity.

Figure 1.2. pK_{BH^+} of some organic superbase examples. Values given in MeCN as solvent.[37]
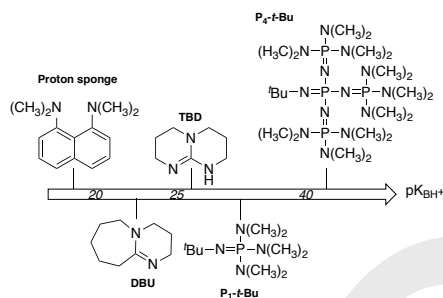
Remarkably, these commercially available superbases have recently been used in a large number of new synthetic methodologies.[38-41] In 2013, the group of Shibata reported the effectiveness of the P4-*t*-Bu superbase for the addition of a trifluoromethyl anion generated from

4

fluoroform to a carbonyl group. The key of this reaction is the formation of a stabilized ion pair between the protonated base and the deprotonated trifluoromethyl anion that prevents the decomposition of the trifluoromethyl carbanion ($^-CF_3$) to the fluoride anion and difluorocarbene (:CF_2).[42]

1.1.2   Heterogeneous catalysis

Heterogeneous catalysis has emerged as an important area of research, both in academia and industry during the last decades.[43-45] However, heterogeneous processes have been on-going for more than a century. An important process in this area is the development of the hydrogenation process by Paul Sabatier in 1897. The process consists of the metal-catalyzed hydrogenation reaction of π-bonds such as alkenes, using heterogeneous catalysts containing palladium, platinum or nickel.[46] Nowadays, a huge number of synthetic organic routes involve heterogeneous catalytic hydrogenations. This reaction is well-established as a type of heterogeneous catalysis, defined as surface chemistry catalysis. Surface catalysis proceeds through chemical and physical reaction steps: Physisorption or physical adsorption, chemisorption, surface reaction, diffusion and desorption.[47, 48]

However, heterogeneous catalysis does not necessarily involve surface chemistry. Indeed, a closer look to the literature gives an overview of the heterogenization of homogeneous catalysts that has been a focus of research more recently.[49-51] The major advantage of the heterogenization of well-established homogeneous catalysts is the easier separation of the catalyst from reactants and products, and its regeneration. The ongoing work on this type of heterogeneous catalysis is focused on the construction of new heterogenous catalysts with tunable reactivity, and with higher stability and selectivity than that of their homogeneous version.[50, 52] In this type of heterogeneous catalysis, the accessibility of the substrates to the active site is considered of great significance. Diffusion becomes important in the reactivity of the system, since fast diffusion leads to an increased number of catalytic turnovers. Therefore, the shape and size of the reactants and the catalyst contribute to the efficiency of the catalytic system. For example, materials on the nanoscale have demonstrated to have a high impact on influence the efficiency of the heterogeneous system.[53]

In order to gain a better insight of the heterogeneous catalysts before and after a reaction proceeds, there are a number of characterization techniques that can be used: X-Ray Powder Diffraction (XRD), Scanning Electron Microscopy (SEM), Transmission Electron Microscopy (TEM), Thermal Gravimetric Analysis (TGA), Infrared Spectroscopy (IR), gas adsorption analysis, Elemental Analysis (EA) or Ultraviolet-visible (UV-vis) spectroscopy, among others.[54] Remarkably, it is possible to get deeper understanding of the mechanism of a heterogeneous-catalyzed reaction while the catalyst is in *operando*. In order to achieve that, *in-situ* characterization techniques can be applied. This kind of characterization may require high-energy synchrotron radiation. The Martín-Matute group contributed in 2018 to this field with the study of the evolution of palladium species during the Heck coupling reaction using a heterogeneous catalyst by *operando* X-Ray Absorption Spectroscopy (XAS) and X-ray Diffraction (XRD) techniques.[55]

Porous materials are among the most widely used heterogeneous catalysts with high surface areas. The porous materials can be classified in three types according to the diameter pore size: microporous (<2 nm), mesoporous (2–50 nm) and macroporous (>50 nm). Metal-Organic Frameworks (MOFs) have risen over the past three decades as one the most popular porous materials used in the scientific community among zeolites, silicates and activated carbons.[56-58]

1.2 Metal-organic frameworks

A Metal-Organic Framework consists of a coordination network between organic linkers and metal ions or clusters in two- or three- dimensions, containing potential voids (**Figure 1.3**).
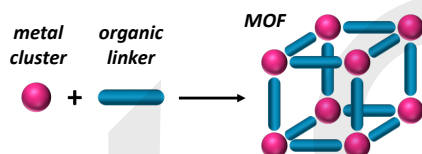

Figure 1.3. General 3D coordination network of a MOF.

MOFs have emerged as potential hybrid materials[59] for gas storage,[60] biosensors,[61] drug delivery[62] and importantly, for catalysis[63] due to their tunable porosity, structural chemical versatility and high surface area.

An extraordinary application of MOFs has been developed by the group of Yaghi and co-workers in order to solve tremendous worldwide problems. They have contributed to the study of how to get water from the air in a landscape like the deserts, where precipitation barely occurs.[64-66] The group of Yaghi demonstrated that MOF-801, based on $Zr_6O_4(OH)_4(fumarate)_6$ and MOF-303, $Al(OH)(HPDC)(H_2O)$ types (**Figure 1.4**) are highly promising for sorbent-assisted water harvesting without using electricity. On average, MOF-303 was able to produce 0.7 L kgMOF^{-1} day^{-1}. Thus, the group of Yaghi have envisioned the design of MOFs as sorbent materials for the production of several tons of liters of water per kilogram of MOF per day.[65]
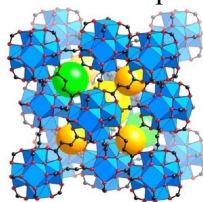
Figure 1.4. MOF-801, atom color scheme: C, black; O, red; Zr, blue polyhedral. Yellow, orange and green spheres indicate the space within the framework. Figure reproduced with permission from ACS.[64]

1.2.1 Synthesis of MOFs

MOFs can be synthesized following different methods. Solvothermal and hydrothermal synthesis, electrochemistry, microwave-assisted, mechanochemistry and sonochemistry methods have been employed over the years.[67, 68] Importantly, different synthetic methods afford the same MOF in different yields, reaction times, particle size, morphology, phase-selectivity and crystallinity. This thesis focuses on the traditional heating and microwave-assisted methods.

In conventional synthesis, the reaction mixture is usually placed in an autoclave controlling pressure, temperature, solvent and concentration. When the reaction temperature is above the boiling point the process is called *solvothermal* (ST, for organic solvents) or *hydrothermal* (when water is employed). If the temperature is lower than the boiling point of the solvent, it is called *non-solvothermal* synthesis.[69]

Conventional methods often require long reaction times, autoclaves and high energy consumption. To overcome some of these limitations, microwave-assisted methods (MW) have shown to be a more efficient alternative,[70] empowering the reduction of reaction times, the crystallization of the process and crystal size and the selective synthesis of polymorphs.[71-73] However, the use of microwave heating lacks reproducibility when different instruments are used due to the intrinsic differences of each reactor's settings (*e.g.* irradiation power).

1.2.2   MOFs as catalysts

As a consequence of the hybrid nature of MOFs, they offer the possibility of having the catalytic sites on different parts of their network (**Figure 1.5**).[74-76]
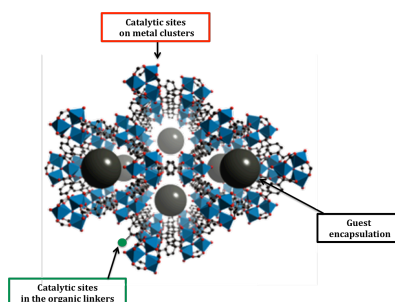
Figure 1.5. Schematic representation of the three catalytic sites in MOFs.

Firstly, the oxo-metal clusters of the MOF can act as a Lewis acid due to the availability of open coordination sites. Labile ligands, such as solvent molecules or any ligand present in the synthesis of the framework can be displaced from the metal cluster in a reversible way, creating a coordinative unsaturated site.[77, 78] Secondly, the catalytic active sites can be present at the organic linkers either *per se* or anchored to another organic or transition metal moieties.[79-81] Lastly, another catalytic site in a MOF could be the generation or encapsulation of enzymes, molecular complexes or metal nanoparticles (MNPs) at the voids of the material without being covalently attached to the host framework.[82]

This thesis is focused on the use of MOFs as catalysts where the catalytic site is introduced into the surrounding linkers. There are several

routes to introduce linkers into MOFs by direct synthesis, post-synthetic exchange (PSE) and post-synthetic modification (PSM, **Figure 1.6**).
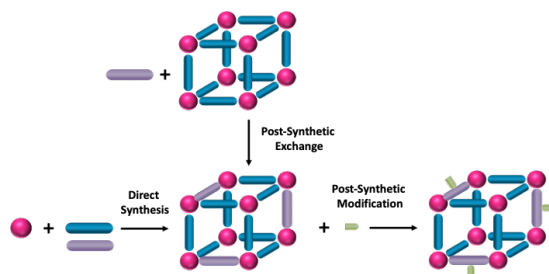
Figure 1.6. Synthetic strategies for MOFs. Pink spheres (metal clusters), purple and blue bars (organic linker counterparts), green bar (organic linker modifications).

Cohen and co-workers reported these three strategies for the functionalization of the UiO-67 MOF with (bis(2,2-bipyridine)(5,5-dicarboxy-2,2-bipyridine)ruthenium(II). Low loadings of Ru were observed when using direct synthesis and PSE. Importantly, PSM enhances the Ru loading up to 10% providing a robust heterogeneous catalyst for the photocatalyst aerobic oxidative hydroxylation of arylboronic acids.[83] Martín-Matute and co-workers also contributed to the synthesis of a MOF with an Ir-NHC complex for the isomerization of allylic alcohols *via* direct synthesis and PSE. The latter route was shown to be a potential approach that can lead to higher metal loadings when comparing to direct synthesis routes.[84]

1.3 Allylic alcohols

1.3.1 Relevance and general reactivity

Allylic compounds are molecules constituted by a double bond attached to a saturated carbon which bears a functional group (**Figure 1.7**). Importantly, natural products and biologically active organic compounds such as terpenes and steroids present on their structure allylic systems (*e.g.* androstenediol, a weak steroid that controls certain hormone processes and carveol, a monoterpenoid found in spearmint commonly used as flavoring in food and tea).[85] Steroids and terpenes are important scaffolds for the synthesis of significant pharmaceutical molecules.[86]

Y = OR, Cl, Br, I, NRR and SR
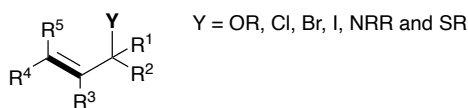
Figure 1.7. General representation of allylic substrates.

The reactivity of allylic moieties is due to the presence of an olefin which strongly activates the functional group allowing the system to undergo a variety of substitution reactions.[87] For example, Claisen re-arrangements[88] that might give access to complex molecules such as stereodefined polysubstituted olefins.[89] Importantly, the activating effect of the hydroxyl group in the allylic alcohol in olefin metathesis has been found to be an important strategy for the synthesis of natural products (**Scheme 1.5**).[90]
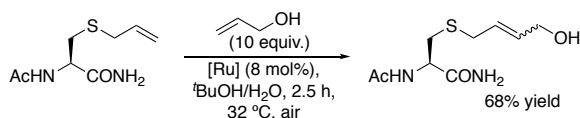
Scheme 1.5. Cross-metathesis of *S*-allylcysteine.

1.3.2   Isomerization of allylic alcohols

Traditionally, the transformation of allylic substrates into saturated car-bonyl compounds requires a two-step process for stoichiometric oxida-tion/reduction reactions. Therefore, high amounts of waste are gener-ated after the processes. From an atom-economical perspective this is not desirable. Therefore, during the last 50 years the use of transition-metal catalysts[91] have become an attractive pathway to overcome this issue. One of the first reports, $Fe(CO)_5$ was used as catalyst for this transformation although low yields and selectivity were obtained (**Scheme 1.6a**).[92] Subsequently, a considerable amount of articles have been published to enhance the efficiency of this transformation compare to the previous reports (**Scheme 1.6b**).[93-97] Recently, the group of Mar-tín-Matute contributed to the isomerization of primary and secondary allylic alcohols using a commercially available Ir(III) catalyst under very mild conditions in aqueous solvents (**Scheme 1.6c**).[98, 99]

10

a)

R₂ OH → Fe(CO)₅ (10–20 mol%) / octane or pentane, 2-6 h, 110–125 °C → R₂ O

R_1 ... R_4 / R_3 → R_1 ... R_4 / R_3

b)

R_1 ... OH / R_3 — [Ir] (0.25–10 mol%) / THF, rt, 0.5–22 h → R_1 ... H / R_3

c)

R_1 ... R_4 / R_3 — [Cp*IrCl₂]₂ (1 mol%) / Acetone/H₂O (2:1), rt or 60 °C → R_1 ... R_4 / R_3
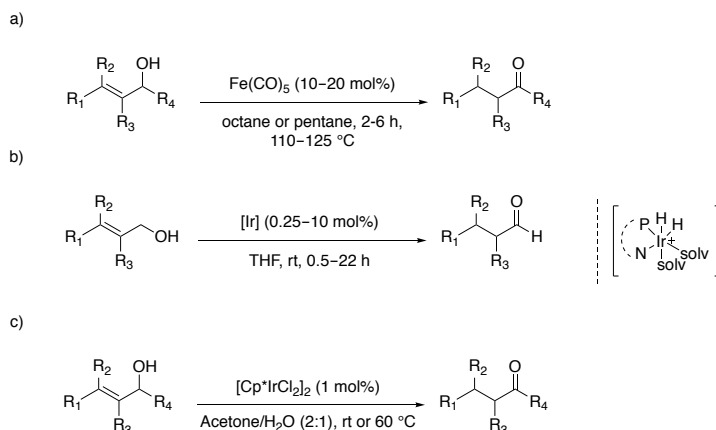
Scheme 1.6. Transition metal-catalyzed isomerization of allylic alcohols.[92, 95, 98]

The enantioselective isomerization of allylic alcohols into the corresponding chiral ketones has been widely studied. However, these processes rely on the use of sophisticated transition-metal catalysts containing chiral ligands (**Scheme 1.7a**), and with a very few exceptions, it is limited to primary allylic alcohols.[96, 100-104] Another approach to access chiral ketones from allylic alcohols is the use of enantiomerically pure substrates that are then isomerized *via* a stereospecific mechanism using non-chiral catalysts (**Scheme 1.7b**).[105-107]

a)

R^1 ... R^3 / R^2 — [Rh(COD)₅]BF₄ (2 mol%) / (R)-BINAP (5 mol%) / Ag₂CO₃, 24 °C, 20 h → H O / R^1 ... R^3 / R^2

up to 94% yield
up to 90% *ee*

b)

F₃C ... R^1 / R^2 OH — [RuCl₂(PPh₃)₃] (1 mol%) / Toluene, Cs₂CO₃, 30 °C, 2 h → F₃C ... R^1 / R^2 O

High enantioselecitivity   High stereospecificity
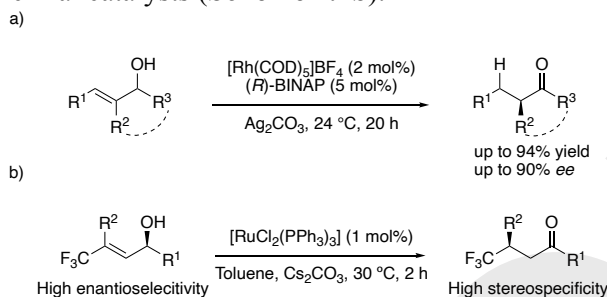
Scheme 1.7. a) Enantioselective[102] and b) stereospecific isomerization of allylic systems.[105]

1.3.3 Transition-metal-free isomerization of allylic alcohols
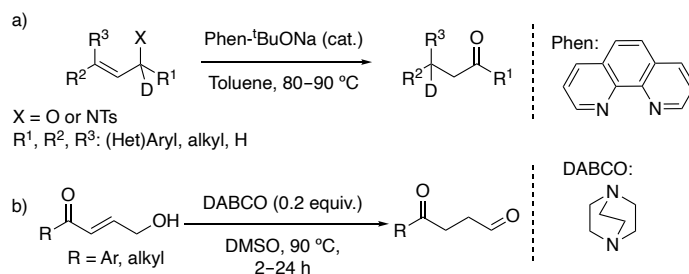
The isomerization of allylic alcohols has also been reported without the presence of transition metals. In 1928[108] the use of Brønsted bases for this transformation was published for the first time, although the field

has not progressed substantially since then. The protocols usually require stoichiometric amounts of strong bases and the reactions are limited to the substrate structure because of functional group compatibility.[109, 110]

Recently, protocols for the base-catalyzed isomerization of allylic alcohols have been reported in the literature. A combination of phenanthroline and *tert*-butoxide as radical initiators was developed by the group of Tang in 2015 (**Scheme 1.8a**) for this purpose.[111] And the group of Pan developed an organocatalytic redox strategy for the isomerization of γ-hydroxy enones using DABCO as a catalyst under mild conditions (**Scheme 1.8b**) in 2016.[112]

Scheme 1.8. Examples of base-catalyzed isomerization of allylic alcohols and amines.[111, 112]

In 2016, Martín-Matute and co-workers described the organocatalytic isomerization of electron-poor allylic moieties using a simple guanidine-type base, 1,5,7-triazabicyclo[4.4.0]dec-5-ene (TBD).[113] It was the first time that the base-catalyzed isomerization of allylic alcohols and ethers was reported to be stereospecific. Importantly, the reaction follows a stereospecific pathway due to the formation of a chiral ion-pair intermediate (**Scheme 1.9**). The stereochemical information is transferred with high levels of chirality transfer (*c.t.*, up to 97%) when apolar solvents such as toluene are used. The base-catalyzed protocol has been applied to conjugated allylic alcohols and ethers and to other allylic substrates such as allylic halides and allylamines. The metal-free isomerization was also extended to other conjugated polyenyl alcohols and ethers (*vide infra,* Chapter 3).[114-116]
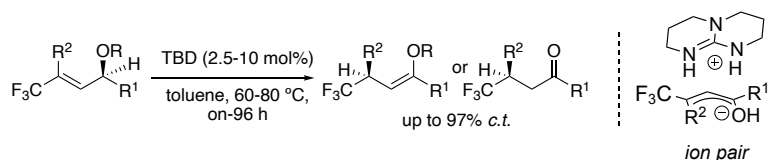
Scheme 1.9. Base-catalyzed isomerization of allylic alcohols and ethers through ion-pair organocatalysis.

Yamazaki and co-workers reported in 2017 a similar protocol for the isomerization of CF$_3$-containing allylic alcohols to saturated ketones using 1,8-diazabicylo[5.4.0]undec-7-ene (DBU) as the base, and under reflux conditions.[117] Recently in 2020, the group of He reported a protocol for the asymmetric allylic substitution-isomerization to axially chiral enamides. This approach first follows an iridium-catalyzed allylic substitution and then base-catalyzed stereospecific isomerization with high central-to-axial levels of chirality transfer.[118, 119]

1.4 Hypervalent iodine reagents

1.4.1 Structure and reactivity of hypervalent iodine reagents

According to the IUPAC, the term hypervalency is defined as "*the ability of an atom in a molecular entity to expand its valence shell beyond the limits of the Lewis octet rule. Hypervalent compounds are common for the second and subsequent row elements in groups 15-18 of the periodic table*".[120] One of the most useful and explored class of such compounds are hypervalent iodine reagents (**Figure 1.8**) due to their ability to adopt several oxidation states (from I to VII) upon oxidation process.[121-123] Thus, they have been employed in oxidation reactions.[123-125]

Togni's reagent   **Dess-Martin Periodinane (DMP)**   **Iodine Heptafluoride**
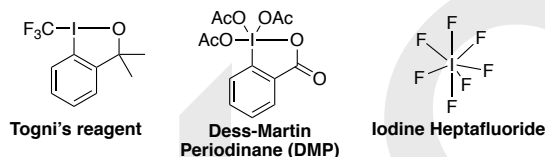
Figure 1.8. Selected examples of hypervalent iodine reagents.

The hypervalency of the iodine(III) reagents is a consequence of the T-shaped geometry (L–I–L) where the two lone pairs of the iodine and the R group reside on the equatorial position while the two ligands are

in the axial position (**Figure 1.9a**). In accordance with the molecular orbital theory, the hypervalent bond in the iodine(III) reagents is defined as a linear 3-center 4-electron bond (3c-4e) (**Figure 1.9b**). One pair of the bonding electrons is delocalized with the two ligands and as a result, the central iodine is described with a partial positive charge while the external ligands accumulate a partial negative charge.[126]
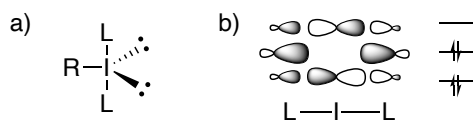
Figure 1.9. a) T-shaped structure of hypervalent iodine molecules. b) Molecular orbital description of the three-center-four-electron bond in hypervalent iodine molecules.

As mentioned above, the central iodine bears a partial positive charge which makes this atom very electrophilic as a consequence of the nature of the hypervalent bond. Therefore, nucleophiles are prompt to react with the electrophilic iodine, replacing one of the two ligands during the ligand exchange process. A new T-shaped intermediate (X) is formed which will undergo through a reductive elimination or a concerted ligand coupling of the two ligands (**Figure 1.10**).[127] Hence, using hypervalent iodine compounds is possible to introduce a number of functional groups at the α-carbon of carbonyl compounds through the formation of enolonium intermediates by switching the polarity of one of the substrates. For example, enol derivatives that are nucleophiles by nature can react with other nucleophiles mediated by hypervalent iodine reagents through an umpolung reaction.[128-131]
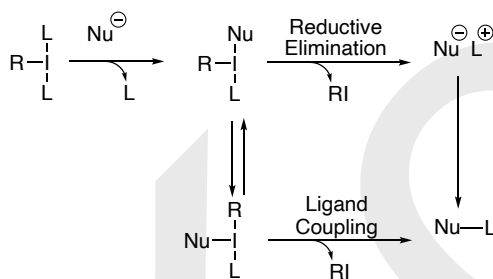
Figure 1.10. General reactivity of hypervalent iodine reagents.

14

1.5 Computational chemistry

Nowadays, computational studies are an essential tool for a better understanding of the mechanism operating in chemical reactions.[132] Computational chemistry provides information of the energy of a system in terms of the position of the atoms that is defined as potential energy surface (PES). In this way, geometries and electronic properties of all molecular entities involved in the energy profile, kinetic simulations and enantiomeric excess can be obtained.

1.5.1 Density Functional Theory (DFT)

In the past decades, DFT has emerged as one of the most popular methods in quantum mechanics (QM).[133] One of its main benefits is the accuracy to computational cost ratio, which is much higher than that of other methods. The fundamentals of DFT were first drawn by Thomas[134] and Fermi[135] but it was the work of Hohenberg and Kohn that set the grounds of modern DFT. In 1998 the Nobel Prize in chemistry was awarded to Walter Kohn for his reformulation of the theory and to John A. Pople for developing computational methods in quantum mechanics.[136, 137]

In 1964 Hohenberg and Kohn proved two theorems to demonstrate the correlation between the total energy of the system and the electron density $E[\rho(r)]$.[138] The first theorem proves that the density of any system determines all ground-state properties of the system uniquely. The second theorem asserts that the ground state energy of the system can only be obtained with the exact electronic density, and that the energy obtained from other calculated electronic densities are an upper bound to it. Instead, DFT-calculated energies depend only on the three spatial coordinates of the electron density. The main drawback of this method is the difficult analysis and resolution of the complex equations at the base of DFT.

For this reason, most of current methods used nowadays in DFT calculations are based on the Kohn-Sham theory, which approximates the kinetic energy of the ground state of the system to the kinetic energy of a non-interacting gas.[139] Thus, the Kohn-Sham expression can be written as described in **Equation 1**, in which all terms are known except for the exchange-correlation energy (E_{XC}). This term is divided into the exchange term (E_X), which representing the interactions between same

spin electrons, and the correlation term (Ec), representing the interactions of electrons with opposite spin. The approximations used to account for these terms in the DFT methods determine the accuracy of the final energy and electron density of the calculations.

$$E_{HK}\left[\rho(r)\right] = E_{ni}\left[\rho(r)\right] + V_{Ne}\left[\rho(r)\right] + J[\rho(r)] + E_{XC}\left[\rho(r)\right]$$

Equation 1. Kohn-Sham theory expression where E_{ni} is the energy of the non-interacting system, V_{Ne} is the nuclei-electron attraction, J is the Coulomb term, and E_{XC} is the exchange-correlation energy.

1.5.2   Computational details

The DFT calculations presented in this thesis were performed with Gaussian 16 software.[140]

Geometry optimizations and frequency calculations in **Chapter 2** were performed with the B3LYP functional and 6-31G(d,p) basis set for all the atoms with the exception of I and Br in which SDD basis set was used. The energies showed in the manuscript have been refined by single-point calculations on the previously optimized structures, by applying the M06 functional and Def2-TZVPP[141] basis set in a solvent model (IEFPCM, solvent = DMF).

The calculations presented in **Chapter 3** were performed using the M06-2X[142] functional. For the geometry, optimizations were carried out by using the 6-311G (d,p) basis set for all the atoms. All final energies were corrected to the Def2TZVPP basis set with single-point calculations in a polarizable continuum solvent model using the integral equation formalism variant (IEFPCM).[143-145]

In chapter 3 all the stationary points were characterized by frequency calculations in order to verify that they have the right number of imaginary frequencies, and the intrinsic reaction coordinates (IRC) were followed to verify the energy profiles connecting the key transition.[146] In chapter 2 the IRC were followed for $TS_{1a'-1a''}$. All the Gibbs free energies values are given in kcal/mol and all reported energies are relative to the initial mixtures of reactants.

1.6   Aim of the thesis

The aim of this thesis is study the mechanisms of new organic transformations of allylic substrates and enol derivatives. For this, DFT in combination with experimental studies will be used to get an understanding of the mechanisms in the reactions in Chapter 2 and 3. Further, a goal in this thesis is also to develop new heterogeneous catalytic transformations and develop an understanding of how the materials (MOFs) can influence on the outcome of the reactions.

The functionalization of ketones with a heteroatom at the α-position requires the use of highly reactive heteroatom-based electrophiles, which also have strong oxidizing properties. In the second chapter, we aim to develop an umpolung method that enables to substitute these highly electrophilic species by nucleophilic counterparts. This will broaden the scope of the reaction, at the same time as provide more efficient alternative reaction pathways, without formation of unwanted side products.

The mechanism for the isomerization of electron-deficient poly-enylic alcohols and ethers with a base catalyst is presented in the third chapter of this thesis. The mechanism has been studied employing DFT calculations and deuterium labelling experiments.

MIL-101-type MOFs have been synthesized employing different methods. However, the use of hydrofluoric acid or long reaction times make the protocols undesirable. In the fourth chapter of this thesis, we present an expedient protocol using microwave-assisted for the synthesis of MIL-101(Cr) and MIL-101(Cr)-NH$_2$ with excellent yields, phase selectivity and short reaction times.

In the fifth chapter of this thesis, our goal is to synthesize a MOF bearing a superbase within its structure. Moreover, we aim to demonstrate that the confinement effect conferred by MOFs enhances the levels of chirality transfer in the isomerization of electron-deficient allylic alcohols.

2 An expedient method for the umpolung coupling of enol nucleophiles with heteronucleophiles. Paper I.

2.1 Background of the project

α-Substituted carbonyl compounds are very important motifs in synthetic and medicinal chemistry.[147-150] Indeed, there is a considerable number of α-functionalized compounds that have important biological activities (**Figure 2.1**).[151] Amfepramone is used as a stimulant drug to suppress the appetite, while glutathione plays an important role for building and repairing tissues.[147, 152]

Amfepramone   **Gluthanione**
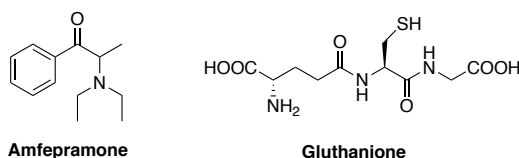
Figure 2.1. Examples of relevant organic α-functionalized carbonyl compounds in synthetic and medicinal chemistry.

The classic synthesis of α-functionalized ketones is based on the reaction of the nucleophilic α-carbon of the carbonyl compound with an electrophile. When it comes to heteroatomic electrophiles leading to formation of C–heteroatom bonds, the reaction usually results in formation of by-products. This is because heteroatomic electrophiles are also strong oxidants[153, 154] Further, in some instances, the limited availability of the heteroatomic electrophile requires to prefunctionalize the reagents before use.[155-158] An alternative approach is the use of nucleophiles rather than electrophiles. However, this route is not straightforward due to the polarity mismatch between the two nucleophilic reagents.

Corey and Seebach originally developed the umpolung concept in the 70s reversing the intrinsic reactivity of acyl carbon atoms that has led to unexplored molecular.[159] The inversion of polarity of carbonyl compounds could be accomplish by the use of transition-metal catalysts,[160, 161] Lewis acids[162] and hypervalent iodanes[163, 164] (**Scheme 2.1**).

a) Tandem umpolung

1. a) R⁴MgX, Et₂O, Copper source b) H⁺

2.

b) Hypervalent iodanes

HTIB
MeCN, Δ

c) Lewis acid

isoxazolidine (2 equiv.)
MgSO₄

CH₂Cl₂, 16 h, rt

R₃Al (2 equiv.)
3 - 5 h, rt
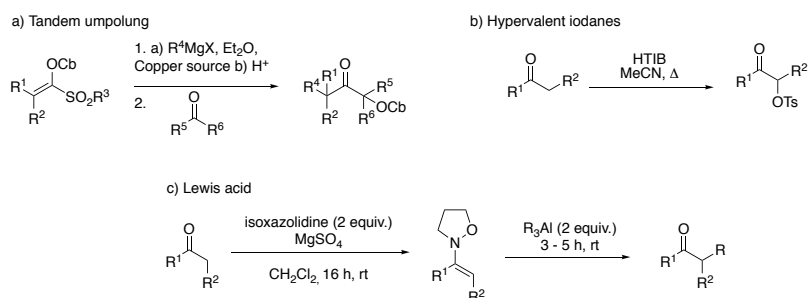
Scheme 2.1. Reported strategies for the synthesis of α-functional-ized ketones following an umpolung event. a) Hoppe[160] b) Koser[163] c) Miyata.[162]

Numerous examples of the α-functionalization of carbonyl com-pounds using hypervalent iodine reagents have been reported, including tosyloxylation, hydroxylation, acetoxylation, halogenation, amination, alkynylation, alkylation and arylation.[165-169] By taking advantage of this reactivity, the α-functionalized ketones give access to many natural products, pharmaceuticals and other organic functional compounds by forming C–C and C–X bonds (X = heteroatom).[170-172] Martín-Matute and co-workers contributed recently to this field with an umpolung strategy using allylic alcohols as enolate synthons, in a reaction cata-lyzed by iridium.[130]

More recently, the Martín-Matute group developed an unprecedented protocol for the synthesis of α-carbamoyl compounds from CO_2 using hypervalent iodine compounds as mediator of the transformation. Dur-ing the investigations, an α-bromoketone was identified as a key inter-mediate.[173]

By taking advantage of the formation of this α-bromoketone, we pre-sent in this chapter the investigation of the generality of the reaction by introducing new heteronucleophiles as partners for their cross-nucleo-phile coupling with enol derivatives mediated by iodine (III) reagents. We also present mechanistic investigations.

2.2 Substrate scope

After evaluating different parameters and screening different hypervalent iodine reagents, the optimal conditions were found (**Scheme 2.2**). Thus, two methods were employed, and its choice was dependent on the nucleophile (*vide infra*). Using Method A 1-Bromo-3,3-dimethyl-1,3-dihydro-1λ3-benzo[d][1,2]iodaoxole (**2**), the corresponding nucleophile (NuH) and sodium hydride are placed in a pressure tube. Then, a solution of (*Z*)-*tert*-butyldimethyl((1-phenylprop-1-en-1-yl)oxy)silane (**1**) in DMF was added and stirred overnight at room temperature. While when using Method B, the reagents **1** and **2** were placed in a pressure tube with DMF and stirred overnight at room temperature. After that, a suspension of the NuH and sodium hydride was added and the mixture is stirred for additional 4 h. The difference between the methods is that Method A is one-pot one step and Method B is one-pot two steps.
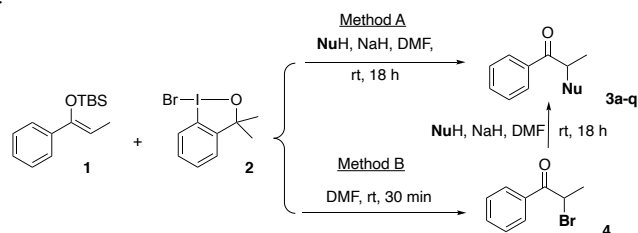
Scheme 2.2. Optimized reaction conditions for the α-functionalization of silyl enol ethers following Methods A and B.

After the application of Method A for the formation of α-carbamoyl carbonyl compounds (**Scheme 2.3**), we moved onto the evaluation of the generality of the cross-nucleophile coupling of TBS-enol ethers with a variety of nucleophiles (**Scheme 2.4**). Unless otherwise noted, the scope was performed following Method A. However, for the cases where a complex mixture of unidentified by-products was obtained Method B was applied. This slight modification was needed in order to preform the key intermediate (α-bromo ketone, **4**) before adding the other nucleophilic reaction partner.
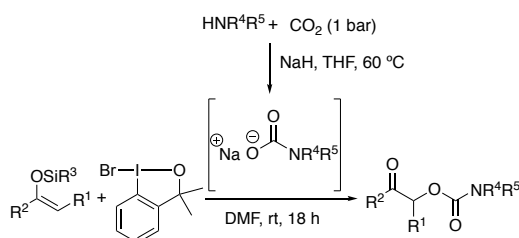
Scheme 2.3. Method A applied for the synthesis of α-carbamoyl carbonyl compounds.

Initially, several *para*-substituted benzoic acid derivatives were investigated as nucleophiles. Both electron-withdrawing and electron-donating groups gave α-carboxylate carbonyl compounds **3a-3c** in very good to excellent yields (80-98%). Method B was applied when phenol was used as nucleophile, yielding the corresponding α-phenolate **3d** in moderate yield. Thiols were then evaluated, thiophenol provided **3e** in 60% yield following Method A. The yield of the reaction was increased to 82% using Method B, which gave also quantitative yield for ^{t}BuSH (**3f**). Interestingly, alkyl- and cyclo-substituted amines were also well tolerated when applying Method B. Benzylamine gave the product **3g** in 67% yield and cyclopropylamine functionalization **3h** could be obtained following both procedures, although Method B resulted in higher yields. Piperidine and morpholine derivatives (**3i** and **3j**) were obtained in good yields of 77% and 80%, respectively. Importantly, 1,3-dicarbonyl compounds as carbon nucleophiles reacted smoothly and **3k** was formed in 72% yield when using Method B. Finally, azides were also very well tolerated and the **3l** was provided in a good yield (73%) following Method B, and in 50% yield following Method A.

Different natural products and pharmaceuticals containing carboxylic acids motifs in their structure were tested as nucleophiles in their umpolung reaction with TBS-enol ether **1**. When using a simple Boc-protected amino acid derivative, **3m** was obtained in a moderate yield of 55%. Biotin gave compound **3n** in 40% yield, as an equimolar mixture of diastereomers. Acetyl salicylic acid **3o** and ibuprofen **3p** yielded the corresponding α-carboxylate carbonyl compound quantitatively, 98% and 89%, respectively. When using oleic acid (**3q**), the corresponding product was obtained in very good yields 70%.
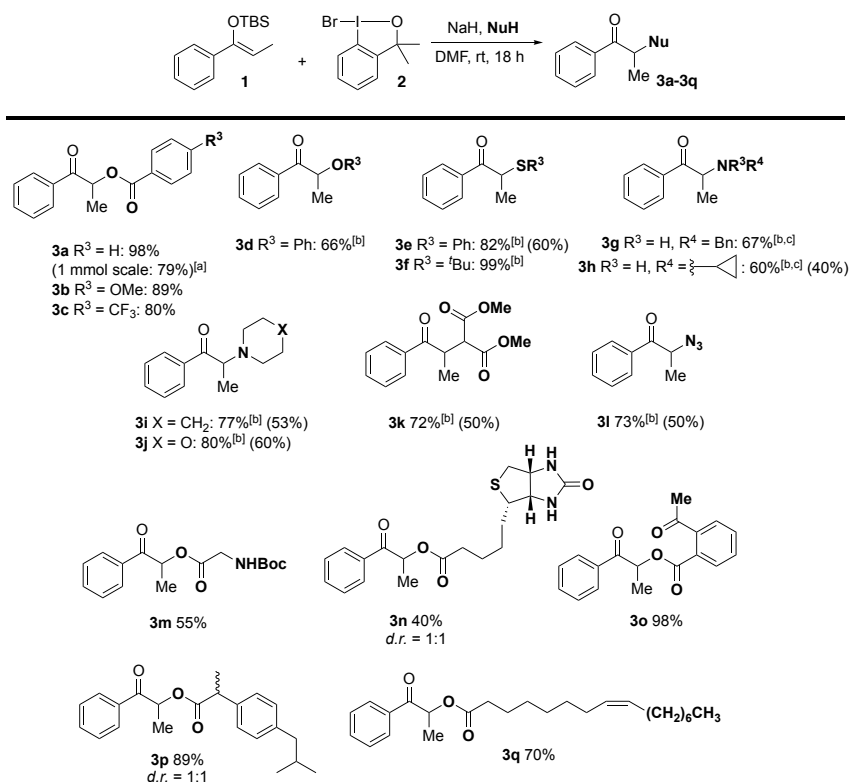
Scheme 2.4. Scope of the umpolung strategy for the cross-nucleo-phile coupling of heteronucleophiles with enol derivatives. Method A: **1** (0.1 mmol, 1 equiv.), **2** (0.15 mmol, 1.5 equiv.), NaH (0.15 mmol, 1.5 equiv.), nucleophile (NuH, 0.2 mmol, 2 equiv.), DMF (0.1 M), rt, 18 h. Method B: **1** (0.1 mmol, 1 equiv.), **2** (0.15 mmol, 1.5 equiv.), DMF (0.1 M), rt, 18 h. After completion, NaH (0.15 mmol, 1.5 equiv.) and nucle-ophile (NuH, 0.2 mmol, 2 equiv.) were added. [a]: Reaction was run on 1 mmol scale. [b]: The reactions were carried out following Method B. c: The reactions were run without NaH. Isolated yields.

2.3 Mechanistic investigations

To gain some insights into the mechanism of the transformation, the reaction was monitored by ^{1}H NMR spectroscopy (**Figure 2.2**).[1] The

---

[1] Kinetic study performed by Víctor García Vázquez.

reaction profile showed that after 10 min, the mixture contained unreacted silyl enol ether **1** in 47% yield, together with α-carbamoyl product **5** in 10% yield and α-bromoketone **4** in 43% yield. The reaction progressed with increasing concentrations of **5**, until a maximum of 68% after 180 min. It can be concluded that the reaction proceeds through formation of a key brominated intermediate **4**, which is consumed via S_N2 of the bromide atom by the heteronucleophile, affording the α-functionalized ketone.
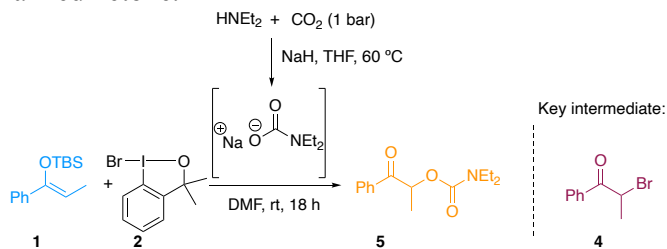
Kinetic studies
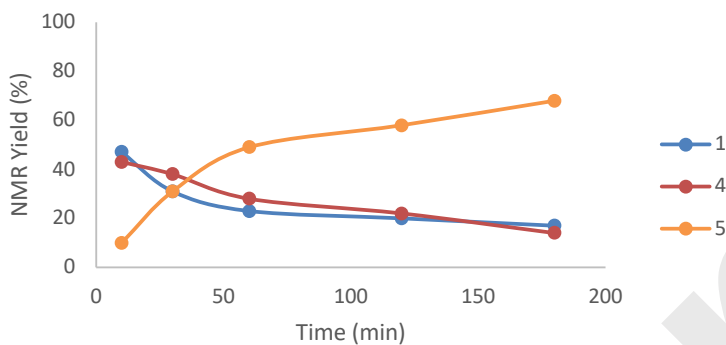
Figure 2.2. NMR profiling of the α-functionalization of silyl enol ether **1** upon reaction with diethylcarbamate in the presence of **2**.

We then performed a number of control experiments to gain more insights into the reaction mechanism. First, when silyl enol ether **1** and the benzoiodoxole **2** reacted in DMF in the absence of the second nucleophile, α-bromoketone **4** was obtained in quantitative yields (**Scheme 2.5a**). Then, the anionic carbamate generated *in-situ* was reacted with **4**, giving the α-carbamoyl carbonyl compound **5** in high yields (**Scheme 2.5b**). This type of transformation has been previously

studied by other groups as a way to avoid using strong electrophilic reactants in the context of poor functional group tolerance.[174-176] We then tested other brominating reagents, replacing **2** by NBS and Br_2 under the optimized reaction conditions (Method A). However, they both led to the formation of overbrominated and unknown by-products, whereas the desired α-carbamoyl carbonyl **5** compound could not be observed in significant yields (**Scheme 2.5c**). In an attempt to understand the selectivity of the reaction, we then tested the effect of excess of sodium hydroxide. Water has been reported to be a good nucleophile for the displacement of I(III) in the enolonium intermediates to give α-hydroxyketone **6**. However, in our case the formation of α-bromoketone **4** in quantitative yields was observed (**Scheme 2.5d**). These control experiments suggest that the mechanism proceeds with an electrophilic bromination of the enolonium intermediates followed by a nucleophilic substitution reaction, giving the desired α-functionalized ketones.
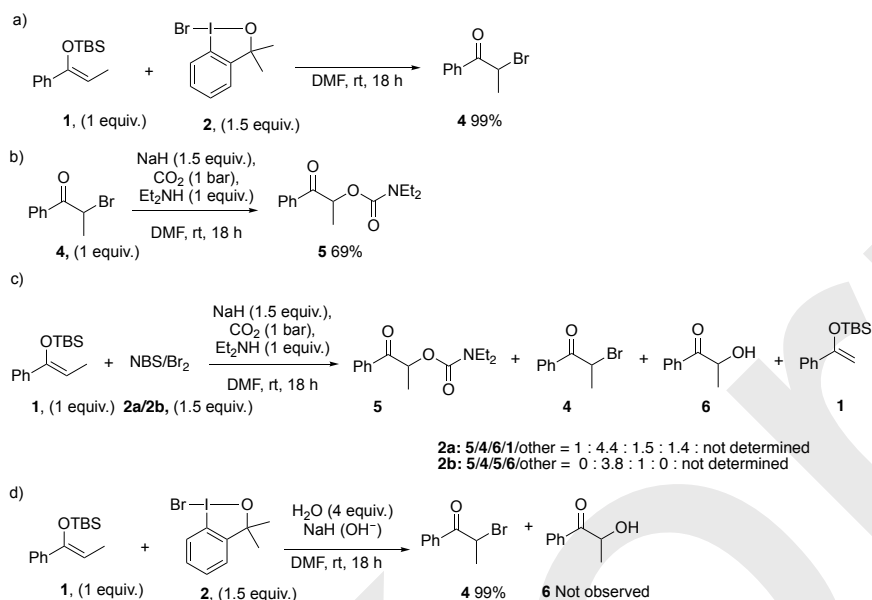
Scheme 2.5. Control experiments.

With all the experimental results on hand, we then set out to calculate the mechanism operating in this transformation. The structure of the silyl enol ether has been reduced to the enolate motif **1a**, as it is likely to be formed under basic conditions in DMF.[177-179] Furthermore, it is

plausible to suggest that an intramolecular silyl transfer[180-183] could occur between the oxygen of **1a** and that of **2**. The starting point of this calculations is the sum of the energies of enolate **1a** and the benzoiodoxole **2**.

There are three pathways (A, B and C) that might be operating in this transformation. In Pathway A (**Figure 2.3**), the reaction starts with the attack of enolate **1a** to the iodine (III) center, forming the **O-enolonium intermediate-1a** (−2.0 kcal/mol). Formation of the enolate-iodane bond takes place in the *trans* position to the Ar–I substituent leading to a lengthening of the I–Br bond (from 2.90 to 3.17 Å). It has been reported that structures with I and Br atoms can present halogen bond distances up to 4 Å.[184, 185] After the formation of the intermediate, the reductive coupling between the enolate and the Br occurs via **TS$_{1ao-4}$** with an activation energy of 20.5 kcal/mol.
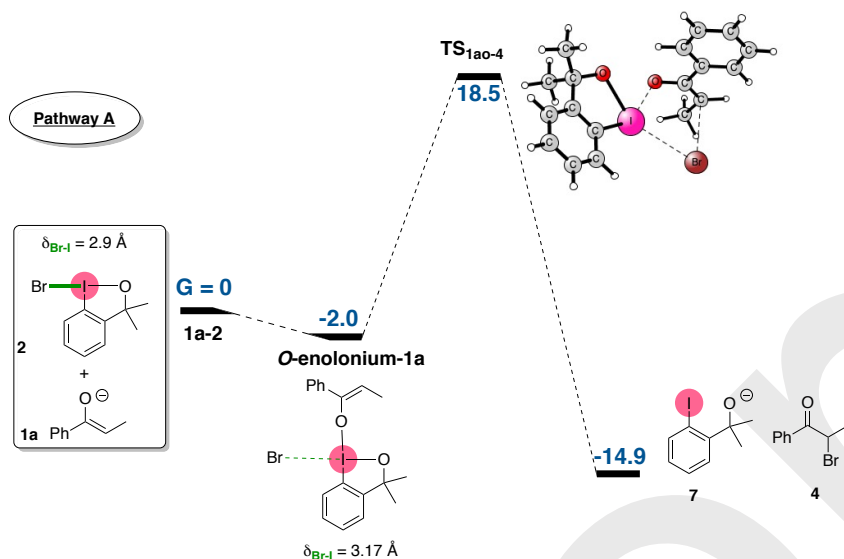
Figure 2.3. Energy profile for Pathway A.

In Pathways B and C (**Figure 2.4**), the enolate attacks the iodine atom through the carbon of the enolate leading to **C-enolonium-1a** (0.2 kcal/mol) and **C-enolonium-1a'** (-3.0 kcal/mol). After the attack, the I–Br halogen bond is elongated to 3.20 Å in the case of pathway B, and even more for pathway C, where it reaches 3.29 Å. Pathway B follows with a reductive elimination giving the key intermediate **4** *via* **TS$_{1a-4}$**

25

with an energy of 18.5 kcal/mol. Intringuingly, for **C-enolonium-1a'** the rotation of the enolate substituent takes places through a low energy transition state, **TS$_{1a'-1a''}$** of 16.2 kcal/mol. The enolate moves from the *trans* to the *cis* position in relation to the Ar–I bond, giving **C-enolonium-1a''** intermediate. As a consequence of the rotation, the Br atom goes out from the coordination sphere of the iodine atom and there is no halogen bond in this case, as the I–Br distance is long, of 5.16 Å. From here, two transitions states have been found. On the one hand, the backside attack of the bromide on the α-carbon of the enolate, that results in the lowest activation energy values (**TS$_{1a''-4}$**, 15.8 kcal/mol). On the other hand, the bromide could perform a *syn* attack to the α-carbon. However, this option seems to be unfeasible under the reaction conditions (**TS'$_{1a''-4}$**, 35.7 kcal/mol).
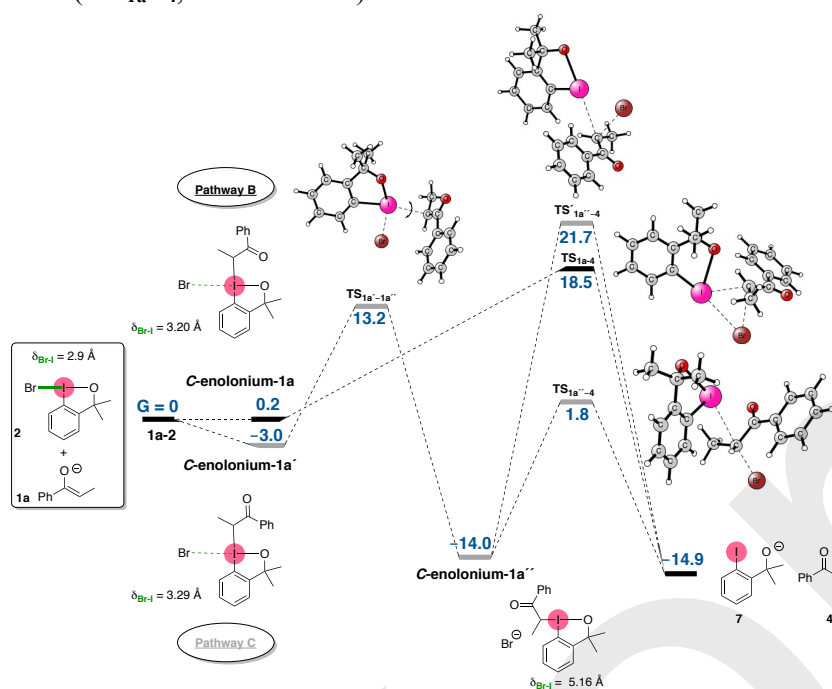
Figure 2.4. Energy profile for Pathways B (black lines) and C (gray lines).

According to the experimental results and the calculations, the I–Br halogen bond seems to be the reason for the absence of by-products in the reaction mixture. This will be the case for the pathways A and B that after formation of the enolonium species, they will follow a ligand

coupling step to provide α-bromoketone **4** in an intramolecular manner. This high selectivity towards **4** under mild conditions is not reported in the literature for the studies of cross-nucleophile coupling mediated by I(III) reagents, since dimerization of the enolate and the attack of other nucleophiles, such as water, are observed.[129] On the contrary, Pathway C undergoes a rearrangement of the ligands bonded to the I(III) center of ***C*-enolonium-1a''**. Therefore, the halogen bond interaction does not happen in this case and the bromide attacks at the very electrophilic carbon of the enolonium intermediate *via* intermolecularly leading to **4** as well. However, by-products will be observed if this would be the case. We would expec ***C*-enolonium-1a''** to react with other nucleophiles present in the reaction mixture, such as enolate **1a** or hydroxyl anions (⁻OH). Therefore, DFT calculations suggest that just pathways A and B are feasible.

2.4 Conclusions

A general umpolung protocol mediated by I(III) reagent **2** for the cross-nucleophile coupling has been described in this chapter, affording α-functionalized carbonyl compounds.

The results obtained for the formation of α-carbamoyl carbonyl compounds encouraged us to develop an umpolung bromination/nucleophilic substitution for the coupling of silyl enol ethers with a broad variety of nucleophiles. The scope with other nucleophiles has been evaluated showing the generality of the protocol. Alcohols, thiols, azide, 1,3-dicarbonyl compounds and primary and secondary amines has reacted. A large number of carboxylic acids can be used under our reaction conditions. This methodology could be applied to natural products and pharmaceuticals as nucleophiles.

Finally, the mechanism of the reaction has been studied experimentally and computationally in this thesis. The experimental investigations and the DFT calculations performed indicates that the high selectivity of this method is due to the formation of a key intermediate (**4**). According to the calculations, pathway A and B are similar involving the ***O*-enolonium-1a** and ***C*-enolonium-1a**, respectively, with a halogen interaction between the bromide and the I(III) center. Both of these pathways can be operating. An alternative pathway C, which involves the formation of ***C*-enolonium-1a''** can be ruled out. Therefore, the plausible pathways involve first the formation of *O*- or *C*-enolonium

intermediates, followed by a nucleophilic substitution affording the desired α-functionalized carbonyl compounds.

3 Base-catalyzed [1,*n*]-proton shift in conjugated polyenyl alcohols and ethers. Paper II.

3.1 Background of the project

Polyenyl alcohols and ethers are prevalent moieties in natural products, as well as important motifs in organic chemistry.[186-189] Conjugated trienes are important examples of compounds containing polyenyl alcohols and ethers that presents biological activity, such as in the antibacterial and immunosuppressive agent Rapamycin[190] or in the antitumoral agent Leukotriene B_4[191](**Figure 3.1**).
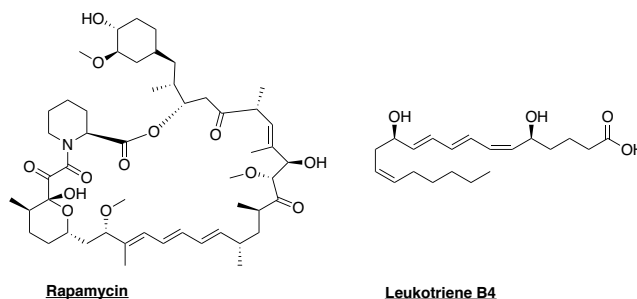
Figure 3.1. Examples natural products containing conjugated polyenol moieties.

The transformation of polyenyl alcohols and ethers into the corresponding carbonyl compounds or into conjugated vinyl ethers has not been extensively explored in the literature. Indeed, the metal-catalyzed isomerization of conjugated systems is very challenging, since formation of very stable metal-diene intermediates takes place.[192] Formation of these η^4-complex restrains the hydride shift, and poisons the catalytic system.[192] This issue can be solved by applying metal-free protocols.[110, 112, 193] As mentioned in Chapter 1, the Martín-Matute group reported the first stereospecific [1,3]-proton shift isomerization of electron deficient allylic alcohols and ethers using TBD[113] Although unexplored, we set out to investigate the feasibility of this methodology on polyenyl systems (**Scheme 3.1**).
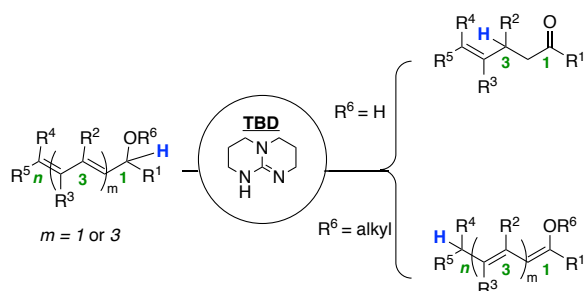
Scheme 3.1. Isomerization of polyenyl alcohols and ethers using TBD as a catalyst.

Due to the fact that the reaction can proceed *via* different [1,*n*]-proton shifts, different isomeric products could be formed. Thus, in this chapter, the mechanistic investigation of the migration of the proton shift in the isomerization of conjugated polyenyl alcohols and ethers is presented. This proton shift migration follows a "chain walking" process. Experimental mechanistic studies[2] and computational are discussed.

3.2 Overview of the reaction conditions

In order to test the protocol on polyconjugated systems, the Martín-Matute group started the investigation with dienyl alcohols. For these cases, the corresponding carbonyl compound was formed in moderate to high yields, but without formation of side-products (**Scheme 3.2a**). The [1,3]-proton shift product was obtained exclusively when a dienyl alcohol was used as a substrate. On the other hand, dienyl ethers could be isomerized under milder conditions, yielding a mixture of [1,5]-proton shift products (**Scheme 3.2b**). The catalyst loading and the temperature could be decreased to 10 mol% and 85 °C, respectively. The major isomeric product is (1*Z*, 3*E*), for all the cases studied in the reaction scope. Finally, the protocol was studied in a more extended conjugated polyenyl ethers yielding the products *via* [1,9]-proton shift, using a slightly higher base loading (**Scheme 3.2c**).

---

[2] The experimental part presented in this chapter has been performed by Dr. Nagaraju Molleti, Dr. Samuel Martinez-Erro and Dr. Amparo Sanz-Marco. I have participated in the discussion regarding the mechanism of the reactions.

a) Isomerization of conjugated dienyl alcohols

b) Isomerization of conjugated dienyl ethers

c) Isomerization of conjugated polyenyl ethers
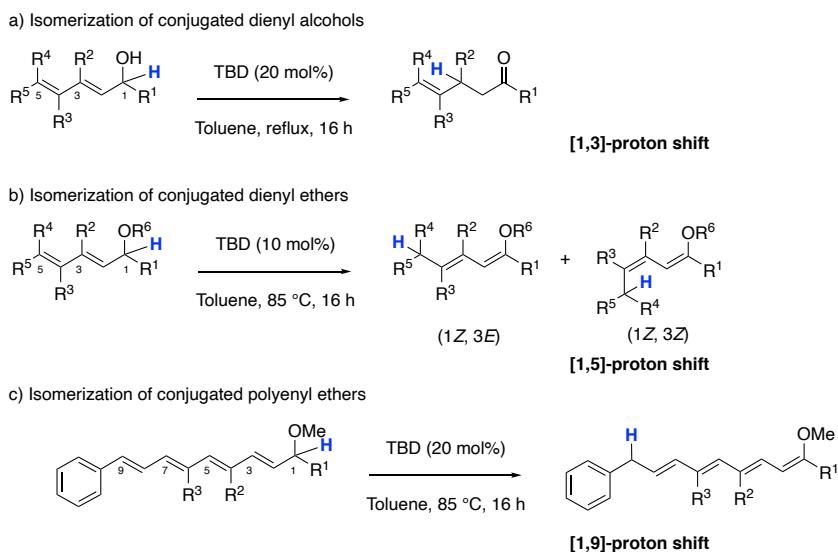
Scheme 3.2. An overview of the TBD-catalyzed isomerization of conjugated dienyl alcohols, dienyl ethers and polyenyl ethers.

3.3 Experimental mechanistic investigations

Experimental mechanistic studies were performed in order to understand the transformation. Kinetic isotope effect studies were carried out for both dienyl alcohols and ethers (**Figure 3.2**), obtaining KIE values of 2.4 ± 0.5 and 3.8 ± 0.5, respectively. Following the reported mechanism for the isomerization of allylic alcohols,[113] these KIE values suggest that the rate-determining step involves breaking of the C–H bond.
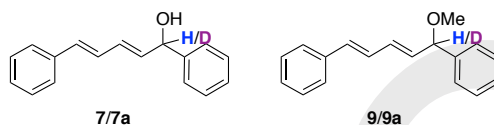
Figure 3.2. Kinetic isotope effect studied with compounds **7**, **7a**, **9** and **9a**.

Deuterium labelling studies were performed in the study of both conjugated systems. Deuterated **7a-d^1** (89% D) afforded the corresponding unsaturated ketone with 24% of D at C^3. No deuterium was found at C^5 indicating that this transformation occurs through a [1,3]-proton shift

31

mechanism (**Scheme 3.3a**). In contrast, in the case of dienyl ethers different positions of the system were deuterated (C^1, C^3 and C^5). Deuterated **9a-d^1** (92% D) transferred the deuterium to both C^3 and C^5 (**Scheme 3.3b**), with 20% and 28% deuterium content, respectively. Thus, the deuterium labelling suggest that the mechanism involves two consecutives [1,3]-proton shift. Then, in order to justify our hypothesis deuterated compound **9a-d^3** (98% D) was subjected to isomerization reaction conditions (**Scheme 3.3c**). A 20% deuterium content was transferred to C^5 which confirms a proton transfer from C^3 to C^5. Finally, starting from a deuterated compound at C^5, namely **9a-d^5** (92% D), a 45% of the deuterium content ends up in that position (**Scheme 3.3d**). This result suggests that the final deuteration at C^5 is irreversible.
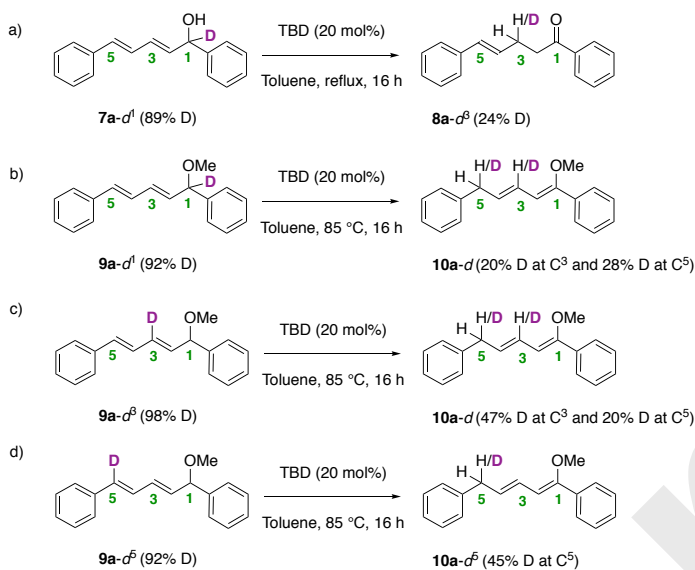
Scheme 3.3. Isomerization of deuterated dienyl alcohols and ethers: a) 7a-d^1, b) 9a-d^1, c) 9a-d^3 and d) 9a-d^5.

3.4 Computational mechanistic investigations

To gain a comprehensive understanding of the reaction mechanism operating in this transformation, DFT calculations were carried out. The study was performed using dienyl ether **I** as a model substrate (**Figure 3.3**). This substrate can interconvert easily to conformer **I´** by rotation of a σ−bond, with an energy barrier calculated to be 6.4 kcal/mol. The

reaction starts with the deprotonation of both conformers **I/I´** by TBD with relative activation free energy barrier of 22.2 (**TS$_{I-II}$**) and 22.5 (**TS$_{I´-II´}$**) kcal/mol, respectively. This is the relative energy for the conformations favored by a hydrogen bond between the oxygen of the dienyl ether and the hydrogen of the base.
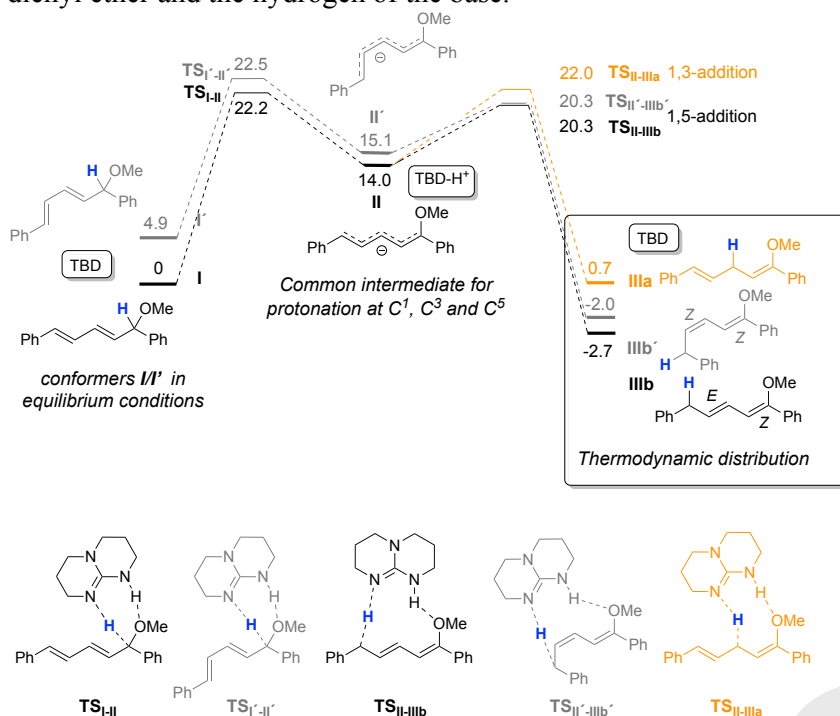
Figure 3.3. Energy profile of the isomerization of dienyl ethers. The Gibbs free energy values are given in kcal/mol.[114]

After the deprotonation step, an ion pair is formed between the dienyl anion and the conjugated acid of the base (**II** and **II´**). These two intermediates cannot be interconverted easily due to calculated energy barrier of +16.9 kcal/mol. Each of these dienyl anion can be protonated in a reversible manner at C^1 (**TS$_{II-I}$**), at C^3 (**TS$_{II-IIIa}$**) or at C^5 (**TS$_{II-IIIb}$** and **TS$_{II´-IIIb´}$**). The protonation energy barriers for this transformation have quite similar relative activation energies: +22.2 for **TS$_{II-I}$** , +22.5 for **TS$_{II´-I´}$**, +22.0 for **TS$_{II-IIIa}$**, +20.3 for both **TS$_{II-IIIb}$** and **TS$_{II´-IIIb´}$**, kcal/mol. These suggest that all the pathways are reversible. Therefore, all possible products formed in the reaction are under thermodynamic equilibrium. Thus, the more stable product will be the major product of

the reaction: **I**, **I′**, **IIIa**, **IIIb** and **IIIb′**. The isomeric product **IIIb** and **IIIb′** are the most stable species of this transformation with calculated energy values of −2.7 and −2.0 kcal/mol respectively. Therefore, the stereoisomeric ratio depends on the relative energy difference between the products. The (1*Z*, 3*E*) stereoisomer **IIIb** is 0.7 kcal more stable than the (1*Z*, 3*Z*) stereoisomer **IIIb′**. Importantly, these results are in agreement with the results found experimentally where the major product observed in the reaction is a mixture of **IIIb**/**IIIb′** with a stereoisomeric ratio of [78:22].

The KIE has also been studied computationally, replacing a hydrogen by deuterium in the reaction profile. An increase in the activation energy barrier for the deprotonation step (**TS$_{I-II}$** and **TS$_{I′-II′}$**) was calculated to be 0.6 and 1.2 kcal/mol, respectively. These results are in agreement with the KIE value obtained experimentally for the dienyl ether system, 3.8 ± 0.5, suggesting that the rate-determining step is the deprotonation at C^1 position.

DFT calculations suggest that the reaction proceeds *via* [1,*n*]-proton shift until formation of the most thermodynamically stable product. This agrees well with the experimental deuterium labelling studies that showed the irreversibility of the formal [1,5]-proton shift (*vide supra*, **Scheme 3.3d**).

Additionally, the reaction kinetics were simulated in order to understand the ratio of the stereoisomers **IIIb**:**IIIb′** = 78:22 using COPASI (Complex Pathway Simulator 4.24). The rate constant (*k*) of the reaction, either forward (k_f) or backward (k_r), is calculated from the Gibbs free energy obtained by the DFT calculations using the Eyring equation (**Equation 2**).

$$k = \frac{k_B T}{h} e^{\frac{-\Delta G^\ddagger}{RT}}$$

Equation 2. The Eyring equation. T = temperature (358 K); k_B = Boltzmann constant ($1.3806e^{-23}$ J/K); h = Planck′s constant ($6.6261e^{-34}$ J·s); $\Delta G^\ddagger$ = Gibbs free energy difference between the intermediates involved (J/mol); R = ideal gas constant (8.3414 J/K·s).

For the simulation, all the steps were considered reversible. The plotted simulations were obtained performing a Time Course calculation (**Figure 3.4**). The reaction proceeds quickly at the very beginning of the

34

plot to the formation of the most thermodynamically stable product **IIIb**. However, since the starting material **I** could interconvert easily to provide conformer **I'** the reaction also forms the corresponding **IIIb′**, slightly less stable than **IIIb**. A simulated stereoisomeric ratio between **IIIb**:**IIIb′** = 71:29 can be calculated from this data, in strong agreement to the one experimentally observed (**IIIb**:**IIIb′** = 78:22).
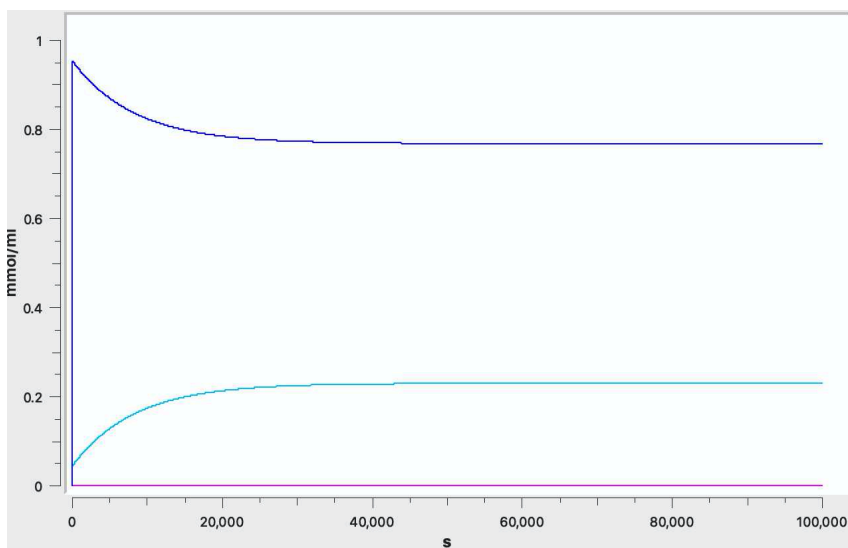
Figure 3.4. Plot of the simulated concentration of **IIIb** (dark blue) **IIIb′** (light blue) stereoisomers and **IIIa** (pink) *versus* time.

3.5 Conclusions

In this chapter, the mechanism of the metal-free protocol for the isomerization of polyenyl ethers into dienyl ethers has been studied by DFT calculations and kinetic simulations. These studies revealed that the reaction starts by a rate-determining deprotonation at the C^1. After that, an intimate ion pair is formed between the dienyl anion and the protonated TBD. Later, follows the protonation at C^1, C^3 or C^5 giving the corresponding products.

The replacement of hydrogen by deuterium in the reaction profile confirmed that the rate determining step of the reaction is the deprotonation at C^1 which is also in agreement with the experimental studies.

35

The computational results revealed that the reaction is under thermodynamic control. Thus, the ratio of the stereoisomers depends on the relative energy difference between them. A simulated kinetic profile was performed based on the $\Delta G^{\ddagger}$ values obtained in the theoretical calculations using the COPASI software. Indeed, the simulated ratio of the stereoisomers was found to be almost identical to the one obtained experimentally.

Experimental and computational studies suggested that the reaction proceeds *via* two consecutive proton shifts, a [1,3] followed by a [3,5], alongside the studied conjugated system or by a direct [1,5]-proton shift. In other words, the proton shift "chain walk" continues until the formation of the most thermodynamically stable product. Therefore, the proton shift walking will depend on how long the chain is.

4 A novel microwave-assisted synthesis of amino functionalized chromium (III) terephthalate MIL-101-NH₂. Paper III.

4.1 Background of the project

In 2005 the group of Feréy and co-workers developed the ideal combination of computer simulation and targeted chemistry to synthesize a new powdered solid, MIL-101 (MIL stands for Material of Institut Lavoisier; **Figure 4.1**).[194] The material was synthesized following a conventional hydrothermal method that consisted of the reaction of terephthalic acid (TA) with $Cr(NO_3)_3·9H_2O$, hydrofluorhydric acid and H_2O for 8 h at 220 °C in an autoclave. The result is a green powder with the molecular formula $[CrF(H_2O)_2O(TA)_3]·nH_2O$. The resulting zeotype architecture led to two large cages with internal diameters of 29 and 34 Å and a high surface area of 4100 m^2g^{-1} that makes it an excellent candidate for gas storage or drug delivery. It was Férey and co-workers who defined a general methodology for the assembly of the organic and inorganic units within the framework using the concept of secondary building blocks (SBU).[195-197] For example, MIL-101(Cr) and MIL-88B(Cr)[198] are polymorphic materials since they share the same formula but the combination of the SBU is different. Consequently, the diverse interconnection of the SBU results in two MOFs with different topologies and features.
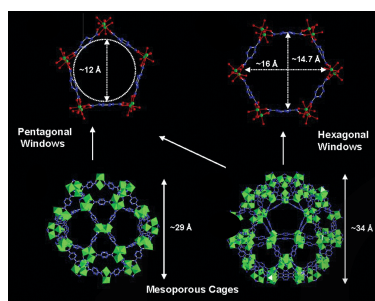

Figure 4.1. Computational simulation of the two cages of the MIL-101(Cr) MOF. Figure from Férey and co-workers, used with permission from Science AAAS.[194]

To this date, a number of groups have reported the synthesis of MIL-101(Cr) either by minor modifications of the traditional method or employing other methods such as microwave-assisted, sonochemical or mechanochemical.[199-202]

A post-synthetic modification of MIL-101(Cr) for the introduction of an amino group was described years later by the group of Stock leading to MIL-101(Cr)-NH$_2$.[203] This material has raised as a potential heterogeneous catalyst. The unusual large pore volume offers the possibility of immobilization of transition metal catalysts or organic species and makes it the perfect host for metal nanoparticles.[204, 205] The resulting MOF can be synthesized either *via* direct synthesis of the MIL-101(Cr)-NO$_2$ using 2-nitroterephthalic acid (2-NTA) and subsequent reduction by SnCl$_2$·2H$_2$O, or by the direct synthesis of plain MIL-101(Cr) followed by an electrophilic aromatic substitution (MIL-101(Cr)-NO$_2$) and subsequent reduction of the nitro to the amino group MIL-101(Cr)-NH$_2$. Unfortunately, the direct synthesis from 2-aminoterephthalic acid (2-ATA) leads to the decomposition of the material under hydrothermal methods. This is due to the high affinity of the amino groups to chromium, interfering with the 3D coordination of both the metal cluster and the organic linker to yield the desired MOF under the mentioned reaction conditions.[206] Nonetheless, the direct synthesis of the MIL-101(Cr)-NH$_2$ under hydrothermal conditions has been reported leading to a material with moderate crystallinity.[199] The yields are unfortunately not reported in this work. Furthermore, under solvothermal conditions the crystallinity improves but requires longer reaction times and non-environmentally friendly solvents (i.e. DMF).[207]

Microwave-assisted methods have gained interest in the recent years within the MOF community due to a number of advantages compared to the traditional methods, such as faster reaction rates, high yields and remarkable phase selectivity, size control from microcrystals to nanosized particles, and lower costs in terms of energy.[70, 71] In this chapter, we present a single step synthesis of chromium(III) terephthalate MIL-101(Cr) and amino-functionalized chromium(III) terephthalate MIL-101(Cr)-NH$_2$, directly from 2-ATA, using microwave-assisted method in water.

4.2 Optimization of the microwave-assisted protocol

We started our investigations by screening the effect of different reaction parameters, such as the effect of the modulator and its concentration, temperature, reaction time, nature of the chromium salt and the number of equivalents of all the species in the mixture. The reaction mixture contains a chromium(III) source, 2-ATA, the modulator and H_2O in a 20 mL microwave vial.

Modulators are used in MOF synthesis in order to control defects, crystallinity and to obtain bigger crystals.[208] The modulator is any species that could either deprotonate the organic linker or compete with it to form bonds with the metal cluster [*i.e.* hydrofluoric acid for the direct synthesis of MIL-101(Cr)].[209] Consequently, the rates for the nucleation and crystal growth processes decrease allowing for a better control over the size and morphology of the crystals.

We tested a series of acids and bases, TFA, HCl, DMF, NH4F, 4DMAP, NH4OH and NaOH. In all cases, characterization by PXRD showed that amorphous materials were obtained. Interestingly, when using salts such as LiF, NaF, KF and CsF crystalline materials were obtained (**Figure 4.2**). The PXRD patterns at larger 2Ɵ showed the peaks of the corresponding salts for the case of CsF and KF, together with other impurities. This could be a result of the retention of the cations within the framework due to a poor efficiency in the diffusion during the washing, as a consequence of the large size of the cations. Using NaF, a clearer PXRD pattern was observed when comparing to the theoretical diffraction pattern of the MIL-101(Cr) than the one obtained with LiF. Importantly, when running the reactions with the modulators following the hydrothermal method no crystalline material was obtained, unveiling the *in-situ* generation of hydrofluoric acid when applying microwave heating.
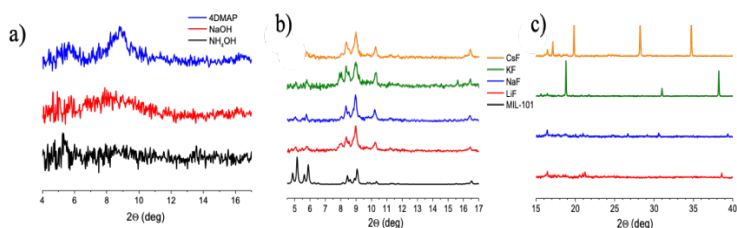
Figure 4.2. PXRD patterns (2θ = 4–17 deg) of Chromium(III)-2-ATA polymers; a) using NH₄OH, NaOH and 4DMAP as modulators. b) using LiF, NaF, KF and CsF as modulators and c) PXRD patterns (2θ = 15–40 deg).

The results obtained showed NaF as the best salt to promote the formation of the porous material. This is achieved by an optimal deprotonation of the benzoic acid linkers, producing fluoride and hydroxy anions that coordinate to the Cr metal, and by promoting a slow nucleation and crystal growth.

Then, we studied the effect of the temperature when using 1.35 mmol of Cr(III) chloride, 1.35 mmol of 2-ATA and 3.3 mmol of NaF in 10 mL of water for 1 h. When running the reaction at 160 °C for 1 h, an amorphous material was obtained, as shown by the broad diffraction signals in the PXRD pattern. When the temperature was increased to 175 °C, the reaction yielded a pure crystalline MIL-101(Cr)-NH₂, while at 190 °C the crystallinity was much lower (**Figure 4.3a**). The next parameter to be evaluated was reaction time. The reaction was studied employing the same quantities of the reactants for different reaction times: 30, 60, 120, 300 and 900 min. In all the cases, crystalline porous polymers were obtained (**Figure 4.3b**). At longer reaction times, the reaction conditions favor the formation of hydrofluoric acid. Consequently, other unknown species are obtained what turned out to give lower crystallinity of the material. Moreover, when running the reaction at shorter times (30 min), the crystals did not have considerable amount of time to grow. The optimized reaction time for high crystallinity was found to be 60 min.
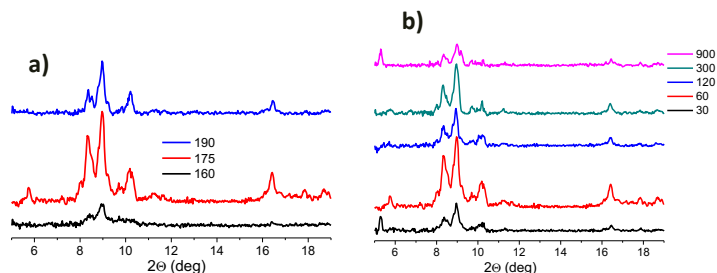
Figure 4.3. a) PXRD patterns (2Θ = 5-19 deg) of Cr(III)-2-ATA polymers obtained at different temperatures (160, 175 and 190 °C). b) PXRD patterns (2Θ = 5-19 deg) of Cr(III)-2-ATA polymers obtained at different reaction times (30, 60, 120, 300 and 900 min).

Later, we examined different amounts of NaF in the reaction mixture. The reactions were studied using 1 equiv. of $CrCl_3$, 1 equiv. of 2-ATA and NaF (0.0, 1.25, 2.50 and 5.00 equiv. compared to the amount of chromium(III)) in 10 mL of H_2O at 175 °C for 1 h. For this study, well-defined crystals were obtained only when using 2.5 equiv. (3.36 mmol) of NaF (**Figure 4.4a**). Different chromium sources (1 equiv., 1.35 mmol) were also investigated at 175 °C for 1 h in 10 mL with 1 equiv. of 2-ATA and 2.5 equiv. of NaF. Only when using chromium(III) chloride, nitrate and sulfate the desired MIL-101(Cr)-NH_2 was formed (**Figure 4.4b**). However, the optimal crystallinity was obtained with chromium(III) chloride hexahydrate.
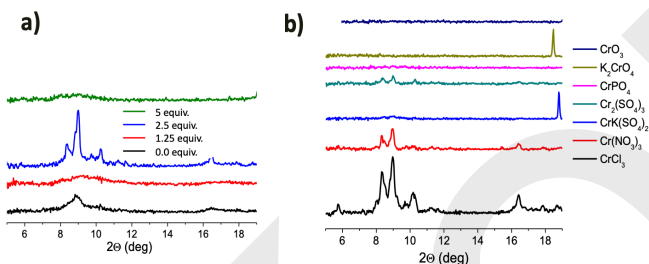
Figure 4.4. a) PXRD patterns (2Θ = 5-19 deg) of Cr(III)-2-ATA polymers when using different amounts of NaF (0.0, 1.25, 2.50 and 5.00 equiv.). b) PXRD patterns (2Θ = 5-19 deg) of Cr(III)-2-ATA polymers obtained using different Cr sources ($CrCl_3$, $Cr(NO_3)_3$, $CrK(SO_4)_2$, $Cr_2(SO_4)_3$, $CrPO_4$, K_2CrO_4 and CrO_3).

41

Lastly, the concentration of all the species was analyzed in order to study the scale up of the method using microwave heating. Different dilutions of Cr(III)/2-ATA/NaF were studied in the reaction (0.2, 0.3, 0.6, 1.2 and 2.4 M, **Figure 4.5a**). The initial molar ratio of the substrates was kept (1.35 mmol of chromium(III) chloride, 1.35 mmol of 2-ATA and 3.36 mmol of NaF at 175 °C for 1 h). Decreasing the total concentration to 0.2 M resulted in the obtention of poor crystallinity of MIL-101(Cr)-NH$_2$. However, when increasing the concentration to 0.3 M the mass of the material obtained was decreased when compared to the amount obtained with 0.6 M. Interestingly, 1.2 M gave better defined crystallinity and the amount of MOF obtained was higher than the one obtained when using 0.6 M (**Figure 4.5b**). A four-fold increase of the total concentration led to both polymorphs, MIL-101(Cr)-NH$_2$ and MIL-88B(Cr)-NH$_2$, revealing that increasing the concentration of the system favors the interconnection of the SBU for the design of the other polymorph which is thermodynamically more stable than MIL-101(Cr)-NH$_2$.
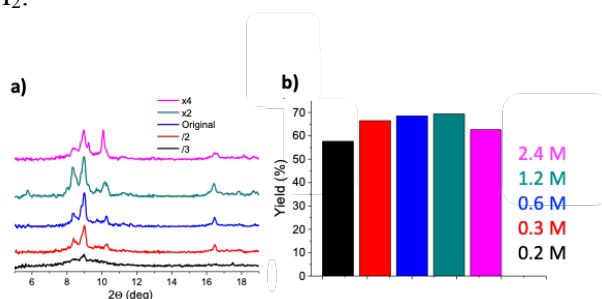
Figure 4.5. PXRD patterns (2Θ = 5-19 deg) of Cr(III)-2-ATA polymers obtained using NaF at different total concentration of reagents (0.2, 0.3, 0.6, 1.2 and 2.4 M). b) Yield of the obtained polymers at different concentrations.

After the evaluation of the effect of all the parameters the final chosen conditions for the synthesis of MIL-101(Cr)-NH$_2$ were: 1.35 mmol of chromium(III) chloride, 1.35 mmol of 2-ATA, 3.36 mmol of NaF in 10 mL of water at 175 °C for 1 h (**Scheme 4.1**), resulting in a yield of 73%.
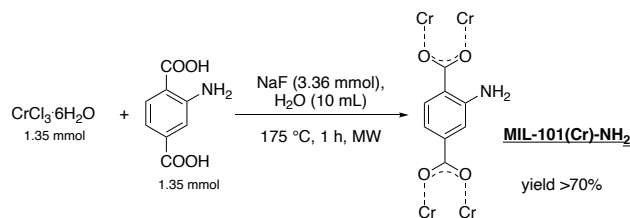
Scheme 4.1. Optimal reaction conditions for the synthesis of MIL-101(Cr) and MIL-101(Cr)-NH$_2$ by microwave heating.

4.3 Characterization of MIL-101(Cr) and MIL-101(Cr)-NH$_2$

PXRD was applied as the main tool for the characterization of the material during the optimization of the reaction conditions, since it was used to determine the crystallinity of the MOF and the presence of the desired polymorph.

Importantly, there are a number of characterization techniques that have been employed for the full characterization of the material such as nitrogen adsorption, TGA, SEM, ICP and FTIR.[3] The PXRD patterns of the MOFs obtained using solvothermal and microwave-assisted method were compared to the simulated pattern of the MIL-101(Cr) in order to verify the morphology of the polymer (**Figure 4.6**).
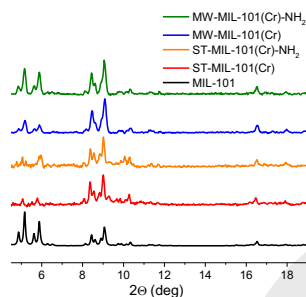
Figure 4.6. PXRD patterns (2Θ = 5-19 deg) of solvothermal (ST) and microwave-assisted (MW) methods compared to the simulated MIL-101(Cr) pattern.

---

[3] Characterizations were performed by Dr. Sergio Carrasco except for PXRD.

Scanning electron microscopy (SEM) images revealed that the MW-MOF protocol produces MIL-101(Cr) and MIL-101(Cr)-NH_2 in the nanometric scale with a smaller particle size compared to the traditional methods, (**Figure 4.7**). Microwave heating favors the process of nucleation, providing almost twice as much yield for MIL-101(Cr)-NH_2 compared to the traditional solvothermal method. However, a much smaller crystal size was observed when employing microwave conditions.
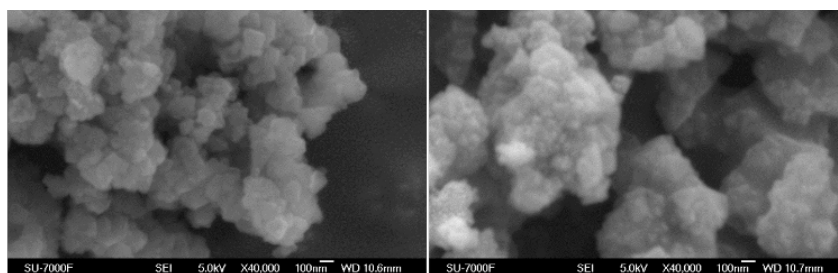
Figure 4.7. SEM images for MIL-101(Cr) (left) and MIL-101(Cr)-NH_2 (right) by microwave-synthesis.

Elemental analysis by ICP-OES was performed in order to calculate the molecular formula per unit cell of the obtained MOFs using the MW protocol. The formulae for MIL-101(Cr) and for MIL-101(Cr)-NH_2 were derived to be $Cr_3F(H_2O)_2O[(O_2C)-C_6H_4-(CO_2)]_3(CH_3CH_2OH)_4(HF)_3$ and $Cr_3F(H_2O)_2O[(O_2C)-C_6H_3NH_3^+F^--(CO_2)]_3(CH_3CH_2OH)_4(HF)_3$, respectively. This was confirmed by TGA analysis, which showed three weight losses (**Figure 4.8**). For temperatures between 50 °C to 200 °C, the guest molecules within the pores are removed. Afterwards, in the range of 200-350 °C the water molecules coordinated to the clusters are detached. Finally, the linker starts to decompose at 350 °C until around 600 °C. This means that following the MW protocol the MOF is stable until 350 °C.
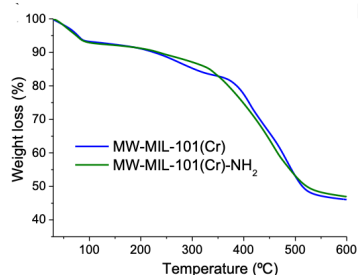
Figure 4.8. Thermogravimetric (TGA) curves of MW-MIL-101(Cr) (blue) and MW-MIL-101(Cr)-NH2 (green).

Finally, the surface area of the MW-MIL-101(Cr) and MW-MIL-101(Cr)-NH$_2$ were studied by nitrogen adsorption isotherm at 77 K, which resulted in 2651 and 2014 m^{2}g^{-1}(**Figure 4.9**), respectively. These values matched with those found in the literature.[194] A significant decrease on the surface area value for the MW-MIL-101(Cr)-NH$_2$ compare to MW-MIL-101(Cr) confirms the occupancy of the framework voids by the amino moieties.

The surface area values when employing the conventional solvothermal method are lower compared to the ones obtained in this project. Therefore, it can be concluded that the smaller crystal size favors the diffusion of other species through the cavities of the material resulting in larger BET surface area values.
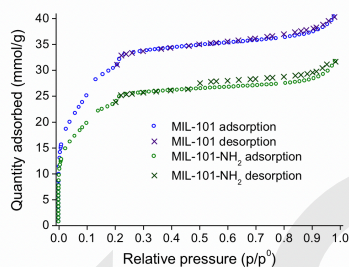
Figure 4.9. Nitrogen adsorption isotherms at 77 K of MW-MIL-101(Cr) in blue and MW-MIL-101(Cr)-NH$_2$ in green. Circles indicates adsorption and crosses indicate desorption.

45

4.4 Conclusions

The syntheses of the MIL-101(Cr) and MIL-101(Cr)-NH$_2$ have been described in this chapter using microwave-assisted heating and avoiding the direct handling of hazardous reagents as hydrofluoric acid.

The full optimization of the protocol has been described and analyzed focusing on the PXRD patterns. Other characterization techniques have been used to compare the characteristics of the MW-materials with those synthesized using conventional methods. The presented MW methodology has been shown to give higher yields in less reaction time, better phase-selectivity and use of more environmentally friendly solvents when compared to ST methods.

5 Enhancing the chirality transfer in the isomerization of electron-deficient allylic alcohols. Paper IV.

5.1 Background of the project

Ruthenium-, iridium- and rhodium-based transition metal catalysts have been demonstrated to be efficient catalysts for the redox neutral isomerization of allylic alcohols into saturated carbonyl compounds. When it comes to accessing chiral ketones from allylic alcohols, the most common approach is to use a chiral transition metal complex. An alternative to this was presented in 2012, when the group of Cahard presented a new approach to synthesize enantioenriched (98% *ee*) trifluoromethylated carbonyl compounds, by subjecting a chiral enantiopure allylic alcohol to a stereospecific isomerization mediated by a non-chiral ruthenium catalyst (**Scheme 5.1a**).[101, 105]

In this regard, the Martín-Matute group contributed to this area of research with a stereospecific isomerization of electron-deficient allylic alcohols and ethers using a metal-free catalyst, namely the base TBD (**Scheme 5.1b**). Other guanidine type bases were studied under the optimized reaction conditions, but none of them gave the desired product when the based was used in catalytic amounts. Another important feature found in this study was that the presence of an N–H bond was crucial for the reaction to occur, since the yield obtained using MTBD (7-methyl-1,5,7-triazabicyclo(4.4.0)dec-5-ene) was negligible (less than 5% yield). During the years, the Martín-Matute group expanded the scope of the reaction to other allylic systems such as allylic halides (**Scheme 5.1c**) and allylic amines (**Scheme 5.1d**).[115, 116]
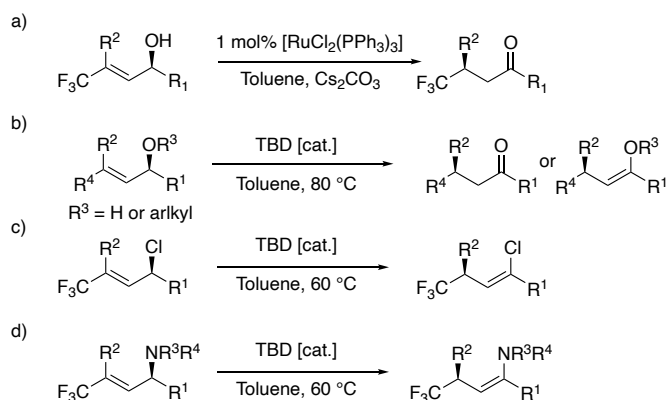
Scheme 5.1. Stereospecific isomerization of γ-trifluoromethylated allylic systems: a) alcohols[105] b) alcohols and ethers[115] c) halides[115] and d) aliphatic amines.[116]

The group also studied the mechanism operating in this type of transformation for the first transition metal-free, base-catalyzed stereospecific isomerization of electron-deficient allylic alcohols (**Scheme 5.2**). The calculations showed that the mechanism starts with the deprotonation of the C^1 leading to the formation of a tight ion pair between the allylic anion and the protonated base. This step has been calculated to have an activation energy barrier of 19.6 kcal/mol. The combination of both experimental and computational results suggested that the deprotonation is the rate determining step. After formation of the tight ion pair, the protonation at C^3 takes place, and for this to happen, the calculations showed that it could occur either in an intermolecular or intramolecular manner, with activation energy barriers of 17.1 and 16.9 kcal/mol, respectively.
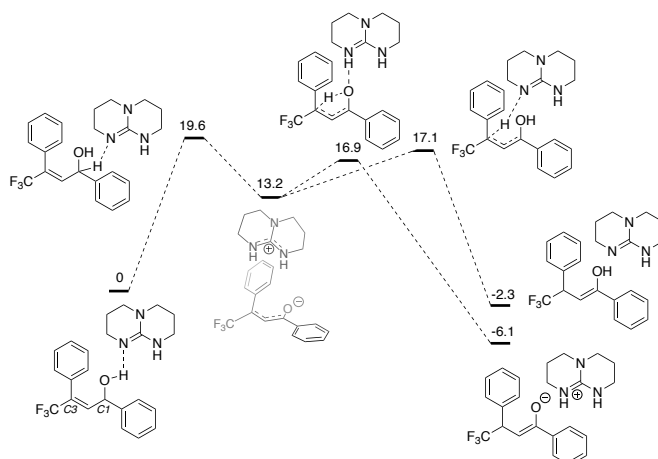
Scheme 5.2. Reaction profile for the base-catalyzed isomerization of electron-deficient allylic alcohols. The energies are given in kcal/mol. (Calculations performed by Mårten S. G. Ahlquist).

The loss of chirality transfer could happen for two reasons. First, the polarity of the solvent used in the reaction plays a role on keeping tight the ion pair. Indeed, excellent levels of chirality transfer may be obtained in apolar solvents such as toluene, whilst using more polar solvents (e.g. THF) results in lower levels of chirality transfer. Secondly, experimental studies revealed that the presence of an electron-withdrawing group on the phenyl ring at C^3 resulted in lower levels of chirality transfer (**Scheme 5.3**). The reason for this could also be related to an lower stability of the ion pairing of the allylic anion and the cationic conjugated acid of TBD (TBD-H$^+$)

11a, X = H (99% *ee*) **12a**, X = H (95% *c.t.*)
11b, X = CF$_3$ (97% *ee*) **12b**, X = CF$_3$ (61% *c.t.*)
11c, X = Cl (97% *ee*) **12c**, X = Cl (89% *c.t.*)
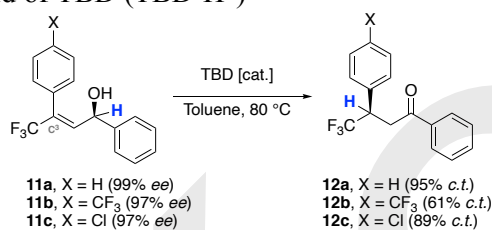
Scheme 5.3. Stereospecific isomerizations with lower chirality transfer.

It was hypothesized that to increase the levels of chirality transfer it was required to maintain the ion pair as tight as possible in order to

49

prevent the racemization of intermediates. To do so, we proposed the synthesis of a porous material where the cavities could limit the dissociation of the ion pair and, as a consequence, the transfer the chirality would take place in a highly efficient manner. As porous materials, we aimed to investigate polymeric materials and MOFs bearing superbases on their structures.

In this chapter, we explore the synthesis of a new heterogeneous material containing a base capable of performing the isomerization of electron-deficient allylic alcohols. Importantly, DFT calculations have been carried out in order to correlate the stability of the ion-pairs with the experimental levels of chiral transfer upon reaction with TBD.

5.2 Ion pair stability

A number of allylic alcohols bearing an electron-donating and electron-withdrawing group at the para position of the aryl group at C^3 were chosen to study the ion pair energy dissociation by DFT (**Figure 5.1**).
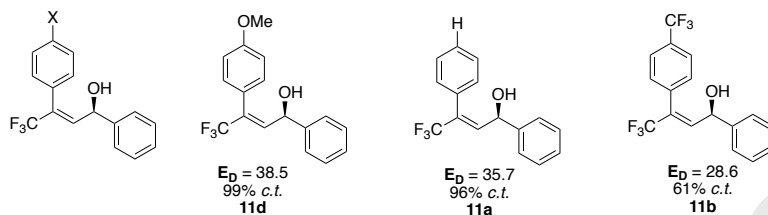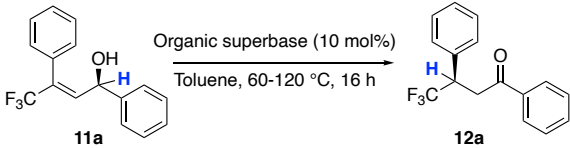
Figure 5.1. Dissociation energies (E_D) of the ion pair and experimental chirality transfer values.[113] E_D values given in kcal/mol (Calculations performed by Dr. Li Man).

From these results, it can be concluded that when placing an electron-withdrawing group in that particular position of the allylic system (C^3), the stability of the ion pair is significantly affected. Therefore, the more EWG X is, the less tight the ion pair is, and the lower the levels of chirality transfer are.

5.3 Heterogenization study

Before moving onto the heterogenization of the homogeneous counterpart, we first carried out several experiments in order to have an overview of the different superbases that could perform the transformation of allylic alcohols into saturated carbonyl compounds, **Table 1**. The superbases chosen for this study were TBD (pK_a = 26.02 in MeCN), DBU (pK_a = 24.34 in MeCN) and a phosphazene (pK_a = 30.25 in MeCN). Compared to the previous work (Table 1, Entry 1)[113], when increasing the temperature of the reaction to 120 ºC, DBU was able to isomerize substrate **11a** with the same level of chirality transfer (Table 1, Entry 2). However, when using a stronger base, the chirality transfer was inefficient (Table 1, Entry 3).

Table 1. Isomerization of **11a** catalyzed by organic superbases.

Entry	T (°C)	Superbase (0.1 equiv.)	Yield 12a (%)	*c.t.* (%)
1	60	TBD*	85	91
2	120	DBU	81	97
3	120	Phosphazene P$_4$-*t*-Bu	78	45

11a (0.1 mmol, 1 equiv.), superbase (0.01 mmol, 0.1 equiv.), toluene (0.1 M), from 60-120 ºC, 16 h. * Reaction carried out for 6 h.

To start our investigations with heterogenous materials functionalized with a base, we used commercially available functionalized polymers. DBU, TBD and P$_4$ phosphazene immobilized on polystyrene were tested on allylic alcohol **11b**, a substrate which gave lower levels of *c.t.* in our previous work[113] (**Scheme 5.4**). TBD-PS (**13a**) did not give good yields. This was expected, as it is the case of MTBD, there is no NH functionality. The amino groups are bound to the polystyrene. Phosphazene-PS (**13b**) afforded the desired ketone **12b** in very good yields. However, the chirality transfer was essentially the same as that obtained with the homogeneous TBD (60% *c.t.*). Pleasingly, DBU-PS (**13c**) afforded quantitative yields of the desired product, with levels of

c.t. much higher compared to those obtained with TBD, 95% *vs* 52% yield, respectively.
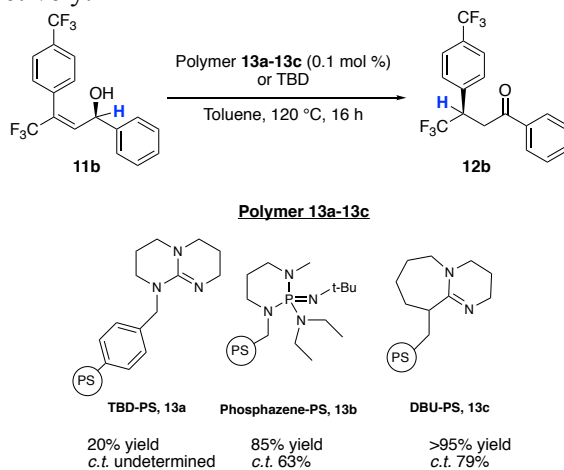
Scheme 5.4. Isomerization reaction of **11b** using PS immobilized superbases compared to TBD. Reaction run with TBD (5 mol%) at 80 ºC for 48 h, **12b** was obtained in 52 % yield and 61 % of *c.t.*

We went on by evaluating other base-functionalized materials. However, all our attempts to access heterogeneous superbases containing DBU or TBD subunits failed in our hands due to intrinsic synthetic problems observed in the different routes that we explored. Therefore, we decided to focus on the phosphazene-type superbases, which have been recently explored by the group of Dixon, and that are synthesized from easily accessible azides (**Figure 5.2**).[210, 211] The superbases reported by Dixon's group have pK_a values between 22 and 25 in MeCN depending on the electronics of the triarylphosphine motif. Therefore, according to the results presented in **Table 1** and **Scheme 5.4**, we expected that the Dixon´s iminophosphoranes would provide high levels of chirality transfer. As shown previously, strong bases with pK_{BH}^+ values above 30 displayed poor performance (*vide supra* **Table 1**, entry 3).

Dixon's bifunctional iminophosphorane organocatalysts: **pK$_{BH}^+$ studies on derived iminophosphorane superbases:**
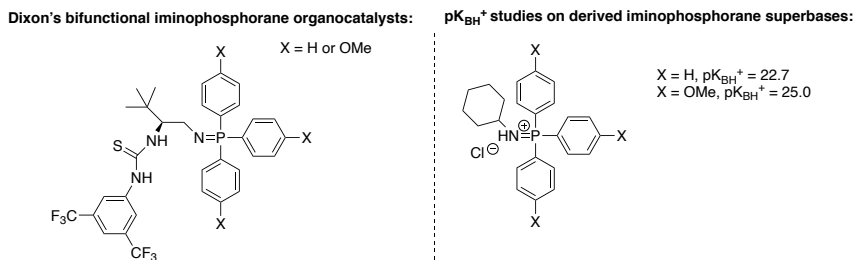
Figure 5.2. Examples of Dixon's BIMP (Bifunctional Iminophosphorane) organocatalysts and their basicity study in MeCN.

To test our hypothesis, we first attempted to use MIL-101(Cr), as we had developed a scalable and reproducible method for its preparation (*vide supra,* Chapter 4). However, our preliminary attempts failed. We then focused our attention on the use of UiO-67[212] derivatives, and studied the activity of this hybrid system towards the transformation of allylic alcohols into saturated carbonyl compounds. This family of MOFs was chosen due to their high chemical and thermal stability.[212, 213] MOFs are not stable under strongly basic conditions. However, the synthetic route applied enabled us to synthesize BIMP-functionalized MOFs. To the best of our knowledge, this is the first example of a MOF functionalized with such a basic motif.

5.4 Synthesis of the MOF

The synthesis of the targeted iminophosphorane-functionalized structure (H$_2$bpdc-az, **Scheme 5.5**) can be achieved in four synthetic steps. First, Suzuki-Miyaura cross-coupling afforded the unsymmetrical methyl-functionalized diaryl intermediate.[214] Then, benzylic radical bromination followed by displacement of the bromide by the azide anion, and basic hydrolysis of the ester yielded the desired linker, H$_2$bpdc-az.
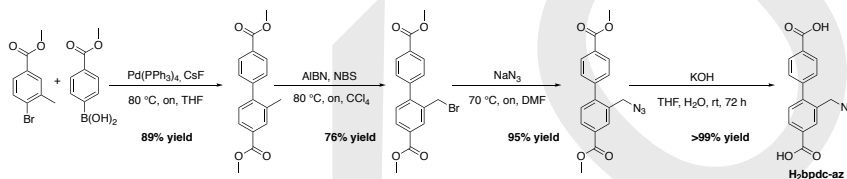
Scheme 5.5. Synthesis of the organic linker H$_2$bpdc-az.

53

UiO-67-bpdc-az was then synthesized in DMF at 130 °C, using benzoic acid as modulator and water as additive, according to a slightly modified reported procedure used for the synthesis of the plain MOF UiO-67.[215] The resulting MOF UiO-67-bpdc-az, was reacted following the Staudinger reaction conditions with tris(4-methoxyphenyl)phosphine in anhydrous diethyl ether and stirred overnight at room temperature (**Scheme 5.6**). The subsequent crystalline solids of UiO-67-bpdc-ip were filtered and washed with Et_2O, and the solid was dried under vacuum overnight.
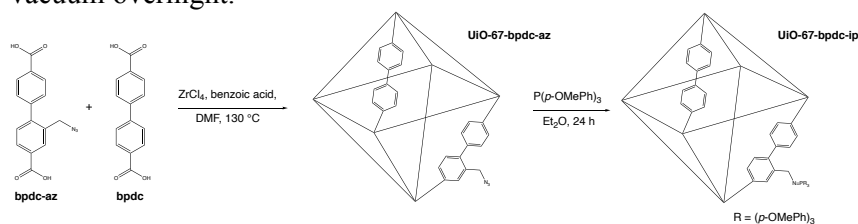
Scheme 5.6. Schematic representation of the synthesis of MOFs UiO-67-bpdc-az and UiO-67-bpdc-ip.

5.5 Characterization of the MOFs

Examination by ^1H NMR spectroscopy of both MOFs, UiO-67-bpdc-(bpdc-az) and UiO-67-bpdc-(bpdc-ip) was done by first digesting them upon treatment with NaOH in 1 M D_2O, to identify the amount of functionalized linker incorporated in each of the MOFs. In the case of UiO-67-bpdc-(bpdc-az) MOF, a 43% of the MOF linker was observed to be the azide one, which was then transformed completely into the corresponding iminophosphorane linker UiO-67-bpdc-(bpdc-ip). This transformation was confirmed by observing the amount of amine-substituted linker present in the UiO-67-bpdc-ip MOF after the digestion. The ratio for both MOFs was confirmed by elemental analysis which revealed that the molecular formula of UiO-67-bpdc-az is $Zr_6(bpdc)_{3.42}(bpdc-az)_{2.58}$ with a molecular mass of 1916 g/mol. The molecular formula for the UiO-67-bpdc-ip is $Zr_6(bpdc)_{3.42}(bpdc-ip)_{2.58}$ with a molecular mass of 2756 g/mol and was also confirmed by elemental analysis. The reproducibility of the obtained ratio was confirmed by several synthesized batches.

Powder X-ray diffractions of UiO-67-bpdc-az and UiO-67-bpdc-ip were done to confirm their isoreticular nature and high crystallinity

compared to the plain MOF UiO-67 (**Figure 5.3**). The patterns indicated that the 3D architecture is retained after incorporation of the bpdc-az linker and upon Staudinger reaction. Therefore, each cluster contains six zirconium(IV) atoms forming an octahedron, and each of these zirconium atoms are 8-coordinated in a square anti-prismatic geometry.
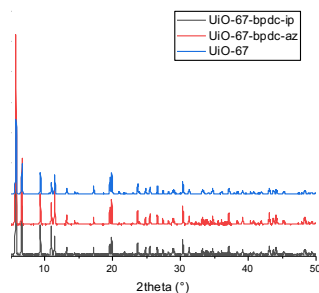
Figure 5.3. PXRD patterns of UiO-67, UiO-67-bpdc-az and UiO-67-bpdc-ip MOFs.

Importantly, the analysis by scanning electron microscopy disclosed that both UiO-67 derivatives form a single and pure phase with an octahedral homogeneous crystal particle size of approximately 1 μm, **Figure 5.4**.[4]
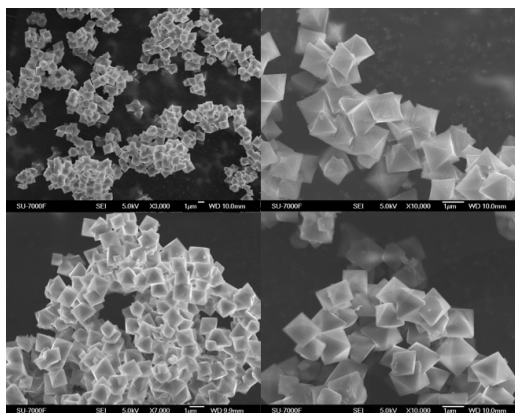
Figure 5.4. SEM images of UiO-67-bpdc-az on the top (5 kV, left: 3000 and right: 10000) and UiO-67-bpdc-ip on the bottom (5 kV, left: 7000 and right: 10000).

---

[4] SEM images were performed by Dr. Gurpreet Kaur.

Additionally, the porosity of the MOFs was determined by nitrogen adsorption isotherms with a BET surface area of 1846 m^2 g^{-1} for UiO-67-bpdc-az and 850 m^2 g^{-1} for UiO-67-bpdc-ip (**Figure 5.5**). The reported surface for the UiO-67 is 2700 m^2 g^{-1}. Therefore, these results indicate that the decrease in surface area for the MOFs UiO-67-bpdc-az and UiO-67-bpdc-ip is due to the invasion of the new organic linkers in the cavities of the MOF.
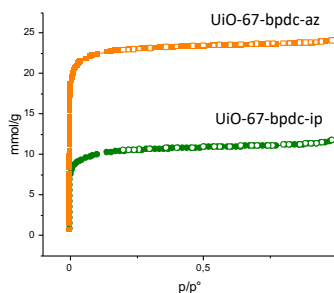
Figure 5.5. Nitrogen isotherm for UiO-67-bpdc-ip. Colored circles and squares indicate adsorption and uncolored circles and squares indicates desorption.

TGA analyses between 50 to 600 °C were performed for both UiO-67 derivatives to determine the total organic content in the hybrid materials (**Figure 5.6**). For both UiO-67 derivatives the first loss that takes place near 100 °C is due to the dehydration in the MOF. Two main weight losses were observed for the UiO-67-bpdc-az; near 300 °C agrees with the removal of the azide motif and near 500 °C corresponds to the combustion of the remaining organic components of the material. However, UiO-67-bpdc-ip shows one weight loss near 450 °C that corresponds to the combustion of the organic components. At 600 °C it is assumed that only ZrO$_2$ remains and this is in accordance for both UiO-67 derivatives.
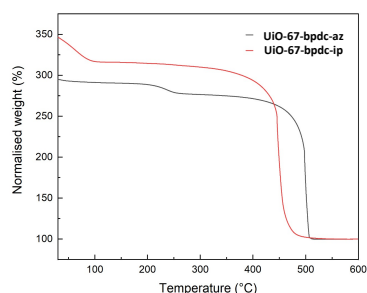
Figure 5.6. TGA analysis from 50 to 600 °C for UiO-67-bpdc-ip (red) and UiO-67-bpdc-az (gray).

The pK_a of the homogeneous counterpart was calculated following a reported procedure according to the literature.[216] The synthesized homogeneous iminophosphorane shows a pK_{BH^+} of 24.45 in acetonitrile.

5.6 Proof of concept

With UiO-67-bpdc-ip in our hands, we focused our attention on the efficiency of the system in the isomerization reaction. First, we tested the catalytic activity of the homogeneous counterpart, as well as the effects of heterogenization into a MOF. Unless otherwise noted, reactions were carried out at 120 °C in toluene (0.1 M) for 48 h with different loadings of the determined $Zr_6O_4(OH)_4(bpdc)_{3.42}(bpdc-ip)_{2.58}$ formula. The reaction was followed using ^{19}F NMR spectroscopy. As seen in **Table 2** the homogeneous counterpart is capable of isomerize substrate **11b** in a 30% conversion after 48 h (Table 2, Entry 1) with a 40% of *c.t.*. Unfortunately, UiO-67-bpdc-ip was not able to promote this transformation in a catalytic fashion (Table 2, Entries 2-5), but afforded **12b** quantitatively when stoichiometric loadings were used (Table 2, Entry 6). The *c.t.* obtained was higher than the results obtained in the previous work. Changing other parameters such as the concentration or temperature of the reaction did not have any effect on the isomerization reaction (Table 2, Entries 7 and 8). When the isomerization reaction was tested with phosphine and phosphine oxide catalyst (Table 2, Entries 9-10), ketone **12b** was not observed in any case. The reaction was also examined with the UiO-67-bpdc-az and UiO-67 MOFs (Table 2, Entries 11 and 12),

and we confirmed that these non-basic MOFs do not catalyze the reaction.

Table 2. Optimization of the reaction conditions.
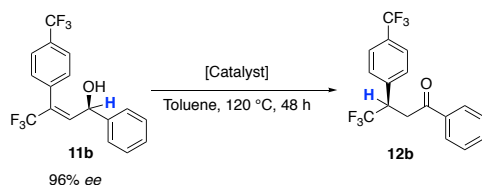
Entry	Catalyst (mol%)	^{19}F NMR Conversion (%)	*c.t.* (%)
1	Homogeneous counterpart (10)	30	40
2	UiO-67-bpdc-ip (10)	<10	n.d.
3	UiO-67-bpdc-ip (20)	10	n.d.
4	UiO-67-bpdc-ip (50)	22	n.d.
5	UiO-67-bpdc-ip (75)	50	78
6	UiO-67-bpdc-ip (100)	>99	78
7[a]	UiO-67-bpdc-ip (10)	10	n.d.
8[b]	UiO-67-bpdc-ip (100)	0	-
9	P(*p*-OMe)$_3$ (100)	0	-
10	O=P(*p*-OMe)$_3$ (100)	0	-
11	UiO-67-bpdc-az (100)	0	-
12	UiO-67 (100)	0	-

Unless otherwise noted: **11b** (0.1 mmol, 1 equiv.), **catalyst** (1 mmol, 1 equiv.), toluene (0.1 M) at 120 ºC, 48 h. n.d.: not determined. [a]: Reaction carried out at 1 M. [b]: Reaction ran at 60 °C.

Post-reaction, UiO-67-bpdc-ip was washed and filtered and characterized by PXRD, showing that the 3D framework was maintained (**Figure 5.7a**). However, ^{1}H NMR of the supernatant revealed the decomposition of the iminophosphorane to the corresponding amine derivative and phosphine oxide (**Figure 5.7b**). This explains the inferior results obtained with substoichiometric amounts of the heterogeneous base. Furthermore, the stability of the MOF under hydrothermal conditions was explored. The MOF was placed on a pressure vial at 120 ºC for 48 h using water as a solvent. A ^{1}H NMR spectrum of this experiment showed that decomposition of the iminophosphorane takes place under hydrothermal heating. Therefore, this suggests that the moisture within the MOF results in the decomposition of the base catalyst.
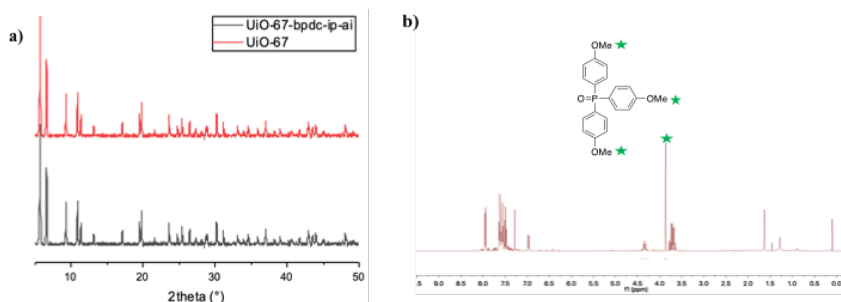
Figure 5.7. a) PXRD of UiO-67-bpdc-ip-ai (black) taken after isomerization compared to UiO-67 (red). b) ^{1}H NMR spectrum showing decomposition of the base into phosphine oxide after isomerization reaction.

Additionally, we studied the recyclability of the hybrid material and its activity in sequential reactions. UiO-67-bpdc-ip was reused up to 4 times (**Table 3**). The material can be reused for two runs without observing a dramatic decrease in the chirality transfer (**Table 3, Entries 1** and **2**). However, after the second run a significant loss of yield and chirality transfer is observed, likely related to the decomposition of the iminophosphorane functional group in the reaction (**Table 3, Entries 3** and **4**). In order to evaluate any change in the morphology of the material, the MOF was analyzed by SEM after the recycling studies. The comparison of the SEM analysis reveals that there is no modification of the morphology observed (**Figure 5.8**).

Table 3. Recyclability studies of the UiO-67-bpdc-ip.
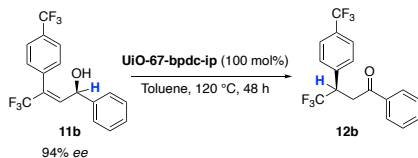
Entry	^{19}F NMR Conversion 12b (%)	*c.t.* (%)
1	>99	78
2	55	69
3	37	58
4	12	58

11b (0.1 mmol, 1 equiv.), **UiO-67-bpdc-ip** (1 mmol, 1 equiv.), toluene (0.1 M), 120 ºC, 48 h.
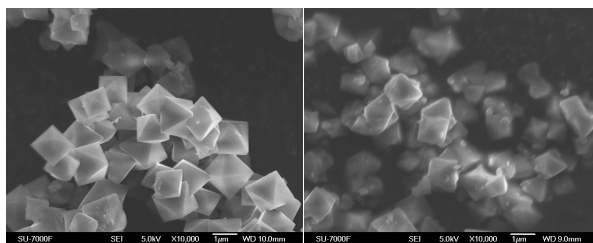
Figure 5.8. SEM images: before (left) and after 4 consecutive runs (right).

For a better understanding of the mechanism operating in this transformation, another allylic system was studied (**Scheme 5.7**). When using an allylic halide (**14**) the reaction did not give the corresponding vinyl halide **15**. In other words, the proton source after deprotonation could come from another proton source of the reaction mixture rather than from the iminophosphorane superbase. As mentioned before, (*vide supra,* **Scheme 5.2**) the proton shift could take place in an intramolecular manner for the case of the allylic alcohols. Therefore, this could explain the different results of the isomerization transformation when employing different allylic systems, alcohols *versus* halides.
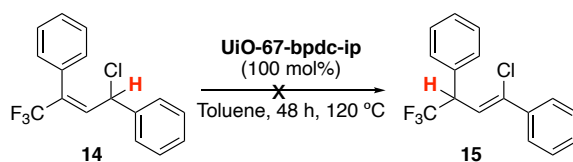
Scheme 5.7. Isomerization of allylic halides catalyzed by UiO-67-bpdc-ip.

At this stage, it cannot be concluded whether the reaction is taking place either on the outer sphere of the MOF or within the pores.

5.7 Conclusions

To the best of our knowledge, we have synthesized the first heterogeneous superbase MOF, UiO-67-bpdc-ip. The heterogeneous material has been fully characterized using several techniques: PXRD, nitrogen adsorption analysis, TGA, SEM and ^{1}H NMR. Elemental analysis has been also carried out. The characterization of the MOF revealed that the crystallinity and the morphology are preserved upon functionalization with the superbase. The surface area decreases since the pores are partly occupied by azide or iminophosphorane groups on the organic linkers.

In this study, we have shown that heterogeneous materials such as polymers and MOFs enhance the chirality transfer of some electron-deficient allylic alcohols when compared to its homogeneous version.

This investigation is in a preliminary stage. Other MOFs with higher pore size and superbases with lower pK_a should be considered for the synthesis of a heterogeneous superbases with better catalytic properties.

6 Concluding remarks

In the present thesis, computational studies for the mechanism of two newly developed organic transformations have been performed. These studies involve the transformation of allylic substrates and enol derivatives. This thesis also describes the synthesis of MOFs using microwave-assisted and conventional methods, together with their use in catalysis.

In the second chapter of this thesis the reaction of silyl enol ethers with heteronucleophiles through an umpolung protocol mediated by a hypervalent iodine reagent is described. After optimizing the reaction conditions, a number of nucleophiles has been tested yielding the desired α-functionalized ketones in good to high yields. The mechanism of the reaction has been studied by DFT calculations and it is suggested that high selectivity of the reaction is due to the formation of a key enolonium intermediate with a halogen-bonded bromide.

The synthesis of the MIL-101(Cr) and MIL-101(Cr)-NH$_2$ employing microwave radiation has been described in the third chapter of this thesis. The described method is faster, highly efficient, phase selective and avoids the use of hydrofluoric acid compared to other methods. The method can be scaled to obtain up to 1 g of the desired MOF in a short reaction time.

In chapter 4, the base-catalyzed [1,n]-proton shift in conjugated polyenyl ethers has been studied computationally. The calculations and mechanistic experiments revealed that after a rate-limiting deprotonation step, the guanidine base is able to go through a number of consecutive [1,n]-proton shifts until formation of the most thermodynamically stable product. Deuterium studies confirmed the KIE values obtained experimentally. Kinetic simulation of the reaction has been performed in order to understand the ratio of the stereoisomers obtained in the reaction, which agreed with the ratio obtained experimentally.

Last chapter describes the synthesis of a UiO-67 derivative containing a superbase to study the effect of the MOF in the stereospecific isomerization of allylic alcohols. An improvement on the chirality transfer has been obtained. However, it cannot be concluded that the

levels of chirality transfer are due to the confined environment. The material has been fully characterized employing techniques such as PXRD, ^{1}H NMR, SEM, N_2 sorption analysis and TGA.

7 Appendix A: List of Contributions

Paper I Contributed equally to Víctor García Vázquez in the experimental part reflected in the article. Amparo Sanz-Marco developed the concept, and together with Víctor performed the optimization. I performed part of the experimental studies and fully contributed to the computational analysis. I contributed to the writing of the manuscript for the scope of the nucleophiles that are not carbamates and the DFT part.

Paper II Participated in the computational study of the reaction. Performed the theoretical kinetical and deuterium studies. Wrote the DFT contribution of the manuscript and the supporting information.

Paper III Performed the optimization of the method and participated in the characterization analysis using PXRD. Participated on writing of the first draft of the manuscript.

Paper IV Performed the synthesis of the organic linker together with Víctor García Vázquez and Pablo Martínez Pardo. Performed the synthesis of the MOF and the major characterization of the material. Performed the optimization of the reaction. Wrote the preliminary manuscript and wrote the supporting information.

8 Acknowledgements

First, I would like to express my most sincere gratitude to my supervisor Prof. *Belén Martín Matute* for giving me the chance to join her group and her guidance and support during this time. To Prof. *Enrique Gómez Bengoa* for his help and guidance in the computational field during my secondment and anytime *via* zoom.

I would also like to thank my co-supervisor at Stockholm University Prof. *Fahmi Himo*, and Prof. *Kálmán Szabó* for helping me to improve my thesis. To Prof. *Jose A. Mata* for helping me during my master thesis in Castellón and motive me in my decision to continue my studies.

I would like to thank *Prof. Shu-Li You* for accepting to be the opponent of this doctoral dissertation, Prof. *Abel de Cozar*, Prof. *Daniel Strand* and Prof. *Gulaim A. Seisenbaeva* for being members of the examination committee.

To the proof-readers of the thesis Dr. *Beatriz Saavedra Guillem*, Dr. *Ferran Planas Padros*, Dr. *Matteo Costantini* and Dr. *Víctor García Vázquez* for all your comments and effort on this thesis. To *Axel Furevi* for translating the Populärvetenskaplig sammanfattning and to *Adrian Gual* for designing the cover of the thesis.

To all the *TA* staff, past and present, for their help during these years.

To all my co-workers that have contributed to the projects: Dr. *Amparo Sanz Marco*, Dr. *Li Man*, Dr. *Nagaraju Molleti*, Dr. *Pablo Martínez Pardo*, Dr. *Samuel Martinez Erro*, Dr. *Sergio Carrasco* and Dr. *Víctor García Vázquez*. To the past and present members of BMM group for all the chemistry discussions and the support during this time: Dr. *Aitor Bermejo*, Dr. *Aditya Dharanipragada*, Dr. *Alejandro Valiente*, *Alexandru Postole*, Dr. *Amparo Sanz Marco*, *Anika Schick*, Dr. *Antonio Bermejo*, Dr. *Aya Ismael*, Dr. *Beatriz Saavedra*, Dr. *Elis Erbing*, *Emanuele Silvi*, Dr. *Erik Weis*, Dr. *Greco Gonzalez*, Dr. *Gurpreet Kaur*, Dr. *Li Man*, *Lucia Crespo*, *Majken Raeder*, *Maria Obieta*, Dr. *Mathias Salomon*, Dr. *Nagaraju Molleti*, Dr. *Pablo Martínez*, *Patrick Maguire*, *Pedro Tortajada*, *Phan Vu Duc Ha*, Dr. *Samuel Martínez*, *Sarko Jabari*, Dr. *Sergio Carrasco* and Dr. *Víctor García Vázquez*.

Past and present members of the department, with whom I have had the best time in Stockholm: *Alba Helena Pérez Jimeno*, Dr. *Alberto Abengózar*, Dr. *Alessandro Ruda*, Dr. *Axel Furevi*, *Beatriz Meana*, Dr. *Biswanath Das*, *Bram Peters*, Dr. *Cristiana Margarita*, *Daria Lebedeva*, Dr. *Davide Di Francesco*, *Davide Di Rigo*, Dr. *Elena Subbotina*, Dr. *Elisa Martínez de Castro*, *Ester Maria Di Tommaso*, Dr. *Federico Riu*, Dr. *Ferran Planas Padros*, *Flavia Ferrara*, Dr. *Gabriella Kverofs*, *Gonzalo Castiella*, Dr. *Haibo Wu*, *Igor Lebedev*, Dr. *Jèssica Margalef*, Dr. *Jianping Yang*, *Kevin Dorst*, Dr. *Kuntawit Witthayolankowit*, *Luca Massaro*, *Linus Holm*, *Marie Deliaval*, Dr. *Mario Prejanò*, Dr. *Marc Montesinos*, Dr. *Matteo Constantini*, Dr. *Miguel Cortés*, Dr. *Rajdip Chowdhury*, Dr. *Stefanie Kohlhepp*, Dr. *Stefano Parisotto*, *Suthawan Muangmeesri*, Dr. *Sybrand Jonker*, Dr. *Thanya Rukkijakan*, *Tautvydas Kireilis* and *Victoria López Corbalán*. To other people who are not from the department: *Brando Adranno, Diego Salas Ugalde*, *Fabio Begnini*, *Francesco Nonsenzo, Francois du Plessis*, *Leah Englund* and *Tran Nguyen Quynh Chau.* Also, to Dr. *Andrés Pastor*, *Micke Sandström* and *Pablo Herreras* that made the beginning of my time in Stockholm incredible.

To the SURFACE team at Stockholm University for offering a mentorship programme that gave me the opportunity of connecting with such an amazing mentor Prof. *Lucie Delemotte*. Thank you for your help and guidance during the last year and being always on the loop. I really appreciate our meetings and calls.

To all the people that I met during my 9 months secondment in the Basque-country but especially to those with whom I discovered the north of Spain and I shared such wonderful moments: *Arkaitz*, *Fer*, *Lia* and *Marina*.

Mis amigos de Castellón por estar siempre sin importar la distancia: *Anita*, *Bárbara*, *Beatriz*, *Cris*, *Ivan*, *Jesús*, *Jorge, Manolo* y *Víctor*. Y al grupo: the lost to the … por todos los momentos compartidos antes, durante estos años y por los que están por venir.

A mis padres, *Amelia* y *Juanma*, y a mi hermana, *Ana,* por darme el amor más puro e incondicional. A mi tia, *Angus,* por estar siempre ahí. Y a mi abuela, *Modesta,* por cada sonrisa que me hace nacer de nuevo.

9 References

1. Nicolaou, K. C., *Proc Math Phys Eng Sci.* **2014,** *470*, 20130690.

2. Anastas, P. T.; Warner, J. C., *Green Chemistry: Theory and Practice*. Oxford University Press: **1998**.

3. Erythropel, H. C.; Zimmerman, J. B.; de Winter, T. M.; Petitjean, L.; Melnikov, F.; Lam, C. H.; Lounsbury, A. W.; Mellor, K. E.; Janković, N. Z.; Tu, Q.; Pincus, L. N.; Falinski, M. M.; Shi, W.; Coish, P.; Plata, D. L.; Anastas, P. T., *Green Chem.* **2018,** *20*, 1929-1961.

4. Anslyn, E. V.; Dougherty, D. A., *Modern physical organic chemistry*. University Science Books: Mill Valley, California, **2006**.

5. Rothenberg, G. In *Catalysis: Concepts and Green Applications*, **2008**.

6. Oyama, S. T.; Somorjai, G. A., *J. Chem. Educ.* **1988,** *65*, 765.

7. MacMillan, D. W. C., *Nature.* **2008,** *455*, 304-308.

8. List, B., *Chem. Rev.* **2007,** *107*, 5413-5415.

9. Taylor, M. S.; Jacobsen, E. N., *Angew. Chem. Int. Ed.* **2006,** *45*, 1520-1543.

10. Oliveira, V. d. G.; Cardoso, M. F. d. C.; Forezi, L. d. S. M., *Catalysts.* **2018,** *8*, 605.

11. Seebach, D., *Angew. Chem. Int. Ed.* **1990,** *29*, 1320-1367.

12. Hajos, Z. G.; Parrish, D. R., *J. Org. Chem.* **1974,** *39*, 1612-1615.

13. Tu, Y.; Wang, Z.-X.; Shi, Y., *J. Am. Chem. Soc.* **1996,** *118*, 9806-9807.

14. Denmark, S. E.; Wu, Z.; Crudden, C. M.; Matsuhashi, H., *J. Org. Chem.* **1997,** *62*, 8288-8289.

15. Yang, D.; Yip, Y.-C.; Tang, M.-W.; Wong, M.-K.; Zheng, J.-H.; Cheung, K.-K., *J. Am. Chem. Soc.* **1996,** *118*, 491-492.

16. Sigman, M. S.; Jacobsen, E. N., *J. Am. Chem. Soc.* **1998,** *120*, 4901-4902.

17. Corey, E. J.; Grogan, M. J., *Org. Lett.* **1999,** *1*, 157-160.

18. Doyle, A. G.; Jacobsen, E. N., *Chem. Rev.* **2007,** *107*, 5713-5743.

19. Guerrero-Corella, A.; Fraile, A.; Alemán, J., *ACS Organic & Inorganic Au.* **2022,** *2*, 197-204.

20. Mase, N.; Tanaka, F.; Barbas III, C. F., *Angew. Chem. Int. Ed.* **2004,** *43*, 2420-2423.

21. Bui, T.; Syed, S.; Barbas III, C. F., *J. Am. Chem. Soc.* **2009,** *131*, 8758-8759.

22.   Dobish, M. C.; Villalta, F.; Waterman, M. R.; Lepesheva, G. I.; Johnston, J. N., *Org. Lett.* **2012,** *14*, 6322-6325.

23.   Deng, Z.-X.; Xie, Z.-Z.; Zheng, Y.; Xiao, J.-A.; Wang, R.-J.; Xiang, H.-Y.; Yang, H., *Org. Biomol. Chem.* **2019,** *17*, 2187-2191.

24.   Enders, D.; Niemeier, O.; Henseler, A., *Chem. Rev.* **2007,** *107*, 5606-5655.

25.   Ukai, T.; Tanaka, R.; Dokawa, T., *J. Pharm. Soc. Jpn.* **1943,** *63*, 296-300.

26.   Breslow, R., *J. Am. Chem. Soc.* **1958,** *80*, 3719-3726.

27.   List, B.; Lerner, R. A.; Barbas, C. F., *J. Am. Chem. Soc.* **2000,** *122*, 2395-2396.

28.   Ahrendt, K. A.; Borths, C. J.; MacMillan, D. W. C., *J. Am. Chem. Soc.* **2000,** *122*, 4243-4244.

29.   Palomo, C.; Oiarbide, M.; López, R., *Chem. Soc. Rev.* **2009,** *38*, 632-653.

30.   Ting, A.; Goss, J. M.; McDougal, N. T.; Schaus, S. E., *Top. Curr. Chem.* **2010,** *291*, 145-200.

31.   Wynberg, H.; Helder, R., *Tetrahedron Lett.* **1975,** *16*, 4057-4060.

32.   Poulsen, T. B.; Alemparte, C.; Saaby, S.; Bella, M.; Jørgensen, K. A., *Angew. Chem. Int. Ed.* **2005,** *44*, 2896-2899.

33.   Verkade, J., *Angew. Chem. Int. Ed.* **2009,** *48*, 9221-9221.

34.   Oediger, H.; Möller, F., *Angew. Chem. Int. Ed.* **1967,** *6*, 76-76.

35.   Angyal, S. J.; Warburton, W. K., *J. Am. Chem. Soc.* **1951**, 2492-2494.

36.   Schwesinger, R.; Schlemper, H., *Angew. Chem. Int. Ed.* **1987,** *26*, 1167-1169.

37.   Kaljurand, I.; Kütt, A.; Sooväli, L.; Rodima, T.; Mäemets, V.; Leito, I.; Koppel, I. A., *J. Org. Chem.* **2005,** *70*, 1019-1028.

38.   Luo, C.; Bandar, J. S., *J. Am. Chem. Soc.* **2018,** *140*, 3547-3550.

39.   Pal, K. B.; Guo, A.; Das, M.; Báti, G.; Liu, X.-W., *ACS Catal.* **2020,** *10*, 6707-6715.

40.   Sather, A. C.; Lee, H. G.; De La Rosa, V. Y.; Yang, Y.; Müller, P.; Buchwald, S. L., *J. Am. Chem. Soc.* **2015,** *137*, 13433-13438.

41.   Chaoseng Luo, J. S. B., *Synlett.* **2018,** *29*, 2218-2224.

42.   Kawai, H.; Yuan, Z.; Tokunaga, E.; Shibata, N., *Org. Biomol. Chem.* **2013,** *11*, 1446-1450.

43.   Wacławek, S.; Padil, V. V. T.; Černík, M., *Ecol. Chem. Eng. S.* **2018,** *25*, 9-34.

44.   Tanimu, A.; Jaenicke, S.; Alhooshani, K., *Chem. Eng. J.* **2017,** *327*, 792-821.

45.   *Nature.* **1902,** *65*, 522-526.

46.   Sabatier, P.; Mailhe, A., *Compt. Rend.* **1904,** *139*.

47.   Sunil, J.; Renade, V., *Industrial catalytic processes for fine and specialty chemicals*. **2016**.

48.   El-Hout, S. I.; El-Sheikh, S. M.; Hassan, H. M. A.; Harraz, F. A.; Ibrahim, I. A.; El-Sharkawy, E. A., *Appl. Catal. A: Gen.* **2015,** *503*, 176-185.

49.   Collis, A. E. C.; Horváth, I. T., *Catal. Sci. Technol.* **2011,** *1*, 912-919.

50.   Genna, D. T.; Wong-Foy, A. G.; Matzger, A. J.; Sanford, M. S., *J. Am. Chem. Soc.* **2013,** *135*, 10586-10589.

51.   Román-Martínez, M. C.; Salinas-Martínez de Lecea, C., Chapter 3 - Heterogenization of Homogeneous Catalysts on Carbon Materials. In *New and Future Developments in Catalysis*, Suib, S. L., Ed. Elsevier: Amsterdam, **2013**; 55-78.

52.   Ventura-Espinosa, D.; Vicent, C.; Baya, M.; Mata, J. A., *Catal. Sci. Technol.* **2016,** *6*, 8024-8035.

53.   Liu, L.; Corma, A., *Chem. Rev.* **2018,** *118*, 4981-5079.

54.   Ma, Z.; Zaera, F., Characterization of Heterogeneous Catalysts. **2006**; 1-37.

55.   Yuan, N.; Pascanu, V.; Huang, Z.; Valiente, A.; Heidenreich, N.; Leubner, S.; Inge, A. K.; Gaar, J.; Stock, N.; Persson, I.; Martín-Matute, B.; Zou, X., *J. Am. Chem. Soc.* **2018,** *140*, 8206-8217.

56.   Hölderich, W.; Hesse, M.; Näumann, F., *Angew. Chem. Int. Ed.* **1988,** *27*, 226-246.

57.   Isaeva, V. I.; Kustov, L. M., *Pet. Chem.* **2010,** *50*, 167-180.

58.   Xuan, W.; Zhu, C.; Liu, Y.; Cui, Y., *Chem. Soc. Rev.* **2012,** *41*, 1677-1695.

59.   Furukawa, H.; Cordova, K. E.; O'Keeffe, M.; Yaghi, O. M., *Science.* **2013,** *341*, 1230444.

60.   Li, H.; Wang, K.; Sun, Y.; Lollar, C. T.; Li, J.; Zhou, H.-C., *Mater. Today.* **2018,** *21*, 108-121.

61.   Carrasco, S., *Biosensors.* **2018,** *8*, 92.

62.   Wuttke, S.; Lismont, M.; Escudero, A.; Rungtaweevoranit, B.; Parak, W. J., *Biomaterials.* **2017,** *123*, 172-183.

63.   Bauer, G.; Ongari, D.; Xu, X.; Tiana, D.; Smit, B.; Ranocchiari, M., *J. Am. Chem. Soc.* **2017,** *139*, 18166-18169.

64.   Furukawa, H.; Gándara, F.; Zhang, Y. B.; Jiang, J.; Queen, W. L.; Hudson, M. R.; Yaghi, O. M., *J. Am. Chem. Soc.* **2014,** *136*, 4369-81.

65.   Hanikel, N.; Prévot, M. S.; Fathieh, F.; Kapustin, E. A.; Lyu, H.; Wang, H.; Diercks, N. J.; Glover, T. G.; Yaghi, O. M., *ACS. Cent. Sci.* **2019, *5*, 1699-1706.

66.   Fathieh, F.; Kalmutzki, M. J.; Kapustin, E. A.; Waller, P. J.; Yang, J.; Yaghi, O. M., *Sci Adv.* **2018, *4*, eaat3198.

67.   Stock, N.; Biswas, S., *Chem. Rev.* **2012**, *112*, 933-969.

68.   Butova, V. V.; Soldatov, M. A.; Guda, A. A.; Lomachenko, K. A.; Lamberti, C., *Russ. Chem. Rev.* **2016**, *85*, 280-307.

69.   Sun, Y.; Zhou, H.-C., *Sci. Technol. Adv. Mater.* **2015, *16*, 054202.

70.   Klinowski, J.; Almeida Paz, F. A.; Silva, P.; Rocha, J., *Dalton Trans.* **2011, *40*, 321-330.

71.   Carrasco, S.; Sanz-Marco, A.; Martín-Matute, B., *Organometallics.* **2019, *38*, 3429-3435.

72.   Jhung, S. H.; Lee, J.-H.; Forster, P. M.; Férey, G.; Cheetham, A. K.; Chang, J.-S., *Chem. Eur. J.* **2006, *12*, 7899-7905.

73.   Amo-Ochoa, P.; Givaja, G.; Miguel, P. J. S.; Castillo, O.; Zamora, F., *Inorg. Chem. Commun.* **2007, *10*, 921-924.

74.   Pascanu, V.; González Miera, G.; Inge, A. K.; Martín-Matute, B., *J. Am. Chem. Soc.* **2019**, *141*, 7223-7234.

75.   Yang, D.; Gates, B. C., *ACS Catal.* **2019**, *9*, 1779-1798.

76.   Lee, J.; Farha, O. K.; Roberts, J.; Scheidt, K. A.; Nguyen, S. T.; Hupp, J. T., *Chem. Soc. Rev.* **2009, *38*, 1450-1459.

77.   Ji, P.; Feng, X.; Oliveres, P.; Li, Z.; Murakami, A.; Wang, C.; Lin, W., *J. Am. Chem. Soc.* **2019**, *141*, 14878-14888.

78.   Ji, P.; Feng, X.; Veroneau, S. S.; Song, Y.; Lin, W., *J. Am. Chem. Soc.* **2017, *139*, 15600-15603.

79.   McGuirk, C. M.; Katz, M. J.; Stern, C. L.; Sarjeant, A. A.; Hupp, J. T.; Farha, O. K.; Mirkin, C. A., *J. Am. Chem. Soc.* **2015, *137*, 919-925.

80.   Feng, X.; Song, Y.; Li, Z.; Kaufmann, M.; Pi, Y.; Chen, J. S.; Xu, Z.; Li, Z.; Wang, C.; Lin, W., *J. Am. Chem. Soc.* **2019**, *141*, 11196-11203.

81.   Liu, L.; Zhou, T.-Y.; Telfer, S. G., *J. Am. Chem. Soc.* **2017, *139*, 13936-13943.

82.   Pascanu, V.; Bermejo Gómez, A.; Ayats, C.; Platero-Prats, A. E.; Carson, F.; Su, J.; Yao, Q.; Pericàs, M. À.; Zou, X.; Martín-Matute, B., *ACS Catal.* **2015**, *5*, 472-479.

83.   Yu, X.; Cohen, S. M., *Chem. Commun.* **2015**, *51*, 9880-9883.

84.   Carson, F.; Martínez-Castro, E.; Marcos, R.; Miera, G. G.; Jansson, K.; Zou, X.; Martín-Matute, B., *Chem. Commun.* **2015, *51*, 10864-10867.

85. Wild, D., *The immunoassay handbook : theory and applications of ligand binding, ELISA and related techniques*. **2013**.

86. Salvador, J. A. R.; Silvestre, S. M.; Pinto, R. M. A., *Molecules.* **2011,** *16*, 2884-2913.

87. DeWolfe, R. H.; Young, W. G., *Chem. Rev.* **1956,** *56*, 753-901.

88. Bausch, C. C.; Johnson, J. S., *J. Org. Chem.* **2008,** *73*, 1575-1577.

89. Belardi, J. K.; Micalizio, G. C., *J. Am. Chem. Soc.* **2008,** *130*, 16870-16872.

90. Lin, Y. A.; Davis, B. G., *Beilstein. J. Org. Chem.* **2010,** *6*, 1219-1228.

91. Uma, R.; Crévisy, C.; Grée, R., *Chem. Rev.* **2003,** *103*, 27-52.

92. Damico, R.; Logan, T., *J. Org. Chem.* **1967,** *32*, 2356-2358.

93. Trost, B. M.; Martinez, J. A.; Kulawiec, R. J.; Indolese, A. F., *J. Am. Chem. Soc.* **1993,** *115*, 10402-10403.

94. Kress, S.; Johnson, T.; Weisshar, F.; Lautens, M., *ACS Catal.* **2016,** *6*, 747-750.

95. Li, H.; Mazet, C., *Acc. Chem. Res.* **2016,** *49*, 1232-1241.

96. Mantilli, L.; Gérard, D.; Torche, S.; Besnard, C.; Mazet, C., *Angew. Chem. Int. Ed.* **2009,** *48*, 5143-5147.

97. Lorenzo-Luis, P.; Romerosa, A.; Serrano-Ruiz, M., *ACS Catal.* **2012,** *2*, 1079-1086.

98. Erbing, E.; Vázquez-Romero, A.; Bermejo Gómez, A.; Platero-Prats, A. E.; Carson, F.; Zou, X.; Tolstoy, P.; Martín-Matute, B., *Chem. Eur. J.* **2016,** *22*, 15659-15663.

99. Li, M.; Sanz-Marco, A.; Martinez-Erro, S.; García-Vázquez, V.; Mai, B. K.; Fernández-Gallardo, J.; Himo, F.; Martín-Matute, B., *Chem. Eur. J.* **2020,** *26*, 14978-14986.

100. Luca, M.; Clément, M., *Chem. Lett.* **2011,** *40*, 341-344.

101. Cahard, D.; Gaillard, S.; Renaud, J.-L., *Tetrahedron Lett.* **2015,** *56*, 6159-6169.

102. Liu, T.-L.; Ng, T. W.; Zhao, Y., *J. Am. Chem. Soc.* **2017,** *139*, 3643-3646.

103. Li, J.-Q.; Peters, B.; Andersson, P. G., *Chem. Eur. J.* **2011,** *17*, 11143-11145.

104. Arai, N.; Sato, K.; Azuma, K.; Ohkuma, T., *Angew. Chem. Int. Ed.* **2013,** *52*, 7500-7504.

105. Bizet, V.; Pannecoucke, X.; Renaud, J.-L.; Cahard, D., *Angew. Chem. Int. Ed.* **2012,** *51*, 6467-6470.

106. Bizet, V.; Pannecoucke, X.; Renaud, J.-L.; Cahard, D., *J. Fluor. Chem.* **2013,** *152*, 56-61.

107. Dabrowski, J. A.; Haeffner, F.; Hoveyda, A. H., *Angew. Chem. Int. Ed.* **2013,** *52*, 7694-7699.

108. Burton, H.; Ingold, C. K., *J. Am. Chem. Soc.* **1928**, 904-921.

109. Crivello, J. V.; Conlon, D. A., *Journal of Polymer Science: Polymer Chemistry Edition.* **1984,** *22*, 2105-2121.

110. Johnston, A. J. S.; McLaughlin, M. G.; Reid, J. P.; Cook, M. J., *Org. Biomol. Chem.* **2013,** *11*, 7662-7666.

111. Zheng, H.-X.; Xiao, Z.-F.; Yao, C.-Z.; Li, Q.-Q.; Ning, X.-S.; Kang, Y.-B.; Tang, Y., *Org. Lett.* **2015,** *17*, 6102-6105.

112. Mondal, K.; Mondal, B.; Pan, S. C., *J. Org. Chem.* **2016,** *81*, 4835-4840.

113. Martinez-Erro, S.; Sanz-Marco, A.; Bermejo Gómez, A.; Vázquez-Romero, A.; Ahlquist, M. S. G.; Martín-Matute, B., *J. Am. Chem. Soc.* **2016,** *138*, 13408-13414.

114. Molleti, N.; Martinez-Erro, S.; Carretero Cerdán, A.; Sanz-Marco, A.; Gomez-Bengoa, E.; Martín-Matute, B., *ACS Catal.* **2019,** *9*, 9134-9139.

115. Martinez-Erro, S.; García-Vázquez, V.; Sanz-Marco, A.; Martín-Matute, B., *Org. Lett.* **2020,** *22*, 4123-4128.

116. García-Vázquez, V.; Martínez-Pardo, P.; Postole, A.; Inge, A. K.; Martín-Matute, B., *Org. Lett.* **2022,** *24*, 3867-3871.

117. Hamada, Y.; Kawasaki-Takasuka, T.; Yamazaki, T., *Beilstein. J. Org. Chem.* **2017,** *13*, 1507-1512.

118. Sun, C.; Qi, X.; Min, X.-L.; Bai, X.-D.; Liu, P.; He, Y., *Chem. Sci.* **2020,** *11*, 10119-10126.

119. Wang, J.; Qi, X.; Min, X.-L.; Yi, W.; Liu, P.; He, Y., *J. Am. Chem. Soc.* **2021,** *143*, 10686-10694.

120. Minkin, V. I., *Pure Appl. Chem.* **1999,** *71*, 1919-1981.

121. Zhdankin, V. V.; Stang, P. J., *Chem. Rev.* **2008,** *108*, 5299-5358.

122. Preparation, Structure and Properties of Polyvalent Iodine Compounds. In *Hypervalent Iodine Chemistry*, **2013**; 21-143.

123. Yoshimura, A.; Zhdankin, V. V., *Chem. Rev.* **2016,** *116*, 3328-3435.

124. Hyatt, I. F. D.; Dave, L.; David, N.; Kaur, K.; Medard, M.; Mowdawalla, C., *Org. Biomol. Chem.* **2019,** *17*, 7822-7848.

125. Reddy Kandimalla, S.; Prathima Parvathaneni, S.; Sabitha, G.; Subba Reddy, B. V., *Eur. J. Org. Chem.* **2019,** *2019*, 1687-1714.

126. Wirth, T., *Hypervalent Iodine Chemistry*. Springer: **2016**; Vol. 373, p 316.

127. Zhdankin, V., *Hypervalent Iodine Chemistry: Preparation, Structure, and Synthetic Applications of Polyvalent Iodine Compounds*. **2014**; p 1-468.

128. Moriarty, R. M.; Hu, H.; Gupta, S. C., *Tetrahedron Lett.* **1981,** *22*, 1283-1286.

129. Arava, S.; Kumar, J. N.; Maksymenko, S.; Iron, M. A.; Parida, K. N.; Fristrup, P.; Szpilman, A. M., *Angew. Chem. Int. Ed.* **2017,** *56*, 2599-2603.

130. Sanz-Marco, A.; Martinez-Erro, S.; Pauze, M.; Gómez-Bengoa, E.; Martín-Matute, B., *Nat. Commun.* **2019,** *10*, 5244.

131. Chengqun Chen, X. F., Guozhen Zhang, Qin Zhao, Guosheng Huang, *Synthesis.* **2008,** *20*, 3205-3208.

132. Cheng, G.-J.; Zhang, X.; Chung, L. W.; Xu, L.; Wu, Y.-D., *J. Am. Chem. Soc.* **2015,** *137*, 1706-1725.

133. Burke, K., *J. Chem. Phys.* **2012,** *136*, 150901.

134. Thomas, L. H., *Math. Proc. Cambridge Philos. Soc.* **1927,** *23*, 542-548.

135. Fermi, E., *Zeitschrift für Physik.* **1928,** *48*, 73-79.

136. Pople, J. A., *Angew. Chem. Int. Ed.* **1999,** *38*, 1894-1902.

137. Kohn, W., *Rev. Mod. Phys.* **1999,** *71*, 1253-1266.

138. Hohenberg, P.; Kohn, W., *Phys. Rev. Lett.* **1964,** *136,* B864-B871.

139. Kohn, W.; Sham, L. J., *Phys. Rev. Lett.* **1965,** *140*, A1133-A1138.

140. Frisch, M. J.; Trucks, G. W.; Schlegel, H. B.; Scuseria, G. E.; Robb, M. A.; Cheeseman, J. R.; Scalmani, G.; Barone, V.; Petersson, G. A.; Nakatsuji, H.; Li, X.; Caricato, M.; Marenich, A. V.; Bloino, J.; Janesko, B. G.; Gomperts, R.; Mennucci, B.; Hratchian, H. P.; Ortiz, J. V.; Izmaylov, A. F.; Sonnenberg, J. L.; Williams; Ding, F.; Lipparini, F.; Egidi, F.; Goings, J.; Peng, B.; Petrone, A.; Henderson, T.; Ranasinghe, D.; Zakrzewski, V. G.; Gao, J.; Rega, N.; Zheng, G.; Liang, W.; Hada, M.; Ehara, M.; Toyota, K.; Fukuda, R.; Hasegawa, J.; Ishida, M.; Nakajima, T.; Honda, Y.; Kitao, O.; Nakai, H.; Vreven, T.; Throssell, K.; Montgomery Jr., J. A.; Peralta, J. E.; Ogliaro, F.; Bearpark, M. J.; Heyd, J. J.; Brothers, E. N.; Kudin, K. N.; Staroverov, V. N.; Keith, T. A.; Kobayashi, R.; Normand, J.; Raghavachari, K.; Rendell, A. P.; Burant, J. C.; Iyengar, S. S.; Tomasi, J.; Cossi, M.; Millam, J. M.; Klene, M.; Adamo, C.; Cammi, R.; Ochterski, J. W.; Martin, R. L.; Morokuma, K.; Farkas, O.; Foresman, J. B.; Fox, D. J. *Gaussian 16 Rev. C.01*, Wallingford, CT, **2016**.

141. Weigend, F.; Ahlrichs, R., *Phys. Chem. Chem. Phys.* **2005,** *7*, 3297-3305.

142. Zhao, Y.; Truhlar, D. G., *Theor. Chem. Acc.* **2008,** *120*, 215-241.

143. Cances E, M. B., Tomasi J., *J. Chem. Phys.* **1997,** *107*, 3032-3041.

144. Cossi, M.; Barone, V.; Mennucci, B.; Tomasi, J., *Chem. Phys. Lett.* **1998,** *286*, 253-260.

145. Tomasi, J.; Mennucci, B.; Cancès, E., *J. Mol. Struct.* **1999,** *464*, 211-226.

146. Gonzalez, C.; Schlegel, H. B., *J. Phys. Chem. A.* **1990,** *94*, 5523-5527.

147. Allen, L. A. T.; Raclea, R.-C.; Natho, P.; Parsons, P. J., *Org. Biomol. Chem.* **2021,** *19*, 498-513.

148. Prasad, P. K.; Reddi, R. N.; Arumugam, S., *Org. Biomol. Chem.* **2018,** *16*, 9334-9348.

149. Rossi, S.; Puglisi, A.; Raimondi, L.; Benaglia, M., *ChemCatChem.* **2018,** *10*, 2717-2733.

150. Magano, J.; Dunetz, J. R., *Org Process Res Dev.* **2012,** *16*, 1156-1184.

151. Ghosh, A. K.; Brindisi, M., *J. Med. Chem.* **2015,** *58*, 2895-2940.

152. Chauhan, P.; Mahajan, S.; Enders, D., *Chem. Rev.* **2014,** *114*, 8807-8864.

153. Nobrega, J. A.; Gonçalves, S. M. C.; Peppe, C., *Synth. Commun.* **2002,** *32*, 3711-3717.

154. Kösel, T.; Dräger, G.; Kirschning, A., *Org. Biomol. Chem.* **2021,** *19*, 2907-2911.

155. Janey, J. M., *Angew. Chem. Int. Ed.* **2005,** *44*, 4292-4300.

156. Selig, P., *Angew. Chem. Int. Ed.* **2013,** *52*, 7080-7082.

157. Jia, H.; Häring, A. P.; Berger, F.; Zhang, L.; Ritter, T., *J. Am. Chem. Soc.* **2021,** *143*, 7623-7628.

158. Shang, M.; Wang, X.; Koo, S. M.; Youn, J.; Chan, J. Z.; Yao, W.; Hastings, B. T.; Wasa, M., *J. Am. Chem. Soc.* **2017,** *139*, 95-98.

159. Seebach, D.; Corey, E. J., *J. Org. Chem.* **1975,** *40*, 231-237.

160. Chen, Y.-L.; Hoppe, D., *J. Org. Chem.* **2009,** *74*, 4188-4194.

161. Miyata, O.; Miyoshi, T.; Ueda, M., *ARKIVOC.* **2012,** *2013*, 60-81.

162. Nandi, R. K.; Takeda, N.; Ueda, M.; Miyata, O., *Tetrahedron Lett.* **2016,** *57*, 2269-2272.

163. Koser, G. F.; Relenyi, A. G.; Kalos, A. N.; Rebrovic, L.; Wettach, R. H., *J. Org. Chem.* **1982,** *47*, 2487-2489.

164. Eleanor A. Merrit, B. O., *Synthesis.* **2011,** *4*.

165. Nicolaou, K. C.; Montagnon, T.; Ulven, T.; Baran, P. S.; Zhong, Y. L.; Sarabia, F., *J. Am. Chem. Soc.* **2002,** *124*, 5718-5728.

166. Moriarty, R. M.; Berglund, B. A.; Penmasta, R., *Tetrahedron Lett.* **1992,** *33*, 6065-6068.

167. Mizukami, F.; Ando, M.; Tanaka, T.; Imamura, J., *Bull. Chem. Soc. Jpn.* **1978,** *51*, 335-336.

168. Greaney, M. F.; Motherwell, W. B., *Tetrahedron Lett.* **2000,** *41*, 4463-4466.

169. Norrby, P.-O.; Petersen, T. B.; Bielawski, M.; Olofsson, B., *Chem. Eur. J.* **2010,** *16*, 8251-8254.

170. Zanka, A.; Takeuchi, H.; Kubota, A., *Org Process Res Dev.* **1998,** *2*, 270-273.

171. Charpentier, J.; Früh, N.; Togni, A., *Chem. Rev.* **2015,** *115*, 650-682.

172. Mizar, P.; Wirth, T., *Angew. Chem. Int. Ed.* **2014,** *53*, 5993-5997.

173. García-Vázquez, V.; Carretero Cerdán, A.; Sanz-Marco, A.; Gómez-Bengoa, E.; Martín-Matute, B., *Chem. Eur. J. 28*, e202201000.

174. Gonçalves, C. R.; Lemmerer, M.; Teskey, C. J.; Adler, P.; Kaiser, D.; Maryasin, B.; González, L.; Maulide, N., *J. Am. Chem. Soc.* **2019,** *141*, 18437-18443.

175. Zhu, C.; Zhang, Y.; Zhao, H.; Huang, S.; Zhang, M.; Su, W., *Adv. Synth. Catal.* **2015,** *357*, 331-338.

176. Blom, J.; Reyes-Rodríguez, G. J.; Tobiesen, H. N.; Lamhauge, J. N.; Iversen, M. V.; Barløse, C. L.; Hammer, N.; Rusbjerg, M.; Jørgensen, K. A., *Angew. Chem. Int. Ed.* **2019,** *58*, 17856-17862.

177. Chen, B.; Sun, H.-X.; Qin, J.-F.; Wang, B., *Tetrahedron Lett.* **2016,** *57*, 253-255.

178. Fernandes, R. A.; Gholap, S. P.; Mulay, S. V., *RSC Adv.* **2014,** *4*, 16438-16443.

179. Wang, B.; Sun, H.-X.; Sun, Z.-H., *J. Org. Chem.* **2009,** *74*, 1781-1784.

180. Hillier, M. C.; Meyers, A. I., *Tetrahedron Lett.* **2001,** *42*, 5145-5147.

181. Pu, Q.; Tang, X.; Gao, L.; Song, Z., *Org. Chem. Front.* **2018,** *5*, 2035-2039.

182. Kelly, S. S.; Shen, T.-L.; Xian, M., *Org. Lett.* **2021,** *23*, 3741-3745.

183. Hu, T.; Huang, L.; Gao, L.; Song, Z., *Org. Chem. Front.* **2020,** *7*, 543-547.

184. Wang, Y.; Su, P., *ACS Omega.* **2020,** *5*, 21862-21872.

185. Catalano, L.; Cavallo, G.; Metrangolo, P.; Resnati, G.; Terraneo, G., *Top. Curr. Chem.* **2016,** *373*, 289-309.

186. Brandt, D.; Bellosta, V.; Cossy, J., *Org. Lett.* **2012,** *14*, 5594-5597.

187. Zhang, M.; Jiang, H.-F.; Neumann, H.; Beller, M.; Dixneuf, P. H., *Angew. Chem. Int. Ed.* **2009,** *48*, 1681-1684.

188. Barluenga, J.; Fañanás, F. J.; Sanz, R.; García, F.; García, N., *Tetrahedron Lett.* **1999,** *40*, 4735-4736.

189. Dalko, P. I.; Moisan, L.; Cossy, J., *Angew. Chem. Int. Ed.* **2002,** *41*, 625-628.

190. Peter J. Belshaw, S. D. M., Donna D. Johnson, Daniel Romo, Yoshihara Ikeda, Merritt Andrus, David G. Alberg, L. Wayne Schultz, Jon Clardy, Stuart L. Schreiber., *Synlett.* **1994,** *6*.

191. Green, R. H.; Lambeth, P. F., *Tetrahedron.* **1983,** *39*, 1687-1721.

192. Cherkaoui, H.; Soufiaoui, M.; Grée, R., *Tetrahedron.* **2001,** *57*, 2379-2383.

193. Suchand, B.; Satyanarayana, G., *Eur. J. Org. Chem.* **2017,** *2017*, 3886-3895.

194. Férey, G.; Mellot-Draznieks, C.; Serre, C.; Millange, F.; Dutour, J.; Surblé, S.; Margiolaki, I., *Science.* **2005,** *309*, 2040-2.

195. Férey, G.; Serre, C.; Mellot-Draznieks, C.; Millange, F.; Surblé, S.; Dutour, J.; Margiolaki, I., *Angew. Chem. Int. Ed.* **2004,** *43*, 6296-6301.

196. Mellot Draznieks, C.; Newsam, J. M.; Gorman, A. M.; Freeman, C. M.; Férey, G., *Angew. Chem. Int. Ed.* **2000,** *39*, 2270-2275.

197. Mellot-Draznieks, C.; Girard, S.; Férey, G., *J. Am. Chem. Soc.* **2002,** *124*, 15326-15335.

198. Surblé, S.; Serre, C.; Mellot-Draznieks, C.; Millange, F.; Férey, G., *Chem. Commun.* **2006**, 284-286.

199. Lin, Y.; Kong, C.; Chen, L., *RSC Adv.* **2012,** *2*, 6417-6419.

200. Babaee, S.; Zarei, M.; Sepehrmansourie, H.; Zolfigol, M. A.; Rostamnia, S., *ACS Omega.* **2020,** *5*, 6240-6249.

201. Khan, N. A., Kang, I.J., Seok, H., Jhung, S. H., *Chem. Eng. J.* **2011,** *166*, 1152.

202. Jhung, S. H.; Lee, J.-H.; Yoon, J. W.; Serre, C.; Férey, G.; Chang, J.-S., *Adv. Mater.* **2007,** *19*, 121-124.

203. Bernt, S.; Guillerm, V.; Serre, C.; Stock, N., *Chem. Commun.* **2011,** *47*, 2838-2840.

204. Wen, M.; Mori, K.; Kamegawa, T.; Yamashita, H., *Chem. Commun.* **2014,** *50*, 11645-11648.

205. Carson , F.; Pascanu , V.; Bermejo Gómez , A.; Zhang , Y.; Platero-Prats , A. E.; Zou , X.; Martín-Matute , B., *Chem. Eur. J.* **2015,** *21*, 10896-10902.

206. Jiménez, J.-R.; Doistau, B.; Poncet, M.; Piguet, C., *Coord. Chem. Rev.* **2021,** *434*, 213750.

207. Tian, N.; Jia, Q.; Su, H.; Zhi, Y.; Ma, A.; Wu, J.; Shan, S., *J. Porous Mater.* **2016,** *23*, 1269-1278.

208. Schaate, A.; Roy, P.; Godt, A.; Lippke, J.; Waltz, F.; Wiebcke, M.; Behrens, P., *Chem. Eur. J.* **2011,** *17*, 6643-6651.

209. Zahn, G.; Zerner, P.; Lippke, J.; Kempf, F. L.; Lilienthal, S.; Schröder, C. A.; Schneider, A. M.; Behrens, P., *CrystEngComm.* **2014,** *16*, 9198-9207.

210. Núñez, M. G.; Farley, A. J. M.; Dixon, D. J., *J. Am. Chem. Soc.* **2013,** *135*, 16348-16351.

211. Gerard P. Robertson, A. J. M. F., Darren J. Dixon, *Synlett.* **2016,** *27*, 21-24.

212. Cavka, J. H.; Jakobsen, S.; Olsbye, U.; Guillou, N.; Lamberti, C.; Bordiga, S.; Lillerud, K. P., *J. Am. Chem. Soc.* **2008,** *130*, 13850-13851.

213. Katz, M. J.; Brown, Z. J.; Colón, Y. J.; Siu, P. W.; Scheidt, K. A.; Snurr, R. Q.; Hupp, J. T.; Farha, O. K., *Chem. Commun.* **2013,** *49*, 9449-9451.

214. Ding, L.-G.; Yao, B.-J.; Jiang, W.-L.; Li, J.-T.; Fu, Q.-J.; Li, Y.-A.; Liu, Z.-H.; Ma, J.-P.; Dong, Y.-B., *Inorg. Chem.* **2017,** *56*, 2337-2344.

215. Kaur, G.; Øien-Ødegaard, S.; Lazzarini, A.; Chavan, S. M.; Bordiga, S.; Lillerud, K. P.; Olsbye, U., *Cryst. Growth Des.* **2019,** *19*, 4246-4251.

216. Rodima, T.; Kaljurand, I.; Pihl, A.; Mäemets, V.; Leito, I.; Koppel, I. A., *J. Org. Chem.* **2002,** *67*, 1873-1881.

I

An Expedient Method for the Umpolung Coupling of Enols with Heteronucleophiles**

Víctor García-Vázquez[+],[a] Alba Carretero Cerdán[+],[a, b] Amparo Sanz-Marco[+],[a] Enrique Gómez-Bengoa,[b] and Belén Martín-Matute*[a]

Abstract: In this paper, we present an unprecedented and general umpolung protocol that allows the functionalization of silyl enol ethers and of 1,3-dicarbonyl compounds with a large range of heteroatom nucleophiles, including carboxylic acids, alcohols, primary and secondary amines, azide, thiols, and also anionic carbamates derived from CO_2. The scope of the reaction also extends to carbon-based nucleophiles. The reaction relies on the use of 1-bromo-3,3-dimethyl-1,3-dihydro-1λ^3[d][1,2]iodaoxole, which provides a key α-brominated carbonyl intermediate. The reaction mechanism has been studied experimentally and by DFT, and we propose formation of an unusual enolonium intermediate with a halogen-bonded bromide.

Introduction

The introduction of functional groups at the α carbon of carbonyl compounds is a common transformation in synthetic organic chemistry. α-Functionalized ketones are substructures found in many natural products, pharmaceuticals, and other functional organic compounds.[1] The functionalization reaction relies on the inherent nucleophilicity of the α carbon of the enol (or enolate) derivative of the carbonyl compound, which reacts with an electrophilic reaction partner in this process. Many carbon-based electrophiles can be used, leading to the formation of C—C bonds,[2] but the use of heteroatom electrophiles becomes challenging. This is due to the high reactivity, and therefore limited functional-group compatibility of these species. They are typically strong oxidants, and this can lead to the formation of by-products, such as overfunctionalized or oxidized compounds.[3] The structural variety of these species is also limited, and it is difficult to reconcile this with the idea of

producing structurally diverse target compounds. Nevertheless, there are a number of heteroatom electrophiles that can be used in such reactions, designed for specific transformations and with specific functional-group tolerances.[4] Alternatively, organocatalytic methods have overcome some of these difficulties.[5]

An alternative approach is to use nucleophiles rather than electrophiles to react with enol derivatives. Iodine(III) compounds have been used in this context to mediate the coupling of the two nucleophilic reactants through two-electron oxidations, thereby inverting the polarity of one of the reagents.[6] This strategy has recently been termed "cross-nucleophile coupling".[7] This area has evolved significantly[8] since the first report.[9] When it comes to heteroatom nucleophiles, the reaction usually requires a Lewis acid, as well as a low reaction temperature, in a one-pot two-step procedure, to avoid formation of by-products (Figure 1a).[10] First the I(III) reagent and the enol derivative react at low temperature to form an enolonium intermediate.[10a] This ensures that the enol nucleophile is consumed before the second nucleophile is added at higher temperature (Figure 1a). In this way, side reactions such as homocoupling of the enol derivative or α-functionalization with other nucleophiles derived from the I(III) reagent (e.g., OAc) are minimized.[10a] Using this protocol, Szpilman et. al elegantly observed O-enolonium species for the first time using ^{13}C NMR spectroscopy.[10a] The formation of by-products is closely related to the outstanding leaving ability of the I(III) functional group (10^6 better than triflate).[11]

In general, the nature of the second nucleophile is somewhat limited, but excellent results have been reported for arylations,[10b,c,e,12] azidations,[8c] cyanations,[8b] and acetoxylations.[8d,9,13] The somewhat narrow scope is partly due to the fact that the nucleophile may need to be incorporated into the structure of the I(III) reagent.[8b,12–14] General methods for the intermolecular reaction of ketones or enol derivatives with a variety of nucleophiles, using a non-designer I(III) reagent, are scarce. The Wirth group developed an effective

[a] V. García-Vázquez,[+] A. Carretero Cerdán,[+] Dr. A. Sanz-Marco,[+] Prof. B. Martín-Matute
Department of Organic Chemistry
Stockholm University
Stockholm, 10691 (Sweden)
E-mail: belen.martin.matute@su.se

[b] A. Carretero Cerdán,[+] Prof. E. Gómez-Bengoa
Departamento de Química Orgánica I
Universidad Pais Vasco, UPV/EHU
20080, Donostia-San Sebastián (Spain)

[+] These authors contributed equally to this manuscript.

Chem. Eur. J. **2022**, *28*, e202201000 (1 of 10)

© 2022 The Authors. Chemistry - A European Journal published by Wiley-VCH GmbH

Chemistry–A European Journal

Research Article
doi.org/10.1002/chem.202201000

Chemistry Europe
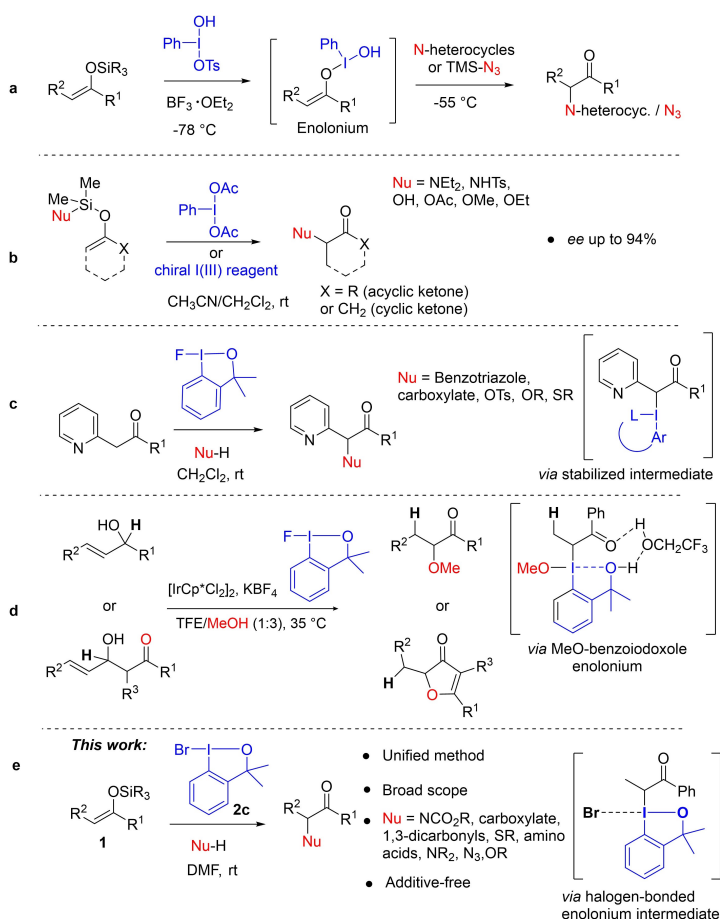European Chemical
Societies Publishing

Figure 1. Strategies for the umpolung α-functionalization of ketones and enol derivatives. a) Cross-nucleophile coupling of silyl enol ethers with nitrogen nucleophiles.[8c] b) Intramolecular cross-nucleophile coupling of nucleophile-functionalized silyl enol ethers.[8a] c) Cross-nucleophile coupling of pyridyl ketones.[14] d) Cross-coupling of allylic alcohols with nucleophiles.[16] e) This work: general method for the cross-nucleophile coupling of silyl enol ethers with nucleophiles.

approach to the formation of nitrogen- and oxygen-α-substituted ketones through an internal umpolung strategy mediated by PhI(OAc)$_2$ (Figure 1b).[8a] Their strategy relied on the use of a tethered nucleophile, i.e., the nucleophile was attached to the silicon center of the enol ether substrate (Figure 1b). Importantly, they were able to extend the scope of the reaction to the synthesis of chiral α-substituted ketones when using chiral I(III) reagents. More recently, the Gulder group reported another elegant approach aimed at expanding the range of nucleophiles that can be used in such reactions. Here, 2-pyridyl ketones react by an umpolung coupling process mediated by a λ³-fluoro iodane (Figure 1c).[15] It was proposed that a noncovalent interaction between the F atom in the iodane and the pyridine moiety in the ketone substrate plays a key role in this reaction. Although this reaction is quite limited in terms of the ketone structure, a large number of nucleophiles could be coupled.

Considering the ketone component, the majority of reported examples, with the exception of the pyridyl ketones used by Gulder,[15] rely on the use of silyl enol ethers.[8a–c,e,10a,b,e] Our own group contributed to this area of research with an umpolung protocol using allylic alcohols as enol synthons, in a reaction mediated by iridium catalysts (Figure 1d). This method gave α-methoxy ketones from allylic alcohols, or 3(2H)-furanones from carbonyl-functionalized allylic alcohols. For all the examples, 1-fluoro-3,3-dimethyl-1,3-dihydro-1λ³-benzo[d][1,2]iodaoxole was used as an oxidant.[16]

Chem. Eur. J. **2022**, *28*, e202201000 (2 of 10)

© 2022 The Authors. Chemistry - A European Journal published by Wiley-VCH GmbH

Chemistry–A European Journal

Research Article
doi.org/10.1002/chem.202201000

Chemistry Europe
European Chemical
Societies Publishing

In this paper, we report the results of our investigations into the development of a method for the general reaction of unbiased silyl enol ethers (**1**) with a wide variety of hetero-nucleophiles, including carboxylic acids, thiols, alcohols, amines, azides, and even CO_2 in the form of carbamate anions for the first time. Conveniently, in all instances, the same I(III) reagent is used. Thus the synthesis of substrate-specific iodanes is avoided, which contributes to the generality and applicability of the method. The mechanism of the reaction has been studied experimentally and by DFT calculations, and an unusual enolonium intermediate with a halogen-bonded bromide atom is proposed. From this enolonium, an α-brominated carbonyl intermediate is formed, which is key for the high efficiency and the broad scope of the umpolung reaction.

Results and Discussion

Initially, we focused on the coupling of silyl ethers (**1**) and CO_2 derivatives, by using carbamates formed in situ from amines (**3**) and CO_2. This umpolung strategy would give access to α-carbamoyl carbonyl compounds, which are important scaffolds in medicinal chemistry.[17] Reported methods for the synthesis of α-carbamoyl carbonyl compounds from CO_2 are very scarce, and typically require the use of high pressures of CO_2 and high temperatures.[18] We started by generating carbamate anions by treating amine **3** with NaH under 1 atm of CO_2, a modification of a procedure described by Trost for the synthesis of carbonates.[19] A variety of hypervalent iodine reagents (**2a–f**)
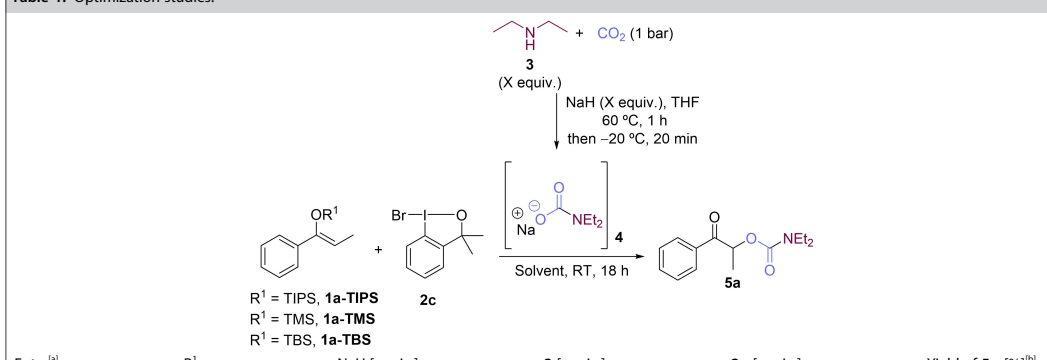
were tested (Scheme 1) for the coupling of silyl enol ether **1a**-TIPS with carbamate **4**. Surprisingly, only those benzoiodoxoles bearing a halide atom on the I(III) (**2a**, **2c**, and **2d**) yielded some amounts of α-carbamoyl carbonyl product **5a**. Of these, it was 1-bromo-3,3-dimethyl-1,3-dihydro-1λ,3[d][1,2]iodaoxole (**2c**) that gave the best result (27% yield of **5a**). Togni reagent **2b**, commonly used in radical additions of CF_3,[20] left the starting silyl enol ether **1a**-TIPS untouched. The use of Koser's reagent **2e** led to the formation of by-products, and with phenyl-λ3-iodanediyl diacetate (PIDA) (**2f**) again the starting enol ether **1a**-TIPS was recovered.

Further optimizations were carried out with reagent **2c** (Table 1). When the number of equiv. of NaH was lowered to 1.5, the yield increased substantially (59%, Table 1, entry 3 vs. entries 1–2). Lowering the amount of NaH further, or lowering the amount of amine **3** did not have a significant effect on the yield (Table 1, entries 4 and 5). On the other hand, with 1.5 equiv. of **2c**, a yield of 68% was obtained (Table 1, entry 6). Importantly, when the triisopropylsilyl group (TIPS, **1a**-TIPS) was replaced by a *tert*-butyldimethylsilyl group (**1a**-TBS, Table 1, entry 7), product **5a** was obtained in 77% yield. The less hindered trimethylsilyl group (**1a**-TMS, Table 1, entry 8) gave a lower yield. We also tested toluene, THF, 2-meth-yltetrahydrofuran, and acetone as reaction solvents, but the desired product was not observed (Table 1, entry 9).

We then applied the optimal conditions (Table 1, entry 7) to a number of TBS-enol ethers (Scheme 2a). With electron-donating groups at the *para* position of the aryl group at R^1, the corresponding carbamates **5b** and **5c** were obtained with high
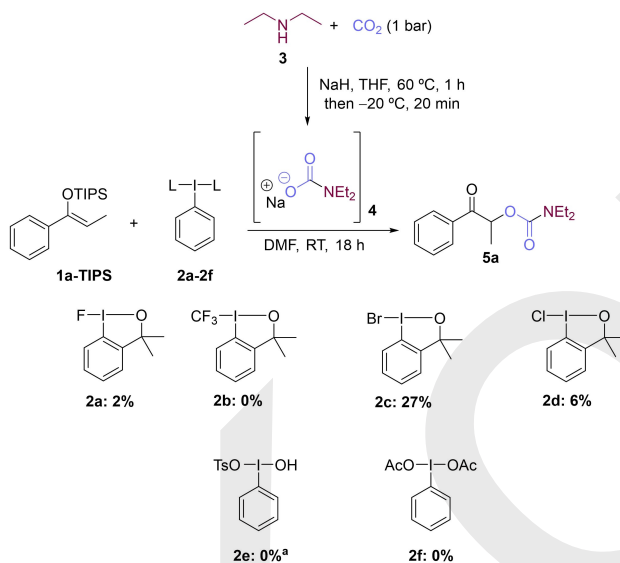
Scheme 1. Screening of hypervalent iodine(III) reagents. Reaction conditions: **1a**-TIPS (0.1 mmol, 1 equiv.), **3** (0.2 mmol, 2 equiv.), iodine(III) reagent **2** (0.12 mmol, 1.2 equiv.), NaH (0.3 mmol, 3 equiv.), DMF (0.33 M), RT, CO_2 (1 bar), 18 h. Yields determined by ^{1}H NMR spectroscopy using 2,3,5,6-tetrachlorobenzene as internal standard. [a] Various products observed.

Chemistry–A European Journal

Research Article
doi.org/10.1002/chem.202201000

Chemistry Europe
European Chemical
Societies Publishing

Table 1. Optimization studies.[a]

Entry[a]	R^1	NaH [equiv.]	3 [equiv.]	2c [equiv.]	Yield of 5a [%][b]
1	TIPS	3	2	1.2	27
2	TIPS	2	2	1.2	43
3	TIPS	1.5	2	1.2	59
4	TIPS	1	2	1.2	51
5	TIPS	1.5	1.5	1.2	43
6	TIPS	1.5	2	1.5	68
7	TBS	1.5	2	1.5	77
8	TMS	1.5	2	1.5	52
9[c]	TBS	1.5	2	1.5	–

[a] Reaction conditions: 1 (0.1 mmol, 1 equiv.) DMF (0.33 M), RT, CO$_2$ (1 bar). [b] Yields determined by ^{1}H NMR spectroscopy using 2,3,5,6-tetrachlorobenzene (0.1 mmol, 1 equiv.) as an internal standard. [c] In toluene, THF, 2-methyltetrahydrofuran, or acetone (0.33 M).
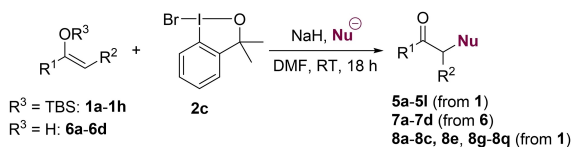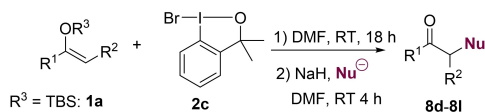
efficiency (80% and 60% yields, respectively). Also, F-substituted silyl enol ether **2d** gave **5d** in 52% yield. Thiophene **1e** gave the corresponding carbamate **5e** in a good yield of 64%. Unsuccessful examples are shown in Scheme S5. Thus, with an ethyl group at R^2, **5f** was obtained in a lower yield (49%). For aliphatic *tert*-butyldimethylsilyl enol ethers **1g** and **1h**, yields of 51% and 46%, respectively, were obtained. To assess the generality of the reaction, we tested different secondary amines to form the carbamate. Symmetrically and unsymmetrically substituted dialkyl amines reacted smoothly to give good yields (**5i–5k**, 60%–80%). Moreover, pyrrolidine substituted carbamate **5l** was also obtained under the reaction conditions in 58% yield. However, carbamates derived from primary amines gave a mixture of unidentified products (not shown), which represents a major limitation of this approach. Significantly, this umpolung strategy is not limited to silyl enol ethers, but could be extended to the use of 1,3-dicarbonyl compounds. A β-ketoester **6a** reacted smoothly under the same conditions to give **7a** in 82% yield. 1,3-Dicarbonyl compound **6b** reacted with carbamate **4** to give **7b** in good yield (56%). The less nucleophilic β-amidoester **6c** and malonate **6d** gave carbamoyl derivatives **7c** and **7d** in good yields (68% and 78%, respectively).

We went on to examine the generality of the cross-nucleophile coupling of silyl enol ethers with a variety of other nucleophiles (Scheme 2b and c). Using both electron-poor and electron-rich benzoic acids as nucleophiles, α-carboxylate-carbonyl compounds **8a–8c** were obtained in excellent yields (80%–98%). W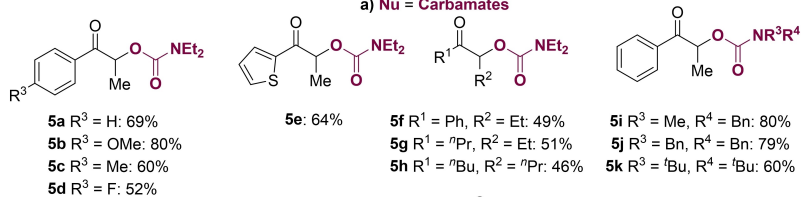hen alcohols were tested as nucleophiles under otherwise identical reaction conditions, complex mixtures of unidentified by-products were formed. However, these difficulties were overcome by modifying the protocol; first silyl enol ether **1a** was treated with I(III) reagent **2c**. This was followed by the addition of the alcohol nucleophile (Method B). Using this procedure, α-phenolate **8d** was obtained in 66% yield. Thiols were also well tolerated, and thiophenol gave **8e** in 60% yield using the standard procedure described above (i.e., Method A), and in 82% yield using Method B. An alkyl-substituted thiol gave a quantitative yield (**8f**, Method B). Importantly, primary amines are also well tolerated, and benzylamine derivative **8g** was obtained in 67% yield when using Method B. Cyclopropyl-amine reacted smoothly to give **8h** in 40% yield, which could be improved to 60% by using Method B. Piperidine gave α-aminoketone **8i** in 53% yield, and morpholine derivative **8j** was obtained in 60% yield. Interestingly, carbon nucleophiles such as malonates also reacted smoothly, and **8k** was formed in 50% yield. α-Azido carbonyl compound **8l** was obtained in 50% isolated yield.

We went on to test a number of natural products and pharmaceuticals as nucleophiles in the reaction with **1a-TBS**. These compounds all contained carboxylic acid moieties in their structures (Scheme 2c). A BOC-protected glycine derivative gave **8m** in 55% yield. With biotin as the nucleophile, compound **8n** was obtained in 44% yield. Acetyl salicylic acid gave **8o** in quantitative yield (98% isolated yield), and ibuprofen gave **8p** in 87% yield. With the aliphatic oleic acid, **8q** was formed in 70% yield.

Chem. Eur. J. **2022**, *28*, e202201000 (4 of 10)

© 2022 The Authors. Chemistry - A European Journal published by Wiley-VCH GmbH

Chemistry–A European Journal

Research Article
doi.org/10.1002/chem.202201000

Chemistry
Europe
European Chemical
Societies Publishing
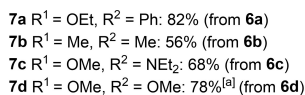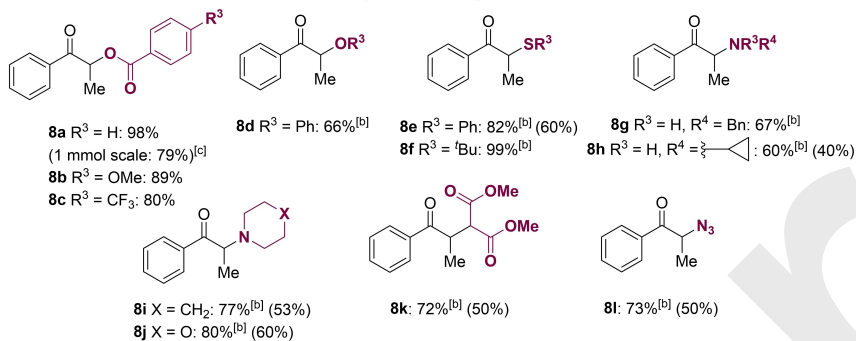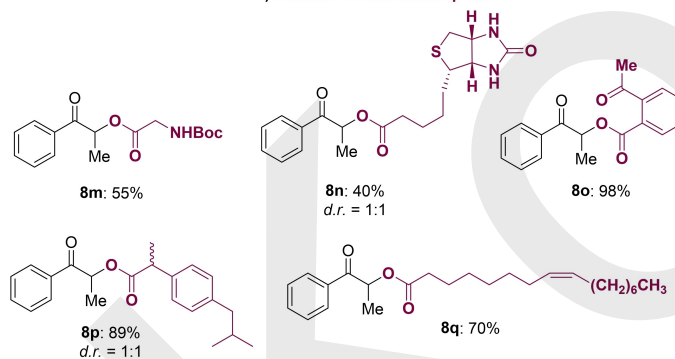
Scheme 2. Substrate scope. Method A: **1a**–**1h** or **6a**–**6d** (0.1 mmol, 1 equiv.), **2c** (0.15 mmol, 1.5 equiv.), NaH (0.15 mmol, 1.5 equiv.), nucleophile (0.2 mmol, 2 equiv.), DMF (0.33 M or 0.1 M), RT, 18 h. Isolated yields. [a]:1-bromo-3,3-bis(trifluoromethyl)-1,3-dihydro-1λ³-benzo[d][1,2]iodaoxole (**2c′**). [b]: Method B: **1a** (0.1 mmol, 1 equiv.), **2c** (0.15 mmol, 1.5 equiv.), DMF (0.1 M), RT, 18 h. After completion, NaH (0.15 mmol, 1.5 equiv.) and nucleophile (0.2 mmol, 2 equiv.) were added. [c]: 1 mmol scale.

Chemistry–A European Journal

Research Article
doi.org/10.1002/chem.202201000

Chemistry Europe
European Chemical
Societies Publishing

Next, we focused our attention on studying the mechanism of the reaction. In an attempt to understand the dramatic effect of DMF as the reaction solvent, a variety of other polar aprotic solvents were tested. When the reaction of **1a**, CO_2, and diethylamine with **2c** was run in MeCN, 2-bromo-1-phenyl-propan-1-one (**9**) was detected as the sole product (Scheme 3a). α-Bromo carbonyl compound **9** was also formed from **1a** and **2c** when the reaction was run in DMF in the absence of the nucleophile, in quantitative yield (Scheme S2b). We found that α-bromo carbonyl derivative **9** reacted with the carbamate anion to give **5a** in quantitative yield (Scheme S3). Therefore, it is reasonable to suggest that the reaction might proceed by umpolung bromination followed by a nucleophilic substitution step with the second nucleophile, in this instance the carbamate generated from CO_2. The formation of α-substituted carbonyl derivatives as intermediates that can react with nucleophiles in S_N2-type reactions has been previously studied by Maulide[21] and Jorgensen[22] among others,[23] as a way to circumvent the inconvenience of using electrophilic reactants. Therefore, **2c** seems to be an unusually mild brominating agent for the bromination of silyl enol ethers and 1,3-dicarbonyl compounds. Other brominating agents such as NBS or Br_2 lead to formation of polybrominated products in their reactions with silyl enol ethers.[24] Moreover, the low compatibility of NBS or

Br_2 with functional groups such as alkynes, alkenes, and electron-rich aromatics hinders their use in the direct α-functionalization of enol derivatives with nucleophiles in a single umpolung step, resulting in a limited scope, and requiring multiple purification steps.[21] Not even with simple unfunctionalized substrates these brominating agents afforded results comparable to those obtained with **2c** (Scheme S4). Therefore, the use of the mild brominating agent **2c** is key for this successful umpolung coupling. Note also that **2c** is compatible with unsaturated functional groups, such as the double bond in **8q**.

In the presence of radical scavengers, silyl enol ether **1a** gave **5a** in yields similar to those obtained in their absence (Scheme 3c and d vs. Scheme 2), suggesting a non-radical pathway. We then tested the selectivity of the reaction towards the formation of α-bromoketone **9** by adding OH^-, as another potential nucleophile, to the reaction mixture (Scheme 3e). It has been shown before that water is able to displace I(III) in the enolonium intermediates, and form α-hydroxy ketones (i.e., **10**). However, when adding a large excess of OH^-, under otherwise identical reactions conditions, only α-bromoketone **9** was formed in 99% yield.

To further understand the mechanism of the cross-nucleo-phile-coupling reaction mediated by bromobenzoidoxole **2c**,
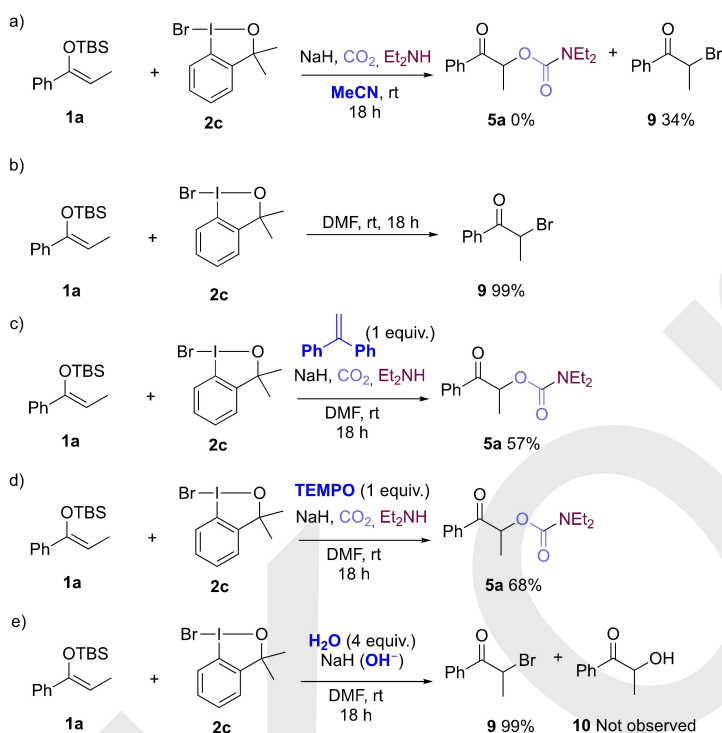
Scheme 3. Control experiments and mechanistic investigations.

Chemistry–A European Journal

Research Article
doi.org/10.1002/chem.202201000

Chemistry Europe
European Chemical
Societies Publishing

we turned to DFT calculations at the B3LYP[25] and M06[26] functional levels using the Gaussian 16 software[27] (see Supporting Information for more details). The calculations were initiated from enolate **I** as the model substrate. Formation of **I** from silyl enol ether **1 c** is likely to occur under basic conditions and in DMF, in agreement with previous reports[28] Additionally, oxygen-oxygen silyl transfer reactions have also been observed in intramolecular process,[29] so it is reasonable to propose that a similar process can be operating between **1 a** and the oxygen atom of **2 c** (see Scheme S6). Therefore, the calculations were carried out using the sum of the energies of enolate species[12] **I**

and iodine(III) reagent **2 c** as the reference point (G = 0 kcal/mol) of the energy profile (Figure 2, middle). The enolate can attack the iodine atom either through the oxygen or through the carbon of the enolate, leading to formation of at least three possible low-energy enolonium intermediates (**O-enolonium-II** (-2.0 kcal/mol), **C-enolonium-II** (− 3.0 kcal/mol), and **C-enolo-nium-II'** (0.2 kcal/mol). In all cases, the formation of the enolate-iodine bond occurs in the position *trans* to the phenyl-I substituent, inducing an elongation of the Br—I bond. In the starting compound **2 c**, the Br—I bond is short, i.e., 2.9 Å. This bond length is increased in **O-enolonium-II** (3.17 Å), and even
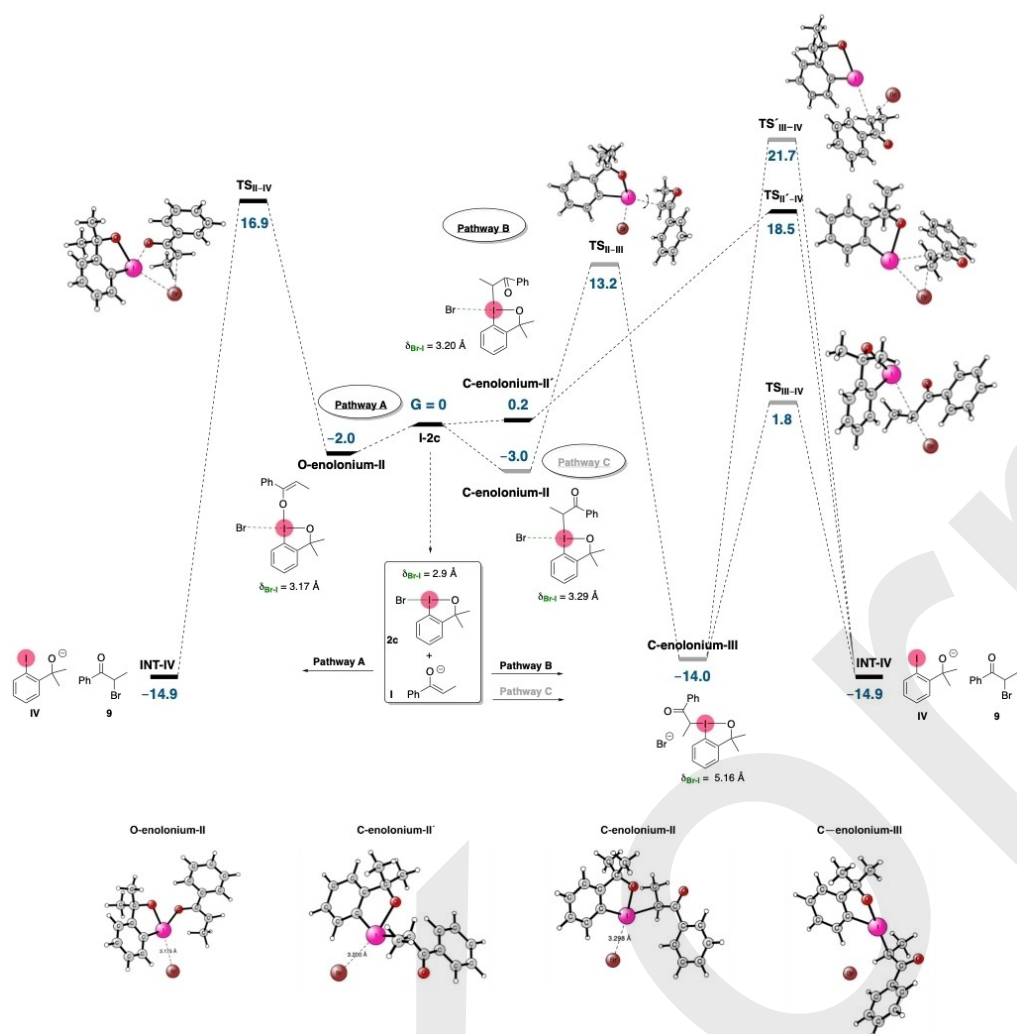

Figure 2. Top: Reaction mechanisms for the umpolung cross-nucleophile coupling of enol derivatives mediated by hypervalent iodine(III) reagent **2 c**. Values are given in kcal/mol. Bottom: 3-D Structures of enolonium intermediates.

Chem. Eur. J. **2022**, *28*, e202201000 (7 of 10)

© 2022 The Authors. Chemistry - A European Journal published by Wiley-VCH GmbH

Chemistry–A European Journal

Research Article
doi.org/10.1002/chem.202201000

Chemistry Europe
European Chemical
Societies Publishing

more so in **C-enolonium-II'** (3.20 Å) and **C-enolonium-II** (3.29 Å). These distances are similar to those found in structures with a halogen bond between iodine and bromine atoms.[30] The three calculated intermediates are almost isoenergetic and they could, therefore, be in equilibrium. The direct reductive ligand coupling of the bromine and enolate fragments of these enolonium intermediates was calculated to be feasible. For example, **TS$_{II-IV}$** and **TS$_{II'-IV}$** have calculated activation energies of 18–19 kcal/mol from their respective enolonium intermediates, **O-enolonium-II** (-2.0 kcal/mol) and **C-enolonium-II'** (0.2 kcal/mol). Interestingly, a transition state was found for the isomerization of the enolate substituent, which rotates from the *trans* to the *cis* position relative to the phenyl-I bond, displacing the bromine atom from the coordination sphere of the iodine. This transition state (**TS$_{II-III}$**, $\Delta\Delta G^{\ddagger} = 16.2$ kcal/mol) is low in energy, and leads to enolonium intermediate **C-enolonium-III**. From here, backside attack by the bromide (**TS$_{III-IV}$**) on the α-carbon in **C-enolonium-III** has the lowest calculated energy for C–Br formation ($\Delta\Delta G^{\ddagger} = 15.8$ kcal/mol). In contrast, the *syn* attack represented by **TS'$_{III-IV}$** is too high energy to take place under these reaction conditions ($\Delta\Delta G^{\ddagger} = 35.7$ kcal/mol). Thus, our DFT calculations show that the formation of the α-bromo ketone intermediate **INT-IV** is feasible under the reaction conditions starting from the enolate and iodine(III) reagent **2c**. This pathway is possible in the absence of any external nucleophilic anion. After that, intermediate α-bromoketone **9** evolves via a nucleophilic displacement upon reaction with the heteronucleophiles (Scheme S2).

Both DFT calculations and experimental studies support the formation of α-bromoketone **9** as an important intermediate in this cross-nucleophile coupling. This umpolung event is mediated by benzoidoxole **2c**, and can occur by three possible mechanisms. Pathway A and pathway B are analogous mechanisms involving **O-enolonium-II** and **C-enolonium-II'**, respectively, in which bromide interacts with the I(III) through a halogen bond (3.17 and 3.20 Å, respectively).[28b] These species then undergo a reductive coupling step to give α-bromoketone **9**. These Br–I interactions might explain the lack of by-products. As mentioned above, the formation of by-products such as dimers (Nu^2 = **1**) or α-hydroxy ketones (Nu^2 = OH$^-$, Scheme 3e) has been a major limitation in similar I(III)-mediated umpolung approaches. We have also observed by-product formation when using other I(III) reagents, for example, with **2a** in our previous work,[16] and with **2e** in the optimization experiments described in this paper (Scheme 1). Alternatively, pathway C can occur via **C-enolonium-III**, which is formed by ligand rearrangement around the I(III) center of **C-enolonium-II**. In pathway C, the bromide is not interacting with the I(III) center (Br–I distance is 5.16 Å) of **C-enolonium-III**. From here, a nucleophilic attack of the Br$^-$ on the very electrophilic[11] α-C of **C-enolonium-III** also leads to α-bromoketone **9** (16.2 kcal/mol for isomerization and 15.8 kcal/mol for the S$_N$2 step). The DFT calculations do not show a strong preference for any of the three pathways explored. However, if **C-enolonium-III** is involved (pathway C), we would expect the highly electrophilic enolonium[11] (**C-enolonium-III**) to react also with any of the nucleophiles present in the reaction mixture, such as starting enol **1** or HO$^-$ (Scheme 3e) to form by-products. The control experiment in Scheme 3b also shows that α-bromoketone **9** is the sole product formed in the absence of the heteronucleophile (Nu^2). The absence of by-products may be explained through a reaction pathway in which an intramolecular reaction results in formation of the C–Br bond formation (pathways A and B), rather than through an intermolecular nucleophilic displacement of I(III) on the enolonium intermediates (pathway C).

Conclusion

We have developed an umpolung method for the cross-nucleophile coupling of enol derivatives with a variety of nucleophiles, using a single iodine(III) reagent. The reactions occur with good efficiency, and by-products are not formed. Using the method described here, CO_2 has been used, in the form of anionic carbamates, in their reaction with silyl enol ethers for the first time. Additionally, benzoic acids, alcohols, thiols, primary and secondary amines, malonate and an azide have been used as nucleophiles in the transformation. We have also used this approach to derivatize natural products and drugs. Compound **2c** has been demonstrated to be an efficient mild brominating agent that allows the umpolung functionalization of enol derivatives in a single step, with higher group functional tolerance than most common electrophilic brominating reagents. Mechanistic evidence and DFT calculations have shown that α-bromoketones are formed as reaction intermediates. DFT calculations indicate that the mechanism may proceed via enolonium species containing I–Br halogen bonds. This may be key for the generality and high selectivity of the reaction.

Experimental Section

General procedures for the cross-nucleophile-coupling reaction

Method A: A solution of the nucleophile (0.2 mmol, 2 equiv.) in DMF (0.33 mL or 1 mL, 0.33 M or 0.1 M of **1**) was added to a vial containing **1** (0.1 mmol, 1 equiv.), NaH (0.15 mmol, 1.5 equiv.), and **2c** (0.15 mmol, 1.5 equiv.). The reaction mixture was stirred at room temperature for 18 h. After this time, the mixture was extracted with EtOAc (3 × 5 mL). The organic phases were combined and washed with water three times. The organic phase was then dried (MgSO$_4$), and the solvent was evaporated under reduced pressure. The residue was purified by flash column chromatography using silica gel as the stationary phase, eluting with a pentane/EtOAc mixture (5 to 100% EtOAc), to give the desired products.

Method B: DMF (0.5 mL, 0.2 M) was added to a vial containing **1** (0.1 mmol, 1 equiv.) and **2c** (0.15 mmol, 1.5 equiv.). The reaction mixture was stirred at room temperature for 18 h. After this time, the formation of **9** was complete. A solution of the nucleophile (0.2 mmol, 2 equiv.) and NaH (0.15 mmol, 1.5 equiv.) in DMF (0.5 mL, to reach 0.1 M of **1**) was added to the mixture. The reaction mixture was stirred at room temperature for a further 4 h. After this time, the mixture was extracted with EtOAc (3 × 5 mL), and the organic phases were combined and washed with water several

times. The organic phase was then dried (MgSO₄), and the solvent was evaporated under reduced pressure. The residue was purified by flash column chromatography using silica gel as the stationary phase, eluting with a pentane/EtOAc mixture (5 to 100 % EtOAc), to give the desired products.

All other experimental data and characterization is provided in the Supporting Information and the raw data can be found at https://zenodo.org/record/6638288

Conflict of Interest

The authors declare no conflict of interest.

Data Availability Statement

The data that support the findings of this study are available in the supplementary material of this article.

[1] a) J. Magano, J. R. Dunetz, *Org. Process Res. Dev.* **2012**, *16*, 1156–1184; b) S. Rossi, A. Puglisi, L. Raimondi, M. Benaglia, *ChemCatChem* **2018**, *10*, 2717–2733; c) P. K. Prasad, R. N. Reddi, S. Arumugam, *Org. Biomol. Chem.* **2018**, *16*, 9334–9348; d) L. A. T. Allen, R.-C. Raclea, P. Natho, P. J. Parsons, *Org. Biomol. Chem.* **2021**, *19*, 498–513.

[2] a) R. Cano, A. Zakarian, G. P. McGlacken, *Angew. Chem. Int. Ed.* **2017**, *56*, 9278–9290; *Angew. Chem.* **2017**, *129*, 9406–9418; b) Y. Liu, S.-J. Han, W.-B. Liu, B. M. Stoltz, *Acc. Chem. Res.* **2015**, *48*, 740–751; c) D. A. Culkin, J. F. Hartwig, *Acc. Chem. Res.* **2003**, *36*, 234–245; d) Z.-T. He, J. F. Hartwig, *J. Am. Chem. Soc.* **2019**, *141*, 11749–11753; e) T. Hama, S. Ge, J. F. Hartwig, *J. Org. Chem.* **2013**, *78*, 8250–8266.

[3] a) E. Differding, G. M. Rüegg, R. W. Lang, *Tetrahedron Lett.* **1991**, *32*, 1779–1782; b) J. A. Nobrega, S. M. C. Gonçalves, C. Peppe, *Synth. Commun.* **2002**, *32*, 3711–3717; c) B. Sreedhar, P. Surendra Reddy, M. Madhavi, *Synth. Commun.* **2007**, *37*, 4149–4156; d) T. Kösel, G. Dräger, A. Kirschning, *Org. Biomol. Chem.* **2021**, *19*, 2907–2911.

[4] a) S. Stavber, M. Jereb, M. Zupan, *Synthesis* **2002**, *2002*, 2609–2615; b) T. Baumann, H. Vogt, S. Bräse, *Eur. J. Org. Chem.* **2007**, *2007*, 266–282; c) H. Jia, A. P. Häring, F. Berger, L. Zhang, T. Ritter, *J. Am. Chem. Soc.* **2021**, *143*, 7623–7628; d) J. M. Janey, *Angew. Chem. Int. Ed.* **2005**, *44*, 4292–4300; *Angew. Chem.* **2005**, *117*, 4364–4372; e) A. M. R. Smith, K. K. Hii, *Chem. Rev.* **2011**, *111*, 1637–1656.

[5] a) P. J. Chevis, S. G. Pyne, *Org. Chem. Front.* **2021**, *8*, 2287–2314; b) P. Chauhan, S. Mahajan, D. Enders, *Chem. Rev.* **2014**, *114*, 8807–8864; c) G. Cecere, C. M. König, J. L. Alleva, D. W. C. MacMillan, *J. Am. Chem. Soc.* **2013**, *135*, 11521–11524; d) B. List, *J. Am. Chem. Soc.* **2002**, *124*, 5656–5657.

[6] V. V. Zhdankin, P. J. Stang, *Chem. Rev.* **2008**, *108*, 5299–5358.

[7] A. Bauer, N. Maulide, *Chem. Sci.* **2021**, *12*, 853–864.

[8] a) P. Mizar, T. Wirth, *Angew. Chem. Int. Ed.* **2014**, *53*, 5993–5997; *Angew. Chem.* **2014**, *126*, 6103–6107; b) H. Jiang, H. Zhang, W. Xiong, C. Qi, W. Wu, L. Wang, R. Cheng, *Org. Lett.* **2019**, *21*, 1125–1129; c) A. A. More, G. K. Pathe, K. N. Parida, S. Maksymenko, Y. B. Lipisa, A. M. Szpilman, *J. Org. Chem.* **2018**, *83*, 2442–2447; d) B. Sundararaju, M. Achard, C. Bruneau, *Chem. Soc. Rev.* **2012**, *41*, 4467–4483; e) L. Jiang, Z. Wang, M. Armstrong, M. G. Suero, *Angew. Chem. Int. Ed.* **2021**, *60*, 6177–6184; *Angew. Chem.* **2021**, *133*, 6242–6249; f) E. A. Merritt, B. Olofsson, *Synthesis* **2011**, *2011*, 517–538; g) G. C. Geary, E. G. Hope, K. Singh, A. M. Stuart, *RSC Adv.* **2015**, *5*, 16501–16506; h) H. K. Minhas, W. Riley, A. M. Stuart, M. Urbonaite, *Org. Biomol. Chem.* **2018**, *16*, 7170–7173.

[9] M. Fujio, A. Moriyasu, T. Tatsuo, I. Juichi, *Bull. Chem. Soc. Jpn.* **1978**, *51*, 335–336.

[10] a) S. Arava, J. N. Kumar, S. Maksymenko, M. A. Iron, K. N. Parida, P. Fristrup, A. M. Szpilman, *Angew. Chem. Int. Ed.* **2017**, *56*, 2599–2603; *Angew. Chem.* **2017**, *129*, 2643–2647; b) S. Maksymenko, K. N. Parida, G. K. Pathe, A. A. More, Y. B. Lipisa, A. M. Szpilman, *Org. Lett.* **2017**, *19*, 6312–6315; c) J. Li, A. Bauer, G. Di Mauro, N. Maulide, *Angew. Chem. Int. Ed.* **2019**, *58*, 9816–9819; *Angew. Chem.* **2019**, *131*, 9921–9924; d) A. Bauer, G. Di Mauro, J. Li, N. Maulide, *Angew. Chem. Int. Ed.* **2020**, *59*, 18208–18212; *Angew. Chem.* **2020**, *132*, 18365–18369; e) B. S. Martins, D. Kaiser, A. Bauer, I. Tiefenbrunner, N. Maulide, *Org. Lett.* **2021**, *23*, 2094–2098; f) J. Borrel, J. Waser, *Org. Lett.* **2022**, *24*, 142–146.

[11] T. Okuyama, T. Takino, T. Sueda, M. Ochiai, *J. Am. Chem. Soc.* **1995**, *117*, 3360–3367.

[12] P.-O. Norrby, T. B. Petersen, M. Bielawski, B. Olofsson, *Chem. Eur. J.* **2010**, *16*, 8251–8254.

[13] a) M. Ochiai, Y. Takeuchi, T. Katayama, T. Sueda, K. Miyamoto, *J. Am. Chem. Soc.* **2005**, *127*, 12244–12245; b) T. Hokamp, T. Wirth, *Chem. Eur. J.* **2020**, *26*, 10417–10421.

[14] a) T. Nabana, H. Togo, *J. Org. Chem.* **2002**, *67*, 4362–4365; b) K. C. Nicolaou, T. Montagnon, T. Ulven, P. S. Baran, Y. L. Zhong, F. Sarabia, *J. Am. Chem. Soc.* **2002**, *124*, 5718–5728; c) M. Yoshida, K. Fujikawa, S. Sato, S. Hara, *Arkivoc* **2003**, *6*, 36–42; d) A. E. Allen, D. W. C. MacMillan, *J. Am. Chem. Soc.* **2010**, *132*, 4986–4987.

[15] G. M. Kiefl, T. Gulder, *J. Am. Chem. Soc.* **2020**, *142*, 20577–20582.

[16] A. Sanz-Marco, S. Martinez-Erro, M. Pauze, E. Gómez-Bengoa, B. Martín-Matute, *Nat. Commun.* **2019**, *10*, 5244.

[17] A. K. Ghosh, M. Brindisi, *J. Med. Chem.* **2015**, *58*, 2895–2940.

[18] a) Y. Peng, J. Liu, C. Qi, G. Yuan, J. Li, H. Jiang, *Chem. Commun.* **2017**, *53*, 2665–2668; b) E. Speckmeier, M. Klimkait, K. Zeitler, *J. Org. Chem.* **2018**, *83*, 3738–3745; c) H. Jiang, H. Zhang, W. Xiong, C. Qi, W. Wu, L. Wang, R. Cheng, *Org. Lett.* **2019**, *21*, 1125–1129.

[19] B. M. Trost, J. Xu, M. Reichle, *J. Am. Chem. Soc.* **2007**, *129*, 282–283.

[20] X. Wang, A. Studer, *Acc. Chem. Res.* **2017**, *50*, 1712–1724.

[21] C. R. Gonçalves, M. Lemmerer, C. J. Teskey, P. Adler, D. Kaiser, B. Maryasin, L. González, N. Maulide, *J. Am. Chem. Soc.* **2019**, *141*, 18437–18443.

[22] J. Blom, G. J. Reyes-Rodríguez, H. N. Tobiesen, J. N. Lamhauge, M. V. Iversen, C. L. Barløse, N. Hammer, M. Rusbjerg, K. A. Jørgensen, *Angew. Chem. Int. Ed.* **2019**, *58*, 17856–17862; *Angew. Chem.* **2019**, *131*, 18020–18026.

[23] C. Zhu, Y. Zhang, H. Zhao, S. Huang, M. Zhang, W. Su, *Adv. Synth. Catal.* **2015**, *357*, 331–338.

[24] a) Y. G. Lee, K. Ishimaru, H. Iwasaki, K. Ohkata, K. Akiba, *J. Org. Chem.* **1991**, *56*, 2058–2066; b) Y. Nakamura, Y. Ozeki, K. Uneyama, *J. Fluorine Chem.* **2008**, *129*, 274–279.

[25] A. D. Becke, *J. Chem. Phys.* **1993**, *98*, 5648–5652.

[26] Y. Zhao, D. G. Truhlar, *Theor. Chem. Acc.* **2008**, *120*, 215–241.

[27] Gaussian 16, Revision C.01, M. J. Frisch, G. W. Trucks, H. B. Schlegel, G. E. Scuseria, M. A. Robb, J. R. Cheeseman, G. Scalmani, V. Barone, G. A. Petersson, H. Nakatsuji, X. Li, M. Caricato, A. V. Marenich, J. Bloino, B. G. Janesko, R. Gomperts, B. Mennucci, H. P. Hratchian, J. V. Ortiz, A. F. Izmaylov, J. L. Sonnenberg, D. Williams-Young, F. Ding, F. Lipparini, F. Egidi, J. Goings, B. Peng, A. Petrone, T. Henderson, D. Ranasinghe, V. G. Zakrzewski, J. Gao, N. Rega, G. Zheng, W. Liang, M. Hada, M. Ehara, K. Toyota, R. Fukuda, J. Hasegawa, M. Ishida, T. Nakajima, Y. Honda, O. Kitao, H. Nakai, T. Vreven, K. Throssell, J. A. Montgomery, Jr., J. E. Peralta, F. Ogliaro, M. J. Bearpark, J. J. Heyd, E. N. Brothers, K. N. Kudin, V. N. Staroverov, T. A. Keith, R. Kobayashi, J. Normand, K. Raghavachari, A. P. Rendell, J. C. Burant, S. S. Iyengar, J. Tomasi, M. Cossi, J. M. Millam, M. Klene, C. Adamo, R. Cammi, J. W. Ochterski, R. L. Martin, K. Morokuma, O. Farkas, J. B. Foresman, D. J. Fox, Gaussian, Inc., Wallingford CT, **2016**.

[28] a) B. Wang, H.-X. Sun, Z. H. Sun, *J. Org. Chem.* **2009**, *74*, 1781–1784; b) R. A. Fernandes, S. P. Gholap, S. V. Mulay, *RSC Adv.* **2014**, *4*, 16438–

Chem. Eur. J. **2022**, *28*, e202201000 (9 of 10)

© 2022 The Authors. Chemistry - A European Journal published by Wiley-VCH GmbH

16443; c) B. Chen, H. -X. Sun, J. -F. Qin, B. Wang, *Tetrahedron Lett.* **2016**, *57*, 253–255.

[29] a) M. C. Hillier, A. I. Meyers, *Tetrahedron Lett.* **2001**, *42*, 5145–5147; b) Q. Pu, X. Tang, L. Gao, Z. Song, *Org. Chem. Front.* **2018**, *5*, 2035–2039; c) S. S. Kelly, T. -L. Shen, M. Xian, *Org. Lett.* **2021**, *23*, 3741–3745; d) T. Hu, L. Huang, L. Gao, Z. Song, *Org. Chem. Front.* **2020**, *7*, 543–547.

[30] a) L. Catalano, G. Cavallo, P. Metrangolo, G. Resnati, Halogen Bonding in Hypervalent Iodine Compounds. In Hypervalent Iodine Chemistry; Wirth, T., Ed.; Topics in Current Chemistry, Springer: Cham, Switzerland, **2016**, p. 289; b) Y. Wang, P. Su, *ACS Omega* **2020**, *5*, 21862–21872.

II

Base-Catalyzed [1,n]-Proton Shifts in Conjugated Polyenyl Alcohols and Ethers

Nagaraju Molleti,[†,⊥] Samuel Martinez-Erro,[†,⊥] Alba Carretero Cerdán,[†,‡] Amparo Sanz-Marco,[†] Enrique Gomez-Bengoa,[‡] and Belén Martín-Matute*,[†]

[†]Department of Organic Chemistry, Stockholm University, Stockholm SE-10691, Sweden

[‡]Department of Organic Chemistry I, Universidad País Vasco, UPV/EHU, 20080 San Sebastián, Spain

Ⓢ *Supporting Information*

ABSTRACT: The isomerization of dienyl alcohols and polyenyl alkyl ethers catalyzed by TBD (1,5,7-triazabicyclo[4.4.0]dec-5-ene) under metal-free conditions is presented. Two reaction pathways have been observed. For dienyl alcohols, the reaction proceeds by a [1,3]-proton shift to give γ,δ-unsaturated ketones exclusively. On the other hand, the reaction with polyenyl alkyl ethers gives the corresponding conjugated vinyl ethers in good yields (up to 85%), with regioselectivities up to >20:1. Experimental and computational investigations suggest that the mechanism proceeds through consecutive "chain-walking" proton shifts ("base walk") mediated by TBD.

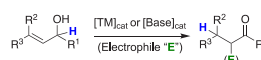**KEYWORDS:** base catalysis, mechanism, superbase, isomerization, proton shift, base walk
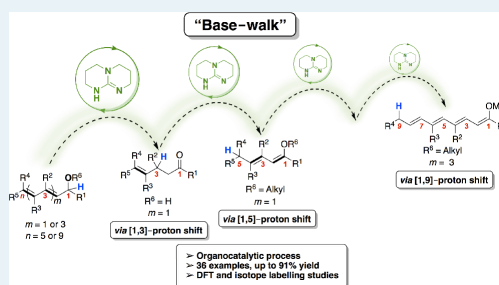
The isomerization of allylic alcohols into carbonyl compounds is a fundamental and powerful tool in organic synthesis. The reaction results in a functional-group interconversion; thus, allylic moieties may be treated as carbonyl equivalents.[1] Since the pioneering work of Logan et al.,[2a] some effort has gone into the development of more efficient catalytic systems for this transformation.[2,3] Our own group has reported the use of a family of complexes with the general structure [Cp*Ir(III)X] for the isomerization of primary and secondary allylic alcohols as well as for the synthesis of α-functionalized carbonyl compounds from allylic alcohols under very mild conditions (Scheme 1a).[4] Although the isomerization of allylic alcohols has traditionally been accomplished using metal catalysts, a few examples of transition-metal-free isomerizations are also known.[5] In 2016, we reported that the isomerization of electron-poor allylic alcohols and allylic ethers could be mediated by a simple base, 1,5,7-triazabicyclo[4.4.0]dec-5-ene (TBD), through a stereospecific [1,3]-proton shift (Scheme 1b).[6]
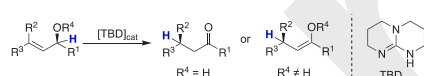
Extended conjugated systems such as dienyl alcohols and dienyl ethers (Scheme 1c) are common structural motifs in biologically active natural products.[7] Compounds containing these structures are also extensively used as key intermediates in organic synthesis.[8−11] Despite the importance of these structural motifs, their isomerization into carbonyl compounds or enol ethers has proved challenging. A reason for this is that transition-metal-catalyzed approaches are ineffective for the isomerization of such complex conjugated systems due to the

Scheme 1. Isomerization of Unsaturated Alcohols and Ethers
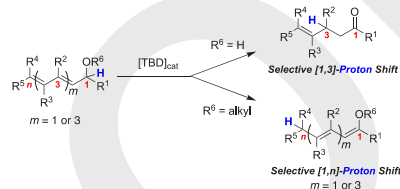
formation of stable diene−metal complexes that prevent hydride migration.[12]

In this paper, we describe the first examples of the isomerization of conjugated allylic alcohols and ethers using a base catalyst (Scheme 1c). The process is reminiscent to the recently explored metal-catalyzed "chain-walking" or "metal-walk" processes, which refer to the ability of certain metal complexes to perform a series of consecutive [1,2]- or [1,3]-hydride shifts along a hydrocarbon chain.[13] This formal alkene migration might be terminated by an enol tautomerization.[14,15] The work presented here consists, in contrast, of a formal proton migration alongside a polyenylic chain, constituting the first example of a "base-walk" process in these type of substrates.[16] The reaction is regioselective: the isomerization of conjugated allylic alcohols proceeds through a [1,3]-proton shift. On the other hand, the analogous ethers follow a formal [1,n]-proton shift where n = 3, 5, or 9. The substrate scope, experimental, and computational mechanistic investigations are presented.

We started by investigating the isomerization of conjugated dienyl alcohols, and we selected dienol **1a** as a model substrate. As the catalyst, we used the base TBD, as it gave excellent results in the isomerization of allylic alcohols.[6] A first attempt conducted with 10 mol % of TBD in toluene at 60 °C overnight did not give any product, and **1a** was recovered. When 20 mol % of TBD was used in refluxing toluene (Scheme 2), dienol **1a** was converted completely and

Scheme 2. Substrate Scope of the Isomerization of Dienyl Alcohols[a]
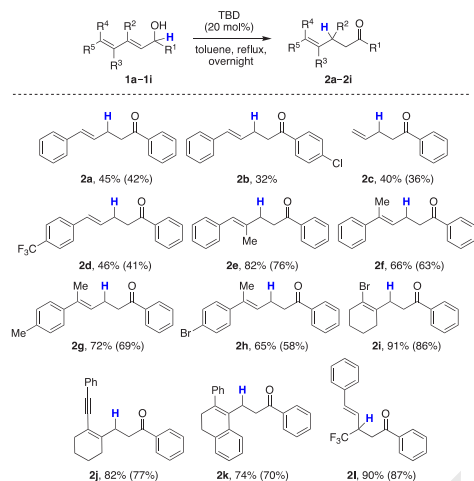
[a]Compounds **1a–1l** (0.1 mmol) and TBD (20 mol %) in toluene (1.0 mL). Isolated yields in parentheses.

exclusively into γ,δ-unsaturated ketone **2a**, albeit in a moderate yield of 45%. The introduction of a chloride group in the *para* position of the aryl ring at R^1 was detrimental to the reaction, and a yield of only 32% of **2b** was obtained. Decomposition was also observed when a terminal dienol **1c** was tested, and **2c** was obtained in a low yield of 40%. Dienyl alcohol **2d** bearing a trifluoromethyl group in the para position of the aryl ring at R^5 was converted to the corresponding γ,δ-unsaturated ketone with a yield of 46%. In contrast, the introduction of

substituents onto the terminal alkene (i.e., R^3 and R^4) prevented the decomposition of the starting dienyl alcohols and significantly enhanced the yields of the products (**2e–2l**). For instance, compounds **1e** and **1f**, bearing a methyl group at either R^3 (**1e**) or R^4 (**1f**), were converted into the corresponding γ,δ-unsaturated ketones in good yields. Both electron-donating and electron-withdrawing substituents in the para position of the aryl ring at R^5 were tolerated ,and ketones **2g** and **2h** were obtained in good yields (72% and 65%, respectively).

Similarly, when the second alkene was part of a cyclic structure (**1i–1l**), very good yields were obtained. The presence of a bromide or an alkyne was tolerated, and compounds **2i** and **2j** were formed in 91 and 82% yields. The introduction of a trifluoromethyl group at R^2 was also found to be beneficial, and **1l** gave the product in an excellent yield of 90%. Products derived from [1,5]-proton shifts were not detected in the isomerization of dienyl alcohols **1a–1l**.

Next, we turned our attention to the isomerization of dienyl ethers. When ((1E,3E)-5-methoxypenta-1,3-diene-1,5-diyl)-dibenzene (**3a**) was treated with TBD (20 mol %) in toluene at 60 °C overnight, interestingly, and in contrast to the reaction of conjugated dienyl alcohols, diene **4a** formed as the major product as a result of a formal [1,5]-proton shift ([1,5]: [1,3] > 20:1). Compound **4a** was obtained in 70% yield as a mixture of stereoisomers [(1Z,3E)/(1Z,3Z) = 78:22] (Table 1,

Table 1. Base-Catalyzed Isomerization of 3a[a]

entry	TBD (mol %)	T (°C)	4a (%)/(1Z,3E)/(1Z,3Z)[b,c]
1	TBD (20)	60	70/78:22
2	DBU (20)	60	<5/−
3	DBU (40)	60	<5/−
4	DABCO (40)	60	<5/−
5	DBU (100)	80	52/77:23
6	TBD (10)	85	83 (80%)[d]/78:22
7[e]	TBD (10)	85	83/78:22
8[f]		85	<5/−

[a]Unless otherwise noted, **3a** (0.1 mmol) in toluene (1 mL). [b]Yields determined by ^{1}H NMR spectroscopy using an internal standard. [c]E/Z ratios were calculated by ^{1}H NMR spectroscopy. [d]Isolated yield in parentheses. [e]Run for 24 h. [f]Without TBD.

entry 1). We also tested other bases and found that 1,8-diazabicyclo[5.4.0]undec-7-ene (DBU) and 1,4-diazabicyclo[2.2.2]octane (DABCO) did not catalyze the reaction under similar reaction conditions (i.e., substoichiometric amount of base, 60 °C, entries 2–4). A stoichiometric amount of DBU (1.0 equiv), on the other hand, gave **4a** in 52% yield (entry 5).

As the best results were obtained with TBD, we carried out further optimization experiments with this base. We found that the catalyst loading could be lowered to 10 mol % when the temperature was raised to 85 °C; under these conditions, **4a** was formed in 83% yield (entry 6). Increasing the reaction time did not have any significant effect on the formation of the product (entry 7). In all instances, the stereoisomeric ratio of the product **4a**, i.e., (1Z,3E)/(1Z,3Z), remained essentially constant, at ca. 78:22, suggesting that a thermodynamic equilibrium was reached. A complete list of the optimization

Scheme 3. Substrate Scope of the Isomerization of Dienyl Ethers[a,b]
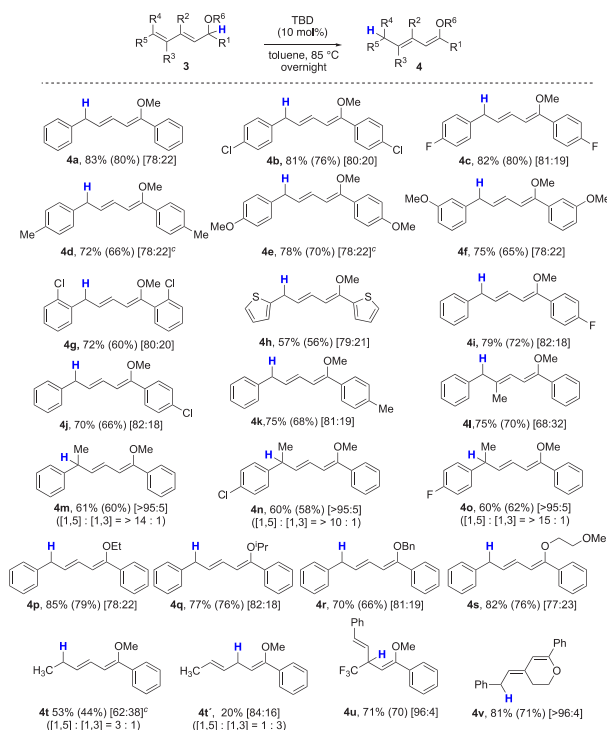
[a]Compounds **3a–3v** (0.1 mmol) and TBD (10 mol %) in toluene (1.0 mL). Isolated yields in parentheses. [b]Ratio of $(1Z,3E)/(1Z,3Z)$ in brackets determined by ^{1}H NMR spectroscopy. [c]110 °C instead of 85 °C.

experiments can be found in the Supporting Information (Table S1). The reaction did not take place in the absence of the base catalyst (entry 8).

We went on to study the substrate scope of the reaction under these optimal reaction conditions. We tested substrates bearing electron-donating and electron-withdrawing substituents on the phenyl groups at R^1 and R^5 (Scheme 3). Dienyl ethers bearing electron-withdrawing groups in both aryl rings (**4b–4c**) were converted into the products in good yields. The introduction of electron-donating substituents in both aryl rings in the *para* position decreased the rate of the reaction (**3d–3e**), but good yields were still obtained at 110 °C. The presence of a methoxy group at the *meta* position of the phenyl ring had no effect on the rate, and **4f** was obtained in 75% yield under standard conditions. A chloride group at the *ortho* position was well tolerated, and **4g** was obtained in 72% yield. Dienyl ether **3h**, bearing two heterocyclic thiophene-yl substituents at R^1 and R^5 gave **4h** in 57% yield. Fluoride, chloride, and methyl groups at the *para* position of the aryl ring at R^1 were all well tolerated, and **4i–4k** were obtained in good yields. Dienyl ethers with additional substituents on the double bonds of the conjugated system, i.e., at R^3 or R^4 (**3l–3o**), underwent the isomerization reaction to give the products in moderate to good yields (60–75%). Interestingly, **4m**, **4n**, and **4o** were obtained with a high $(1Z,3E)/(1Z,3Z)$ ratio of

>95:5. We also tested substrates bearing different substituents at R^6. The [1,5]-proton shift worked well for ethyl (**3p**), isopropyl (**3q**), benzyl (**3r**), and 2-methoxyethyl (**3s**) ethers under the optimized conditions. Next, we investigated the introduction of an aliphatic substituent at R^5 (**3t**). Surprisingly, the reaction gave a mixture of products (3:1) in a total yield of 20%. The major product was derived from the [1,3]-proton shift pathway (**4t′**); the product of the [1,5]-shift (**4s**) was the minor product. However, when the catalyst loading was increased to 20 mol % and the temperature to reflux temperature, **4t** was formed in a better yield of 53%. Notably, compound **3u**, with a CF₃ substituent at R^2, gave only the product derived from the corresponding [1,3]-proton shift (**4u**) in 71% yield. From (E)-6-phenyl-4-styryl-3,6-dihydro-2H-pyran (**3v**), the reaction proceeded smoothly and gave **4v** in very good yield with an excellent E/Z ratio (96:4).

To test the generality of the method, more extended conjugated polyenyl ethers were tested (Scheme 4). Tetraenyl ether **3w** afforded 46% yield of **4w** as a result of an overall [1,9]-proton shift. A tetraenyl ether with additional substituents along the conjugated chain (**3x**) also reacted in a [1,9]-proton shift yielding **4x** in an isolated 69% yield.

Deuterium-labeling studies were carried out with dienyl alcohol **1a-d¹** and dienyl ether **3a-d¹** (Scheme 5). The KIEs[17] were found to be 2.4 ± 0.5 and 3.8 ± 0.5 for the dienol and

Scheme 4. Isomerization of Tetraenyl Ethers[a]

3w–3x

4w–4x

4w, 46% (42%)

4x, 72% (69%), ([1,9] : [1,n] = > 10 : 1)) n = 3,5,7
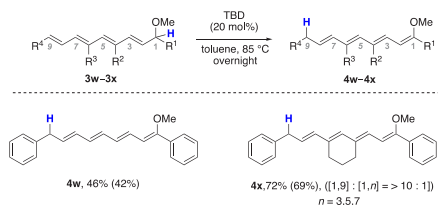
[a]Compounds **3v–3w** (0.1 mmol) and TBD (10 mol %) in toluene (1.0 mL). Isolated yields in parentheses.

Scheme 5. Deuterium-Labeling Studies

a)

1a-d¹ (89% D)

TBD (10 mol%)
toluene, reflux
overnight

2a
24% D at C-3, 12% D at C-2

b)

3a-d¹ (92% D)

TBD (10 mol%)
toluene, 85 °C
overnight

4a
28% D at C-5, 20% D at C-3

c)

3a-d³ (98% D)

TBD (10 mol%)
toluene, 85 °C
overnight

4a
20% D at C-5, 47% D at C-3
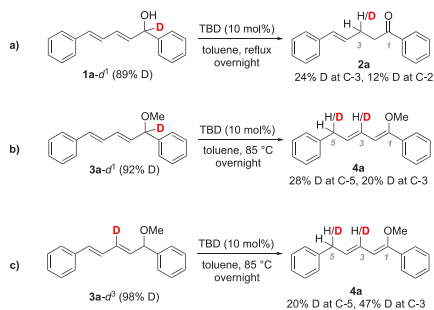
dienyl ether, respectively. These results suggest that in both cases the reaction starts with a rate-determining deprotonation at C-1. In the reaction of **1a-d¹**, 24% deuterium content was found at C-3 (54% of deuterium transfer) and no deuterium

was found at C-5 in the product; this indicates that this substrate reacts exclusively through a [1,3]-proton-shift mechanism (Scheme 5a). The presence of deuterium (12%) at C-2 in the product is due to keto/enol tautomerization. These results are consistent with our previous work.[6] In the reaction of **3a-d¹**, the deuterium content at C-5 was 28% which corresponds to 61% of deuterium transfer to that position (Scheme 5b). The deuterium content at C-3 was found to be 20%, suggesting that the mechanism follows, at least partially, a pathway involving two consecutive [1,3]-proton shifts, i.e., a [1,3]-shift followed by a [3,5]-shift. To test this idea, **3a-d³** was subjected to the reaction conditions; the product of this reaction had 20% deuterium at C-5 (41% of deuterium transfer from C-3 to C-5), which confirms that the [3,5]-proton shift does take place (Scheme 5c). Crossover experiments performed with substrates **3a-d¹** and **3s** at different concentrations suggest that the proton shift does not occur exclusively by an intramolecular pathway (see Scheme S2).

To better understand the reaction, DFT calculations (Figure 1) were carried out on dienyl ethers using the Gaussian 16 software (see the Supporting Information for details). Substrate **3a** was chosen as a simplest model compound for the calculations. This compound exists as an equilibrium mixture of conformers **I/I′** (Figure 1), interconverting by easy rotation around a σ-bond ($\Delta G^{\ddagger}$ = 6.4 kcal/mol). The reaction starts with the rate-limiting deprotonation of the C-1–H bond in **I** or **I′** by the TBD base with activation energies of 22.2 kcal/mol (**TS_{I–II}**) and 24.4 kcal/mol (**TS_{I′–II′}**), respectively. After this step, an intimate ion pair consisting of the dienylic anion and the protonated base is formed; the two intermediates **II** and **II′** cannot interconvert easily ($\Delta G^{\ddagger}$ = 16.9 kcal/mol). Each anion, for example, **II**, can undergo then protonation at C-3 (**TS_{II–III}**), at C-5 (**TS_{II–IV}**), or at C-1 (in a reversible **TS_{I–II}**) to form the three possible adducts **III**, **IV**, and **I**, respectively, with similar energies (22.0 kcal/mol for
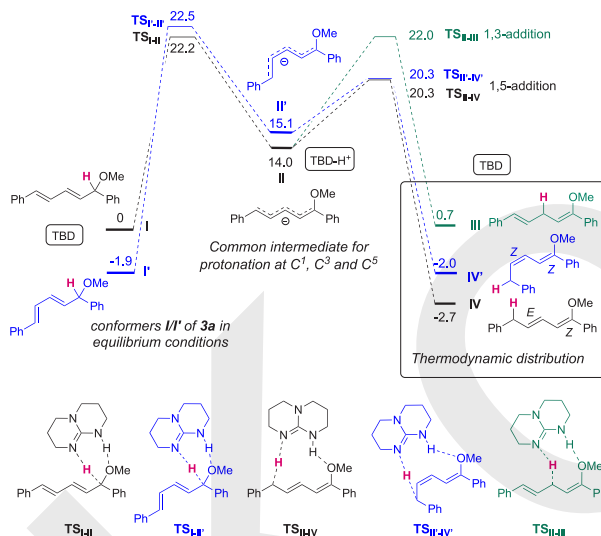

Figure 1. Calculated energy profile of the reaction. Values correspond to Gibbs free energies in kcal/mol.

$TS_{II–III}$, 20.3 kcal/mol for $TS_{II–IV}$, and 22.2 kcal/mol for $TS_{I–II}$). The low activation barriers seem to indicate that all possible adducts might be in equilibrium under the reaction conditions. The fact that the energies of the transition states for the transformations of **I** into the (1Z,3E) product (**IV**) and of **I′** into the (1Z,3Z) isomer (**IV′**) are very similar for both of the two steps (22.2 vs 22.5 and 20.3 vs 20.3 kcal/mol) confirms that the stereoselectivity of this reaction is not expected to be under kinetic control. Rather, the observed experimental selectivities are in good agreement with the relative stabilities of all of the possible products. This indicates that thermodynamic equilibrium is reached between **I**, **I′**, **III**, **IV**, and **IV′**, with the latter two species being the most stable (−2.7 and −2.0 kcal/mol). Thus, the stereoisomeric ratio depends exclusively on the relative stabilities of the products. The (1Z,3E) stereoisomer (**IV**), which is the major isomer observed experimentally, is 0.7 kcal/mol lower in energy than the (1Z,3Z) isomer (**IV′**). The reaction kinetics was also simulated with COPASI software;[18] we calculated a ratio of stereoisomers of 71:29, which is in perfect agreement with the experimental selectivity, 78:22 (Scheme 3), and a >20:1 ratio of [1,5]- vs [1,3]-proton shift. We were also able to explain the results obtained in the deuterium-labeling experiments using DFT calculations. The calculated energies of the rate-determining transition states ($TS_{I–II}$ and $TS_{I–II′}$, Figure 1) increase by 0.6−0.9 kcal/mol when H is replaced with D (see the Supporting Information for further details). This explains the KIE and also the lower rates observed for the deuterated substrate **3a**.

To summarize, we have described the first method for the remote transfer of protons through extended conjugated allylic ethers. As a catalyst, the base TBD was used. The method was found to be remarkably general, and the proton was successfully transferred as far as to eight carbons away, resulting in a formal [1,9]-proton shift. In the case of extended conjugated allylic alcohols, the proton selectively transfers only to C-3 through a [1,3]-proton shift, yielding the corresponding γ, δ-unsaturated carbonyl compounds. On the basis of deuterium-labeling studies, it was established that the rate-determining step is the deprotonation at C-1. For polyenyl ethers, DFT studies suggest that the rate-determining deprotonation is then followed by a consecutive number of proton shifts until the last carbon of the conjugated system. The "base walking" stops when the most thermodynamically stable product is formed. Thus, a simple base enables the isomerization reaction, which cannot be accomplished with transition-metal catalysts due to formation of stable coordination complexes. To the best of our knowledge, this is the first example of a proton being transferred alongside a polyenylic hydrocarbon chain via iterative proton shifts.

■ ASSOCIATED CONTENT

⑤ Supporting Information

The Supporting Information is available free of charge on the ACS Publications website at DOI: 10.1021/acscatal.9b02478.

    Experimental details, spectroscopy data and computational details (PDF)

■ AUTHOR INFORMATION

Corresponding Author

*E-mail: belen.martin.matute@su.se.

ORCID 🄳

Enrique Gomez-Bengoa: 0000-0002-8753-3760
Belén Martín-Matute: 0000-0002-7898-317X

Author Contributions

[⊥]N.M. and S.M.-E. contributed equally to this work.

Notes

The authors declare no competing financial interest.

■ ACKNOWLEDGMENTS

■ REFERENCES

(1) (a) Colquhoun, H. M.; Holton, J.; Thompson, D. J.; Twigg, M. V. *New Pathways for Organic Synthesis—Practical Applications of Transition Metals*; Plenum Press, London, 1984; pp 173−193. (b) Trost, B. M. Atom Economy—A Challenge for Organic Synthesis: Homogeneous Catalysis Leads the Way. *Angew. Chem., Int. Ed. Engl.* **1995**, *34*, 259−281. (c) Trost, B. M. On Inventing Reactions for Atom Economy. *Acc. Chem. Res.* **2002**, *35*, 695−705.

(2) (a) Damico, R.; Logan, T. Isomerization of Unsaturated Alcohols with Iron Pentacarbonyl. Preparation of Ketones and Aldehydes. *J. Org. Chem.* **1967**, *32*, 2356−2358. (b) Uma, R.; Crevisy, C.; Grée, R. Transposition of Allylic Alcohols into Carbonyl Compounds Mediated by Transition Metal Complexes. *Chem. Rev.* **2003**, *103*, 27−52. (c) Cadierno, V.; Crochet, P.; Gimeno, J. Ruthenium-Catalyzed Isomerizations of Allylic and Propargylic Alcohols in Aqueous and Organic Media: Applications in Synthesis. *Synlett* **2008**, *2008*, 1105−1124. (d) Ahlsten, N.; Bartoszewicz, A.; Martín-Matute, B. Allylic Alcohols as Synthetic Enolate Equivalents: Isomerisation and Tandem Reactions Catalysed by Transition Metal Complexes. *Dalton Trans.* **2012**, *41*, 1660−1670. (e) Lorenzo-Luis, P.; Romerosa, A.; Serrano-Ruiz, M. Catalytic Isomerization of Allylic Alcohols in Water. *ACS Catal.* **2012**, *2*, 1079−1086.

(3) For examples of the isomerization of allyl ethers, see: (a) Wille, A.; Tomm, S.; Frauenrath, H. A Highly Z-Selective Isomerization (Double-Bond Migration) Procedure for Allyl Acetals and Allyl Ethers Mediated by Nickel Complexes. *Synthesis* **1998**, *1998*, 305−308. (b) Mereyala, H. B.; Gurrala, S. R.; Mohan, S. K. Study of Metal and Acid Catalysed Deprotection of Propargyl Ethers of Alcohols *via* their Allenyl Ethers. *Tetrahedron* **1999**, *55*, 11331−11342. (c) Taskinen, E. Thermodynamic, Spectroscopic, and Density Functional Theory Studies of Allyl Aryl and Prop-1-Enyl Aryl Ethers. Part 1. Thermodynamic Data of Isomerization. *J. Chem. Soc., Perkin Trans.* **2001**, *2*, 1824−1834. (d) Reid, J. P.; McAdam, C. A.; Johnston, A. J. S.; Grayson, M. N.; Goodman, J. M.; Cook, M. J. *J. Org. Chem.* **2015**, *80*, 1472−1498.

(4) (a) Ahlsten, N.; Martín-Matute, B. Ir-Catalysed Formation of C−F Bonds. From Allylic Alcohols to α-Fluoroketones. *Chem. Commun.* **2011**, *47*, 8331−8333. (b) Ahlsten, N.; Gómez, A. B.; Martín-Matute, B. Iridium-Catalyzed 1,3-Hydrogen Shift/Chlorination of Allylic Alcohols. *Angew. Chem., Int. Ed.* **2013**, *52*, 6273−6276. (c) Gómez, A. B.; Erbing, E.; Batuecas, M.; Vázquez-Romero, A.; Martín-Matute, B. Iridium-Catalyzed Isomerization/Bromination of Allylic Alcohols: Synthesis of α-Bromocarbonyl Compounds. *Chem. - Eur. J.* **2014**, *20*, 10703−10709. (d) Vázquez-Romero, A.; Gómez, A. B.; Martín-Matute, B. An Acid- and Iridium-Catalyzed Tandem 1,3-Transposition/3,1-Hydrogen Shift/Chlorination of Allylic Alcohols. *ACS Catal.* **2015**, *5*, 708−714. (e) Martinez-Erro, S.; Bermejo Gómez, A.; Vázquez-Romero, A.; Erbing, E.; Martín-Matute, B. 2,2-

Diiododimedone: a Mild Electrophilic Iodinating Agent for The Selective Synthesis of α-Iodoketones from Allylic Alcohols. *Chem. Commun.* **2017**, *53*, 9842−9845. (f) Sanz-Marco, A.; Mozina, S.; Martinez-Erro, S.; Iskra, J.; Martín-Matute, B. Synthesis of α-iodoketones from Allylic Alcohols through Aerobic Oxidative Iodination. *Adv. Synth. Catal.* **2018**, *360*, 3884−3888. (g) Sanz-Marco, A.; Martinez-Erro, S.; Martín-Matute, B. Selective Synthesis of Unsymmetrical Aliphatic Acyloins Through Oxidation of Iridium Enolates. *Chem. - Eur. J.* **2018**, *24*, 11564−11567.

(5) (a) Clark, W. M.; Tickner-Eldridge, A. M.; Huang, G. K.; Pridgen, L. N.; Olsen, M. A.; Mills, R. J.; Lantos, I.; Baine, N. H. A Catalytic Enantioselective Synthesis of the Endothelin Receptor Antagonists SB-209670 and SB-217242. A Base-Catalyzed Stereospecific Formal 1,3-Hydrogen Transfer of a Chiral 3-Arylindenol. *J. Am. Chem. Soc.* **1998**, *120*, 4550−4551. (b) Johnston, A. J. S.; McLaughlin, M. G.; Reid, J. P.; Cook, M. NaH mediated isomerisation−allylation reaction of 1,3-substituted propenols. *Org. Biomol. Chem.* **2013**, *11*, 7662−7666. (c) Zheng, H.-X.; Xiao, Z.-F.; Yao, C.-Z.; Li, Q.-Q.; Ning, X.-S.; Kang, Y.-B.; Tang, Y. Transition-Metal-Free Self-Hydrogen-Transferring Allylic Isomerization. *Org. Lett.* **2015**, *17*, 6102−6105. (d) Mondal, K.; Mondal, B.; Pan, S. C. Organocatalytic Redox Isomerization of Electron-Deficient Allylic Alcohols: Synthesis of 1,4-Ketoaldehydes. *J. Org. Chem.* **2016**, *81*, 4835−4848. (e) Suchand, B.; Satyanarayana, G. KOtBu-Mediated Domino Isomerization and Functionalization of Aromatic Allylic Alcohols. *Eur. J. Org. Chem.* **2017**, *2017*, 3886−3895. (f) Hamada, Y.; Kawasaki-Takasuka, T.; Yamazaki, T. Base-promoted isomerization of CF3-containing allylic alcohols to the corresponding saturated ketones under metal-free conditions. *Beilstein J. Org. Chem.* **2017**, *13*, 1507−1512. (g) Zheng, H.-X.; Yao, C.-Z.; Qu, J.-P.; Kang, Y.-B. ^nBu4NOTf-promoted radical self-hydrogen transferring isomerization under transition metal-free conditions. *Org. Chem. Front.* **2018**, *5*, 1213−1216. (h) Liu, Y.; Liu, S.; Li, D.; Zhang, N.; Peng, L.; Ao, J.; Song, C. E.; Lan, Y.; Yan, H. Kinetic Resolution of Allylic Alcohol with Chiral BINOL-Based Alkoxides: A Combination of Experimental and Theoretical Studies. *J. Am. Chem. Soc.* **2019**, *141* (2), 1150−1159.

(6) Martinez-Erro, S.; Sanz-Marco, A.; Bermejo-Gómez, A.; Vázquez-Romero, A.; Ahlquist, M.; Martín-Matute, B. Base-Catalyzed Stereospecific Isomerization of Electron-Deficient Allylic Alcohols and Ethers through Ion-Pairing. *J. Am. Chem. Soc.* **2016**, *138*, 13408−13414.

(7) (a) Thirsk, C.; Whiting, A. Polyene Natural Products. *J. Chem. Soc., Perkin Trans. 1* **2002**, 999−1023. (b) Ghosh, S.; Kumar, S. U.; Shashidhar, J. Total Synthesis of (−)-Bitungolide F and Determination of Its Absolute Stereochemistry. *J. Org. Chem.* **2008**, *73*, 1582−1585. (c) Liu, M.; Yokomizo, T. The Role of Leukotrienes in Allergic Diseases. *Allergol. Int.* **2015**, *64*, 17−26. (d) Schöning, K.−W.; Hayashi, R. K.; Powell, D. R.; Kirschning, A. Synthetic Studies Toward Ansatrienines: Application of the Evans−Tishchenko Reaction to Chiral Enones. *Tetrahedron: Asymmetry* **1999**, *10*, 817−820. (e) Zhang, H.-P.; Kakeya, H.; Osada, H. Biosynthesis of 1-Aminocyclopropane-l-carboxylic acid Moiety on Cytotrienin A in Streptomyces sp. *Tetrahedron Lett.* **1998**, *39*, 6947−6948. (f) Birnbaum, G. I.; Hall, S. R. Structure of the Antibiotic Griseoviridin. *J. Am. Chem. Soc.* **1976**, *98*, 1926−1931.

(8) Synthesis of furans from dienyl ethers: Zhang, M.; Jiang, H.-F.; Neumann, H.; Beller, M.; Dixneuf, P. H. Sequential Synthesis of Furans from Alkynes: Successive Ruthenium(II)- and Copper(II)-Catalyzed Processes. *Angew. Chem., Int. Ed.* **2009**, *48*, 1681−1684.

(9) Barluenga, J.; Fañanás, F. J.; Sanz, R.; García, F.; García, N. New Reduction of Divinylketones to Rearranged Polyenyl Ethers Under Luche Conditions. *Tetrahedron Lett.* **1999**, *40*, 4735−4736.

(10) For applications of dienyl ethers, see: (a) Dalko, P. I.; Moisan, L.; Cossy, J. Modular Ligands for Asymmetric Synthesis: Enantioselective Catalytic Cu^II-Mediated Condensation Reaction of Ethyl Pyruvate with Danishefsky's Diene. *Angew. Chem., Int. Ed.* **2002**, *41*, 625−628. (b) Ashburn, B. O.; Carter, R. G.; Zakharov, L. N. Synthesis of Tetra-ortho-substituted, Phosphorus-Containing and Carbonyl-Containing Biaryls Utilizing a Diels-Alder Approach. *J.*

Am. Chem. Soc. **2007**, *129*, 9109−9116. (c) Tiefenbacher, K.; Arion, V. B.; Mulzer, J. A Diels−Alder Approach to (−)-Ovalicin. *Angew. Chem., Int. Ed.* **2007**, *46*, 2690−2693. (d) Jewett, J. C.; Rawal, V. H. Total Synthesis of Pederin. *Angew. Chem., Int. Ed.* **2007**, *46*, 6502−6504. (e) Batsanov, A. S.; Knowles, J. P.; Lightfoot, A. P.; Maw, G.; Thirsk, C. E.; Twiddle, S. J. R.; Whiting, A. A Novel, Efficient, Diastereo- and Enantioselective Mukaiyama Aldol-Based Synthesis of a Vinyl Cyclopentanone Core Derivative of Viridenomycin. *Org. Lett.* **2007**, *9*, 5565−5568. (f) Ghosh, A. K.; Xi, K. Enantioselective Synthesis of (−)-Platensimycin Oxatetracyclic Core by Using an Intramolecular Diels−Alder Reaction. *Org. Lett.* **2007**, *9*, 4013−4016. (g) Strübing, D.; Kirschner, A.; Neumann, H.; Hübner, S.; Klaus, S.; Gördes, D.; Bornscheuer, U. T.; Beller, M. Synthesis of Enantiomerically Pure Cyclohex-2-en-1-ols: Development of Novel Multicomponent Reactions. *Chem. - Eur. J.* **2005**, *11*, 4210−4218. (h) Dudnik, A. S.; Schwier, T.; Gevorgyan, V. Gold-Catalyzed Double Migration-Benzannulation Cascade toward Naphthalenes. *Org. Lett.* **2008**, *10*, 1465−1468.

(11) Eberle, M. K.; Weber, H.-P. The Regio- and Stereoselectivity of Intramolecular Diels-Alder Reactions of Fumarates: An Unusual Rearrangement-Cyclization. *J. Org. Chem.* **1988**, *53*, 231−235.

(12) Cherkaoui, H.; Soufiaoui, M.; Grée, R. From Allylic Alcohols to Saturated Carbonyls Using $Fe(CO)_5$ as Catalyst: Scope and Limitation Studies and Preparation of Two Perfume Components. *Tetrahedron* **2001**, *57*, 2379−2383.

(13) Crabtree, H. R. *The Organometallic Chemistry of the Transition Metals*; John Wiley & Sons, Inc.: New Haven, CT, 2014; pp 229−231.

(14) (a) Grotjahn, D. B.; Larsen, C. R.; Gustafson, J. L.; Nair, R.; Sharma, A. Extensive Isomerization of Alkenes Using a Bifunctional Catalyst: An Alkene Zipper. *J. Am. Chem. Soc.* **2007**, *129*, 9592−9593. (b) Larionov, E.; Lin, L.; Guénée, L.; Mazet, C. Scope and Mechanism in Palladium-Catalyzed Isomerizations of Highly Substituted Allylic, Homoallylic, and Alkenyl Alcohols. *J. Am. Chem. Soc.* **2014**, *136*, 16882−16894.

(15) Related: (a) Vasseur, A.; Bruffaerts, J.; Marek, I. Remote Functionalization through Alkene Migration. *Nat. Chem.* **2016**, *8*, 209−219. (b) Sommer, H.; Juliá-Hernández, F.; Martin, R.; Marek, I. Walking Metals for Remote Functionalization. *ACS Cent. Sci.* **2018**, *4*, 153−165. (c) Kapat, A.; Sperger, T.; Guven, S.; Schoenebeck, F. E-Olefins through intramolecular radical relocation. *Science* **2019**, *363*, 391−396. (d) Kathe, P.; Fleischer, I. Cooperative Use of Brønsted Acids and Metal Catalysts in Tandem Isomerization Reactions of Olefins. *ChemCatChem* **2019**, *11*, 3343−3354.

(16) The alkyne zipper reaction is an example of "base walk" that isomerizes internal alkynes into more thermodynamically stable terminal alkynes. For more literature about this reaction, see:Avocetien, K.; Li, Y.; O'Doherty, G. A. The Alkyne Zipper Reaction in Asymmetric Synthesis. In *Modern Alkyne Chemistry: Catalytic and Atom-Economic Transformations*; Trost, B. M., Li, C.-J., Eds.; Wiley-VCH, 2015.

(17) Simmons, E. M.; Hartwig, J. F. On the Interpretation of Deuterium Kinetic Isotope Effects in C—H Bond Functionalizations by Transition-Metal Complexes. *Angew. Chem., Int. Ed.* **2012**, *51*, 3066−3072.

(18) (a) Hoops, S.; Sahle, S.; Gauges, R.; Lee, C.; Pahle, J.; Simus, N.; Singhal, M.; Xu, L.; Mendes, P.; Kummer, U. *Bioinformatics* **2006**, *22*, 3067−3074. (b) *COPASI version 4.24*, available free of charge from http://copasi.org. See the Supporting Information for further details.

III

COMMUNICATION

One-Step Microwave-Assisted Synthesis of Amino-Functionalized Chromium(III) Terephthalate MIL-101-NH₂

Alba Carretero-Cerdán,[a] Sergio Carrasco,[a,b]* Amparo Sanz-Marco[a] and Belén Martín-Matute [a]*

A new single-step microwave (MW)-assisted protocol for the synthesis of MIL-101(Cr) and of MIL-101(Cr)-NH₂ is described herein, based on the addition of NaF as the modulator instead of HF to obtain the corresponding polymers in only 1 h with high crystallinity and yields (>70%, >0.5 g).

Metal-organic frameworks (MOFs) are porous coordination polymers based on metal ions or clusters and organic polycomplexant linkers.[1] Owing to their outstanding physicochemical properties these hybrid materials have been widely applied in different fields such as separation,[2] gas storage,[3] energy,[4] biomedicine,[5] water treatment,[6] sensor development[7] and catalysis,[8] among the most relevant.

Because of its kinetic stability and high charge to radius ratio, Cr(III) has been used recurrently as the ion for the construction of the metal cluster constituents in MOFs.[9] However, the number of Cr(III)-based MOFs is still scarce, mainly due to the lability of distorted octahedral Cr(III) complexes under synthetic conditions and the large amount of coordination modes to different organic linkers,[10] resulting in difficult crystal growth. As a consequence, the real potential of Cr-based MOFs remains underdeveloped. Among the few available Cr(III)-based MOFs, MIL-101 (from *Materials Institute Lavoisier*) called the attention of the scientific community because of its outstanding stability and physicochemical and textural properties.[11] After its activation, two coordinatively unsaturated open metal sites per Cr(III) cluster are generated,[12] essential for the capture of target molecules in environmental applications, and acting as open metal sites for catalytic purposes. The organic linker in MIL-101 consists of terephthalic acids, and a broad variety of post-synthetic modifications on the aromatic ring has been reported.[13,14]

a. *Department of Organic Chemistry, Stockholm University, Stockholm 10691, Sweden (belen.martin.matute@su.se).*
b. *Current address: Advanced Porous Materials Unit, IMDEA Energy Institute, Móstoles 28935, Spain (sergio.carrasco@imdea.org).*
Electronic Supplementary Information (ESI) available: experimental section, synthesis, optimization, and characterization (PXRD, SEM, elemental analysis, TGA, nitrogen sorption and infrared spectroscopy). See DOI: 10.1039/x0xx00000x
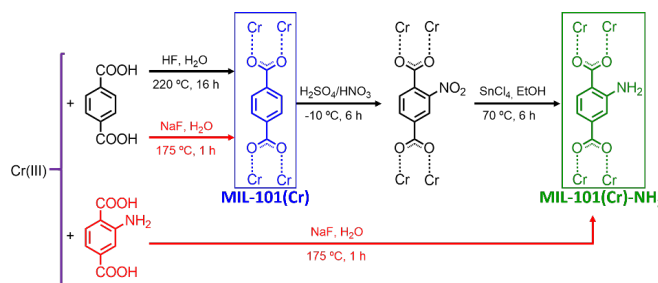
Since 2005, several publications have demonstrated that the topology and crystal size of MIL-101 strongly depend on synthesis factors, i.e. temperature, time, pH, solvent, and reagent concentration.[15] Thus, matching the optimal synthetic conditions is sometimes a non-negligible time-consuming effort, requiring a precise equilibrium between all these parameters. In 2011, Stock and coworkers described the post-synthetic modification of this MOF to quantitatively introduce the -NH₂ moiety within the framework,[16] to yield MIL-101(Cr)-NH₂, which has emerged as a prominent porous material in the area of catalysis. Thus, a broad variety of organometallic species have been introduced onto this NH₂-functionalized framework,[17-20] and metal nanoparticles, stabilized by the amino functionalities, have been grown within its voids.[21, 22]

The direct synthesis of amine-functionalized MIL-101(Cr) from the NH₂-functionalized linkers, i.e. from 2-aminoterephthalic acid, avoiding post-synthetic modifications of MIL-101(Cr), is challenging. In addition to the crystallization issues already mentioned,[9] the NH₂ moieties have high affinity towards Cr(III),[23] complicating the spatial rearrangement of both organic and inorganic components. The first attempt for the direct synthesis of MIL-101(Cr)-NH₂ was reported by Lin and coworkers,[24] who obtained the material in a solvothermal synthesis (150 °C, 12 h) using NaOH as deprotonating agent, resulting in nano-sized MOF particles with moderate crystallinity and showing broad diffraction peaks in the X-ray diffraction pattern. Crystallinity has demonstrated to be a key aspect in MOFs for catalytic purposes because of the better exposure of the metal active sites,[25] the higher porosity and surface area,[26] and the higher stability[27] compared to amorphous materials. In that sense, other authors have improved the crystallinity of MIL-101(Cr)-NH₂ synthesized directly from the NH2-functionalized linker by using DMF as the solvent,[28] which can also act as a base for linker deprotonation, but this procedure is still long-time consuming (72 h) and the solvent is not eco-friendly. Although these methods achieved the synthesis of MIL-101(Cr)-NH₂ directly from the amino-functionalized terephthalic acid, the best yield obtained did not exceed 42% (see **Table S1** in ESI).

Scheme 1. Synthetic procedure to obtain MIL-101(Cr) (blue) and MIL-101(Cr)-NH$_2$ (green) MOFs, under solvothermal (top, black arrows) and microwave conditions (bottom, red arrows). Classical solvothermal synthesis of ST-MIL-101(Cr)-NH$_2$ requires 3 steps via ST-MIL-101(Cr) and ST-MIL-101(Cr)-NO$_2$.

Microwave-assisted MOF syntheses have emerged as an elegant alternative to conventional solvothermal methods,[29] enabling faster reactions, higher efficiency, phase selectivity, and easier morphological control.[30] A few publications have appeared describing the microwave-assisted synthesis of MIL-101(Cr), even in the absence of HF as mineralizing agent with yields up to 37%.[31, 32] However, the direct synthesis of MIL-101(Cr)-NH$_2$ has not been reported to date following this approach. Here a novel one-step HF-free microwave assisted synthesis of MIL-101(Cr) and MIL-101(Cr)-NH$_2$ in water is presented.

We firstly evaluated the effect of different modulators in the pre-polymerization mixture. The use of LiF, NaF, KF and CsF resulted in well-defined diffraction patterns of MIL-101 (**Figure S2a**). It is well known the use of these salts as bases in catalysis,[33] although until now they have not been exploited as bases in MOF syntheses. Microwave heating of aqueous solutions of NaF generates *in situ* HF,[34] that could explain the high crystallinity of the final material compared to reported examples (see also **Table S1**),[16] as chromium clusters of MIL-101 are easily stabilized when F$^-$ or HO$^-$ groups are coordinated to Cr(III).[11] Thus, alkali fluorides accomplish both roles, as deprotonating agents and as a convenient source of fluoride ions for cluster stabilization. Diffraction peaks were sharply defined when using NaF compared to the other fluoride salts, with a better matching between the theoretical and experimental patterns. In addition, some impurities were found when using KF and CsF (**Figure S2b**).

The effect of the temperature on the crystallinity (**Figure S3**) was analyzed by fixing the reaction time to 1 h. At 175 °C pure MIL-101(Cr)-NH$_2$ crystals where obtained, while this crystallinity was much lower at lower (160 °C) or higher temperatures (190 °C), despite the similar yields obtained (68-70%). The effect of time was tested at the optimal temperature, 175 °C (**Figure S4**), and we observed that optimal crystallinity was obtained after 1 h of reaction time. Although well-defined crystalline materials were also obtained after 2 h and 5 h, yields linearly decreased from 69% (1 h) to 64% and 53%, respectively. Thus, at 175 °C the crystal growth process competes with other non-related crystallization events,[35] such as MOF degradation due to the increasing amounts of HF generated in-situ over time.[36]

The amount of NaF was then evaluated at 175 °C in reactions run for 1 h (**Figure S5**), obtaining the optimal results when 3.3 mmol (2.4 equiv. with respect to the organic linker) were used. Different chromium sources were tested at this stage (**Figure S6**). Cr(III) chloride, nitrate and sulfate resulted in MIL-101(Cr)-NH$_2$ showing different degrees of crystallinity, being the first salt (CrCl$_3$·6H$_2$O) the one providing the most intense diffraction peaks. Cr(VI) sources resulted in amorphous materials.

Finally, the concentration of all the species, i.e. Cr(III) salt, 2-aminoterephthalic acid (2ATA) and NaF (1.35:1.35:3.3 mmol, in 10 mL in the original composition used for optimization, i.e. 0.6 M), was tested to probe the scalability of the process in the same monomodal microwave reactor. Decreasing the concentration to 0.3 M resulted in similar diffraction pattern and yield to those observed at 0.6 M (67% vs 69%, **Figure S7c**), but the total amount of material decreased from 250 to 121 mg (**Figure S7b**). Under more diluted conditions, i.e. 0.2 M, polymers were barely crystalline (**Figure S7a**). The synthesis performed at 1.2 M provided similar yields (69%) and more intense diffractions compared to 0.6 M producing 505 mg of MOF (i.e. 73% yield), being these the final conditions chosen for material fabrication. On the other hand, the synthesis performed at 2.4 M resulted in a mixture of MIL-101(Cr)-NH$_2$ and MIL-88B(Cr)-NH$_2$ phases, evidencing that increasing the concentration slightly shifted the polymorphism equilibrium to the thermodynamically more stable polymorph.[37, 38]

Different terephthalic acid linkers substituted at *ortho* position were evaluated, although only the use of 2ATA resulted in crystalline materials (see **Figure S8a** ESI) The absence of substituents at *ortho* position resulted in pure MIL-101(Cr). Thus, this methodology (**Scheme 1**) can be extended for the fabrication of this MOF with remarkable higher yields (97%) and lower reaction times (1 h) than those typically described in the literature under solvothermal conditions, without the need of handling HF, and competitive to similar microwave-assisted syntheses in terms of polymerization extent (**Table S1**).[39]

For comparison purposes, solvothermal MIL-101(Cr) and MIL-101(Cr)-NH$_2$, henceforth named ST-MIL-101(Cr) and ST-MIL-101(Cr)-NH$_2$, were prepared according to classical procedures.[11, 16] Yields for

COMMUNICATION

these materials were 41% and 43%, respectively, that can be compared to 97% and 69% corresponding to MW-MIL-101(Cr) and MW-MIL-101(Cr)-NH$_2$. Interestingly, the aminated MW-MOF was obtained in one single step just by mixing CrCl$_3$, 2ATA and NaF in water after 1 h, while ST-MIL-101(Cr)-NH$_2$ firstly requires the synthesis of ST-MIL-101(Cr) using HF (16 h) and two additional steps.[16]
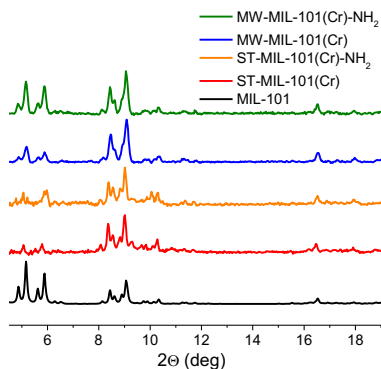

Figure 1. PXRD diffraction patterns (2Θ = 4-19 deg) of both solvothermal (ST-) and microwave (MW-) MIL-101(Cr) and MIL-101(Cr)-NH$_2$ MOFs compared to the simulated MIL-101(Cr) pattern.

All polymers were characterized by powder X ray diffraction (PXRD) and compared to the simulated pattern of MIL-101(Cr) (**Figure 1**). The first remarkable difference between ST- and MW-MOFs concerns the signal-to-noise ratio of diffraction patterns. As all of them were measured under the same instrumental conditions, crystal quality was evidently enhanced under microwave conditions. In fact, we have observed such worse quality when long reaction times and/or high temperatures were considered in solvothermal syntheses, evidencing that the reaction conditions for ST-MOFs compromised their structural integrity. This aspect supported our previous claim: the synthesis of this kinetically stable MOF is a delicate equilibrium between crystallization, degradation, and polymorphism.[40, 41]

On the other hand, a peak broadening effect is observed in MW-MOFs compared to ST- materials, merging the characteristic diffraction twin peaks of MIL-101, those at 8.44 and 8.60 deg, and at 8.90 and 9.06 deg. This phenomenon has been broadly studied in crystallography, related to small crystal sizes,[42] in agreement with scanning electron microscopy (SEM) observations (**Figure 2**). After data treatment (**Figure S10**), we observed a negligible variation of the unit cell size (±0.12%) in both MW-MOFs compared to the reported value (a = 88.869 Å).[11]

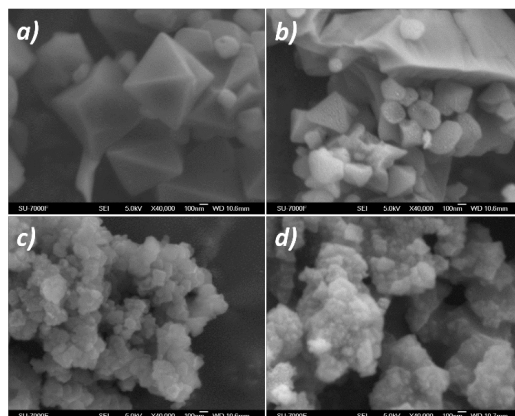**Figure 2**. Scanning electron microscopy (SEM) images of: a) ST-MIL-101(Cr), b) ST-MIL-101(Cr)-NH$_2$, c) MW-MIL-101(Cr) and d) MW-MIL-101(Cr)-NH$_2$.

SEM images (**Figure 2**) showed the shape of octahedral crystals within the micrometric range for ST-MOFs. Crystal size of ST-MIL-101(Cr)-NH$_2$ particles was remarkably smaller (360±90 nm) than the parent counterpart ST-MIL-101(Cr) (1000±200 nm), some of them lacking the octahedral shape because of the crystal attrition during the nitration and reduction steps.[22] The control over the dispersity in the case of MW-MOFs is higher, producing nanometric crystals with narrower particle size distributions (**Figure S11**), for both MW-MIL-101(Cr) and MW-MIL-101(Cr)-NH$_2$ (130±30 and 80±10 nm, respectively). MW heating resulted in nano-sized MOF particles compared to ST methods, with higher control over polydispersity as a consequence of favoring nucleation instead of crystal growth that increased, in return, the amount of material obtained.[43]

The combined results of elemental analysis by ICP-OES (**Table S2**) and TGA (**Figure S12**) suggested that the new unit cell formula of MW-MIL-101(Cr) and MW-MIL-101(Cr)-NH$_2$ was Cr$_3$F(H$_2$O)$_2$O[(O$_2$C)-C$_6$H$_4$-(CO$_2$)]$_3$·(CH$_3$CH$_2$OH)$_4$(HF)$_3$ (1029.0 g/mol) and Cr$_3$F(H$_2$O)$_2$O[(O$_2$C)-C$_6$H$_3$NH$_3^+$F$^-$-(CO$_2$)]$_3$·(CH$_3$CH$_2$OH)$_3$(HF)$_3$ (1022.1 g/mol), with water being replaced by ethanol and HF during both washing and synthesis steps. In the case of MW-MIL-101(Cr)-NH$_2$ the F content was twice the value found for MW-MIL-101(Cr), ascribed to the presence of -NH$_2$ moieties that appeared in the form of -NH$_3^+$F$^-$. Experimental C/Cr and Cr/F ratios and Cr$_2$O$_3$ residues were in good agreement with the proposed compositions (**Table S2**).

Both MW-MIL-101(Cr) and MW-MIL-101(Cr)-NH$_2$ showed a type-I nitrogen sorption isotherm with 2651 and 2014 m^2/g of BET surface area (**Figure S13**).[11, 24] These results evidenced that the presence of -NH$_2$, or -NH$_3^+$F$^-$ moieties within the framework significantly decreased the porosity of the material. This aspect also supports the BET surface area values found for ST-MIL-101(Cr) and ST-MIL-101(Cr)-NH$_2$ of 2328 and 1778 m^2/g (**Table S3**). The surface areas found in this work (2000-2700 m^2/g) matched those reported by other authors.[44] Remarkably, because of the smaller crystal size of

MW-MOFs, the narrower particle size distribution and the better accessibility and diffusion of species throughout the internal pores, BET surface areas were larger than those of ST-MOFs.

Finally, MW-MOFs were characterized by ATR-FTIR (**Figures S14 and S15**). Upon ligand binding to chromium clusters the absorbance of C=O and C-O stretching vibrations (ca. 1650 and 1250 cm^{-1}) dramatically decreased and a new Cr-O band could be observed at 585 cm^{-1}, demonstrating the interaction between them. The C-H stretching vibrations from ethanol (2975 cm^{-1}) supported the location of this solvent as guest molecules within the pores. The presence of $NH_3^+F^-$ in MW-MIL-101(Cr)-NH$_2$ was probed by the band observed at 730 cm^{-1} in this MOF, characteristic of F attached to NH$_2$ in aromatic ammonium salts.[45]

This work provides an efficient, elegant, fast, green and non-toxic microwave-assisted synthesis of MW-MIL-101(Cr) and MW-MIL-101(Cr)-NH$_2$. The methodology stands over classical solvothermal protocols, that either require at least two long time consuming post-synthetic modifications or only one single step but compromising both the crystallinity and yield. It is competitive as well towards other microwave assisted syntheses of MOFs from the MIL family, providing the highest crystallinity, phase selectivity, yields and amounts obtained to date for both polymers in one single step (0.5-0.7 g, yields > 70% in 1 h). Alkali fluorides have revealed to be essential for cluster stabilization and as a convenient source of F atoms for Cr(III) coordination. We believe that the use of NaF as modulator in MW-assisted reactions will pave the way for the stabilization, nucleation and growth of other different MOFs that cannot be obtained otherwise.

Notes and references

1. S. R. Batten, N. R. Champness, X.-M. Chen, J. Garcia-Martinez, S. Kitagawa, L. Öhrström, M. O'Keeffe, M. Paik Suh and J. Reedijk, *Pure Appl. Chem.*, 2013, **85**, 1715-1724.
2. A. A. Kotova, D. Thiebaut, J. Vial, A. Tissot and C. Serre, *Coordination Chemistry Reviews*, 2022, **455**, 214364.
3. H. Li, L. Li, R.-B. Lin, W. Zhou, Z. Zhang, S. Xiang and B. Chen, *EnergyChem*, 2019, **1**, 100006.
4. L. G. Gordeeva, Y. D. Tu, Q. Pan, M. L. Palash, B. B. Saha, Y. I. Aristov and R. Z. Wang, *Nano Energy*, 2021, **84**, 105946.
5. S. Carrasco, in *Metal-Organic Frameworks for Biomedical Applications*, ed. M. Mozafari, Woodhead Publishing, 2020, DOI: https://doi.org/10.1016/B978-0-12-816984-1.00026-3, pp. 525-551.
6. F. Yang, M. Du, K. Yin, Z. Qiu, J. Zhao, C. Liu, G. Zhang, Y. Gao and H. Pang, *Small*, 2021, **n/a**, 2105715.
7. S. Carrasco, *Biosensors*, 2018, **8**.
8. A. Bavykina, N. Kolobov, I. S. Khan, J. A. Bau, A. Ramirez and J. Gascon, *Chemical Reviews*, 2020, **120**, 8468-8535.
9. H. Yang, F. Peng, A. N. Hong, Y. Wang, X. Bu and P. Feng, *Journal of the American Chemical Society*, 2021, **143**, 14470-14474.
10. O. Staples, A. Reinholdt and D. J. Mindiola, in *Comprehensive Coordination Chemistry III*, eds. E. C. Constable, G. Parkin and L. Que Jr, Elsevier, Oxford, 2021, DOI: https://doi.org/10.1016/B978-0-08-102688-5.00013-1, pp. 508-551.
11. G. Férey, C. Mellot-Draznieks, C. Serre, F. Millange, J. Dutour, S. Surblé and I. Margiolaki, *Science*, 2005, **309**, 2040-2042.
12. D.-Y. Hong, Y. K. Hwang, C. Serre, G. Férey and J.-S. Chang, *Advanced Functional Materials*, 2009, **19**, 1537-1552.
13. P. Á. Szilágyi, P. Serra-Crespo, I. Dugulan, J. Gascon, H. Geerlings and B. Dam, *CrystEngComm*, 2013, **15**, 10175-10178.
14. M. Kim, J. F. Cahill, H. Fei, K. A. Prather and S. M. Cohen, *Journal of the American Chemical Society*, 2012, **134**, 18082-18088.
15. A. J. Howarth, A. W. Peters, N. A. Vermeulen, T. C. Wang, J. T. Hupp and O. K. Farha, *Chemistry of Materials*, 2017, **29**, 26-39.
16. S. Bernt, V. Guillerm, C. Serre and N. Stock, *Chemical Communications*, 2011, **47**, 2838-2840.
17. A. Santiago-Portillo, S. Remiro-Buenamañana, S. Navalón and H. García, *Dalton Transactions*, 2019, **48**, 17735-17740.
18. S. Babaee, M. Zarei, H. Sepehrmansourie, M. A. Zolfigol and S. Rostamnia, *ACS Omega*, 2020, **5**, 6240-6249.
19. H. M. A. Hassan, A. A. Betiha, S. K. Mohamed, E. A. El-Sharkawy and E. A. Ahmed, *Applied Surface Science*, 2017, **412**, 394-404.
20. S. Wang, S. Hou, C. Wu, Y. Zhao and X. Ma, *Chinese Chemical Letters*, 2019, **30**, 398-402.
21. M. Wen, K. Mori, T. Kamegawa and H. Yamashita, *Chemical Communications*, 2014, **50**, 11645-11648.
22. F. Carson, V. Pascanu, A. Bermejo Gómez, Y. Zhang, A. E. Platero-Prats, X. Zou and B. Martín-Matute *Chemistry – A European Journal*, 2015, **21**, 10896-10902.
23. J.-R. Jiménez, B. Doistau, M. Poncet and C. Piguet, *Coordination Chemistry Reviews*, 2021, **434**, 213750.
24. Y. Lin, C. Kong and L. Chen, *RSC Advances*, 2012, **2**, 6417-6419.
25. A. Tombesi and C. Pettinari, *Inorganics*, 2021, **9**.
26. H. Ji, S. Lee, J. Park, T. Kim, S. Choi and M. Oh, *Inorganic Chemistry*, 2018, **57**, 9048-9054.
27. C.-Y. Sun, S.-X. Liu, D.-D. Liang, K.-Z. Shao, Y.-H. Ren and Z.-M. Su, *Journal of the American Chemical Society*, 2009, **131**, 1883-1888.
28. N. Tian, Q. Jia, H. Su, Y. Zhi, A. Ma, J. Wu and S. Shan, *Journal of Porous Materials*, 2016, **23**, 1269-1278.
29. J. Klinowski, F. A. Almeida Paz, P. Silva and J. Rocha, *Dalton Transactions*, 2011, **40**, 321-330.
30. S. Carrasco, A. Sanz-Marco and B. Martín-Matute, *Organometallics*, 2019, **38**, 3429-3435.
31. A. Demessence, P. Horcajada, C. Serre, C. Boissière, D. Grosso, C. Sanchez and G. Férey, *Chemical Communications*, 2009, DOI: 10.1039/B915011K, 7149-7151.
32. N. A. Khan, I. J. Kang, H. Y. Seok and S. H. Jhung, *Chemical Engineering Journal*, 2011, **166**, 1152-1157.
33. P. Gautam and B. M. Bhanage, *Catalysis Science & Technology*, 2015, **5**, 4663-4702.
34. P. Kulkarni, S. Chellam, G. Ghurye and M. P. Fraser, *Environmental Engineering Science*, 2003, **20**, 517-531.
35. K. A. S. Usman, J. W. Maina, S. Seyedin, M. T. Conato, L. M. Payawan, L. F. Dumée and J. M. Razal, *NPG Asia Materials*, 2020, **12**, 58.

36. S. J. Garibay, Z. Wang and S. M. Cohen, *Inorganic Chemistry*, 2010, **49**, 8086-8091.

37. M. Y. Zorainy, M. Gar Alalm, S. Kaliaguine and D. C. Boffito, *Journal of Materials Chemistry A*, 2021, **9**, 22159-22217.

38. N. V. Maksimchuk, O. V. Zalomaeva, I. Y. Skobelev, K. A. Kovalenko, V. P. Fedin and O. A. Kholdeeva, *Proceedings of the Royal Society A: Mathematical, Physical and Engineering Sciences*, 2012, **468**, 2017-2034.

39. S. Bhattacharjee, C. Chen and W.-S. Ahn, *RSC Advances*, 2014, **4**, 52500-52525.

40. L. Pukdeejorhor, K. Adpakpang, P. Ponchai, S. Wannapaiboon, S. Ittisanronnachai, M. Ogawa, S. Horike and S. Bureekaew, *Crystal Growth & Design*, 2019, **19**, 5581-5591.

41. T. Tanasaro, K. Adpakpang, S. Ittisanronnachai, K. Faungnawakij, T. Butburee, S. Wannapaiboon, M. Ogawa and S. Bureekaew, *Crystal Growth & Design*, 2018, **18**, 16-21.

42. K. He, N. Chen, C. Wang, L. Wei and J. Chen, *Crystal Research and Technology*, 2018, **53**, 1700157.

43. L. Feng, K.-Y. Wang, J. Powell and H.-C. Zhou, *Matter*, 2019, **1**, 801-824.

44. M.-L. Chen, S.-Y. Zhou, Z. Xu, L. Ding and Y.-H. Cheng, *Molecules*, 2019, **24**.

45. E. Y. Misochko, I. U. Goldschleger, A. V. Akimov and C. A. Wight, *Low Temperature Physics*, 2000, **26**, 727-735.

SUPPORTING INFORMATION

Chapter V. Enhancing the Chirality Transfer in the Isomerization of Electron-deficient Allylic Alcohols

General Information

All reagents were utilized without any further purification as obtained from commercial sources. Flash chromatography was performed with 60 Å (35-70 µm) silica gel (GC 60A 35- 70 Micron, DAVISIL). Analytical TLC was performed on aluminum plates pre-coated (0-25 mm) with silica gel (Merck, Silica Gel 60 F254). ^{1}H, ^{13}C and ^{19}F NMR spectra were recorded at 400 MHz, 100 MHz and 376 MHz respectively on a Bruker Advance spectrometer. Chemical shifts (δ) are shown in ppm, using as a reference the residual peaks of CDCl$_3$ (δ_H 7.26 and δ_C 77.00) and CD$_3$CN (δ_H 1.94 and δ_C 128.06). Coupling constants (J) are given in Hz. High resolution mass spectra (HRMS) were recorded on Bruker microTOF mass spectrometer using APCI ionization. Enantiomeric excesses were determined using HPLC analysis on an Agilent 1200-series instrument with an autosampler and UV detection and using Chiralcel OD-H and IF columns.

Powder X-ray diffraction (PXRD) patterns were acquired in a PANalytical PROMPD diffractometer using Cu (Kα1) as radiation source in the ranges 4−50 deg., with a scan ratio of 0.0445 deg./s, in terms of 2Ɵ. Elemental analysis was performed by duplicate on a Carlo Erba Flash 1112 elemental analyzer and the metal content was determined by inductively coupled plasma-optical emission spectrometry (ICP-OES) on a Varian Vista MPX ICP-OES at Medac Ltd, Chobham, UK. SEM images were acquired with a JEOL-7000F field-emission scanning electron microscope operating at 5 kV. Thermogravimetric analysis (TGA) was performed under an air flow between 25 and 600 ºC with a heating rate of 5 ºC/min on a thermogravimetric analyzer (TA Instruments Discovery TG) in Al$_2$O$_3$ cups using ca. 10 mg of each polymer. N$_2$ sorption isotherms of UiO-67-bpdc-az and UiO-67-bpdc-ip (ca. 100 mg) were obtained at 77 K (p/p0=0.001−0.98) on a Micromeritics ASAP2020 analyzer. Specific surface areas were calculated from the data in the adsorption branch at p/p$_0$=0.05–0.20. All the samples were previously degassed by heating at 150 ºC for 3 h before the sorption measurements. Centrifugation was performed in a Eppendorf 5452 Minispin centrifuge set at 14000 rpm. 2 min were used as centrifuging time unless other conditions stated.

Procedure for the synthesis of H₂bpdc-az
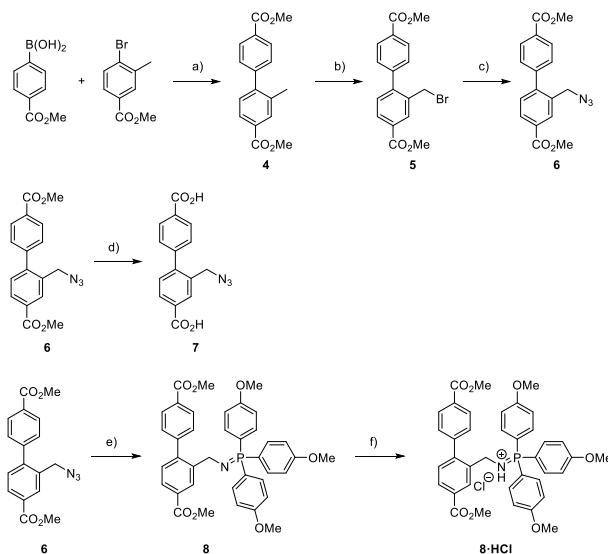
a) Dimethyl 2-methyl-[1,1'-biphenyl]-4,4'-dicarboxylate (**4**)

In a round bottom flask 4-(methoxycarbonyl) phenyl boronic acid (2.8 g, 15.3 mmol, 1 equiv.), methyl 4-bromo-3-methylbenzoate (3.5 g, 15.3 mmol, 1 equiv.), tetrakis(triphenylphosphine)palladium(0) (3.5 g, 3.1 mmol, 0.2 equiv.) and cesium fluoride (9 g, 59.2 mmol, 4 equiv.) were added in a 500 mL round bottom flask. Dry THF (0.1 M, 153 mL) was added under Ar atmosphere and the reaction was stirred under reflux in an oil bath for 18 hours. The crude was filtered with celite and the solvent was evaporated under vacuum. The product was isolated by flash column chromatography (FCC) using silica gel as stationary phase and a mixture of pentane:EtOAc as eluent (5% of EtOAc) and a salmon solid (**4**) was obtained (3.85 g, 13.54 mmol, 89 %).

^{1}H NMR (400 MHz, DMSO-d$_6$): δ 8.05 (d, *J* = 8.4 Hz, 2H), 7.93 (d, *J* = 1.4 Hz, 1H), 7.86 (dd, *J* = 8.0, 1.4 Hz, 1H), 7.54 (d, *J* = 8.4 Hz, 2H), 7.38 (d, *J* = 8.0 Hz, 1H), 3.88 (d, *J* = 4.5 Hz, 6H), 2.29 (s, 3H).

^{13}C NMR (400 MHz, DMSO-d$_6$): δ 166.0, 166.0, 145.0, 144.9, 135.5, 131.1, 129.9, 129.3, 129.2, 129.0, 128.7, 126.9, 52.2, 52.1, 20.0.

For complete characterization see[1]: A. D. Burrows, C. G. Frost, M. F. Mahon and C. Richardson, *Chem. Commun.*, **2009**, 4218-4220.

b) To a round bottom flask charged with a stirrer and dimethyl 2-methyl-[1,1'-biphenyl]-4,4'-dicarboxylate (**4**) (3.85 g, 13.54 mmol, 1 equiv.), AIBN (0.241 g, 1.47 mmol, 0.11 equiv.) and *N*-bromosuccinimide (2.6 g, 14.7 mmol, 1.1 equiv.) were added and purge with Ar. Carbon tetrachloride (76 mL, 0.18M) was added and the reaction was stirred under reflux for 18h in an oil bath. The reaction was followed by TLC until consumption of the starting materials. After the reaction was completed, the solvent was evaporated and the crude mixture was purified

2

by flash column chromatography (FCC) using silica gel as stationary phase and a mixture of pentane:EtOAc (10 % EtOAc) as eluent. The product was obtained as a white solid (**5**) (3.7 g, 10.3 mmol, 76% yield).

^{1}H NMR (400 MHz, CDCl$_3$) δ 8.22 (d, *J* = 1.7 Hz, 1H), 8.14 (d, *J* = 8.4 Hz, 2H), 8.02 (dd, *J* = 8.0, 1,7 Hz, 1H), 7.53 (d, *J* = 8.4 Hz, 2H), 7.33 (d, *J* = 8.0 Hz, 1H), 4.42 (s, 2H), 3.96 (s, 6H).

^{13}C NMR (400 MHz, CDCl$_3$-d$_6$): δ 166.7, 166.2, 145.3, 143.8, 135.6, 132.3, 130.41, 130.37, 129.8, 129.7, 129.5, 128.8, 52.33, 52.25, 30.8.

For complete characterization see: Burrows, A. D., Frost, C. G., Mahon, M. F., Richardson, C., *Chem. Commun.*, **2009**, 4218-4220.

c) Dimethyl 2-(bromomethyl)-[1,1'-biphenyl]-4,4'-dicarboxylate (**5**) (3.7 g, 10.3 mmol, 1 equiv.) and sodium azide (0.736 g, 11.3 mmol, 1.1 equiv.) were placed in a round bottom flask, DMF (0.125M) was added and the reaction was stirred at 60 ºC in an oil bath for 18h. The reaction was diluted with EtOAc and washed with H$_2$O several times to yield the pure azide compound (**6**) (3.35 g, 10.3 mol, 99%).

^{1}H NMR (400 MHz, DMSO-d$_6$): δ 8.15 (d, *J* = 1.8 Hz, 1H), 8.06 (d, *J* = 8.3 Hz, 2H), 8.02 (dd, *J* = 8.0, 1.8 Hz, 1H), 7.56 (d, *J* = 8.3 Hz, 2H), 7.49 (d, *J* = 8.0 Hz, 1H), 4.51 (s, 2H), 3.90 (s, 3H), 3.88 (s, 3H).

^{13}C NMR (400 MHz, DMSO-d$_6$): δ 166.9, 165.7, 145.0, 143.6, 133.7, 130.7, 130.5, 129.3, 129.20,129.17, 129.1, 52.4, 52.3, 51.3.

HRMS (ESI): m/z calculated for [C$_{17}$H$_{15}$N$_3$O$_4$Na]$^+$ 348.0971, found: 348. 0955.

d)Dimethyl 2-(azidomethyl)-[1,1'-biphenyl]-4,4'-dicarboxylate (3.35 g, 10.3 mol) was dissolved in THF (80 mL) then a solution of KOH (3.67g, 206 mmol) in H$_2$O (80 mL) was added. The reaction was stirred at room temperature for 72 hours. Upon completion, all volatiles were removed in vacuo and the remains were acidified with 1M HCl. The precipitated was then filtered through and the residue was washed with H$_2$O before drying in vacuo at 50 ºC to afford a white solid (**7**) (3.00 g, 10.09 mol, 98 %).

^{1}H NMR (400 MHz, DMSO-d$_6$): δ 13.14 (bs, 2H), 8.12 (d, *J* = 1.8 Hz, 1H), 8.04 (d, *J* = 8.3 Hz, 2H), 8.00 (dd, *J* = 7.9, 1.8 Hz, 1H), 7.53 (d, *J* = 8.3 Hz, 2H), 7.47 (d, *J* = 7.9 Hz, 1H), 4.50 (s, 2H).

^{13}C NMR (400 MHz, DMSO-d$_6$): δ 167.0, 166.8, 144.8, 143.4, 133.5, 130.7, 130.6, 130.5, 130.3, 129.5, 129.2, 129.1, 51.4.

HRMS (ESI): m/z calculated for [C$_{15}$H$_{11}$N$_3$O$_4$Na]$^+$ 320.0631, found: 320. 0642.

e) To dimethyl 2-(bromomethyl)-[1,1'-biphenyl]-4,4'-dicarboxylate (**6**) (500 mg, 1.21 mmol) in Et$_2$O (3.0 mL, 0.40 M) under an argon atmosphere was added tris(4-methoxyphenyl)phosphine (426 mg, 1.21 mmol) at room temperature. The reaction was

stirred for 24 h. The solvent was evaporated and the phosphazene (**8**) was used without further purification.

^{1}H NMR (400 MHz, THF-d_8): δ 8.45 (s, 1H), 7.94 (d, J = 8.2 Hz, 2H), 7.83 (dd, J = 7.9, 1.5 Hz, 1H), 7.58 – 7.50 (m, 8H), 7.22 (d, J = 7.9 Hz, 1H), 6.92 (dd, J = 8.7, 1.8 Hz, 6H), 4.12 (d, J = 15.4 Hz, 2H), 3.87 (s, 3H), 3.86 (s, 3H), 3.80 (s, 9H).

^{13}C NMR (101 MHz, THF-d_8): δ 167.5, 167.2, 163.1 (d, J_{C-P} = 2.8 Hz), 146.9, 145.7, 145.5, 145.1, 135.1 (d, J_{C-P} = 9.9 Hz), 132.2, 130.1, 130.4, 130.0, 127.4, 125.0 (d, J_{C-P} = 101.7 Hz), 114.7 (d, J_{C-P} = 12.6 Hz), 55.7, 52.2, 52.0, 47.9.

^{31}P NMR (162 MHz, THF-d_8): δ 5.95 (s).

HRMS (ESI): m/z calculated for $[C_{38}H_{36}NO_7P]H^+$ 650.6202, found: 650.2302.

f) A solution of 2 M HCl in ether (4.60 mL, 9.20 mmol) was added to a solution of **8** in dry diethyl ether. The resulting solution was stirred at rt for 1 h. After evaporation of the solvents, the resulting crude was purified by flash column chromatography (CH_2Cl_2/MeOH 20:1) to obtain **8·HCl** as a colorless foam (300 mg, 0.4 mmol, 30%).

^{1}H NMR (400 MHz, CDCl$_3$): δ 9.09 (s, 1H), 8.48 (d, J = 1.7 Hz, 1H), 7.95 (d, J = 8.3 Hz, 2H), 7.83 (d, J = 8.0, 1.8 Hz), 7.48 (dd, J = 12.3, 8.9 Hz), 7.06 (dd, J = 8.2, 2.5 Hz, 3H), 6.91 (dd, J = 8.9, 2.6 Hz, 6H), 4.25 (d, J = 15.0 Hz, 2H), 3.92 (s, 3H), 3.90 (s, 3H), 3.82 (s, 9H).

^{13}C NMR (400 MHz, CDCl$_3$): δ 166.68, 166.67, 164.1 (d, J_{C-P} = 2.9 Hz), 144.0, 143.5, 136.8 (d, J_{C-P} = 3.2 Hz), 135.3 (d, J_{C-P} = 12.7 Hz), 130.4, 129.9, 129.4, 129.29, 129.27, 129.1, 128.0 115.1

(d, J = 14.3 Hz), 112.3 (d, J = 110.9 Hz), 55.6, 52.2 (d, J = 3.6 Hz), 42.2.

^{31}P NMR (162 MHz, CD$_3$CN): δ 36.89 (s).

HRMS (ESI): m/z calculated for $[C_{38}H_{37}NO_7P]^+$ 650.2302, found: 650.2312.

pK$_{BH+}$ measurement of 8·HCl in CD$_3$CN[2]

8·HCl (30 mg, 0.046 mmol) and tetramethylguanidine (5.77 μl, 0.046 mmol) were dissolved in CD$_3$CN. The ^{13}C NMR was measured and the chemical shift of the **C**H-N=P(ph-p-OMe)$_3$ was used to estimate the equilibrium ratio and the equilibrium constant of the reaction.[3] The equilibrium constant was then used, with the known pK$_{BH+}$ of tetramethylguanidine in CD3CN (pK$_{BH+}$ = 23.3)[4] to determine the estimated pK$_{BH+}$ of salt **8·HCl**. The experiment was repeated three times.

	Estimated pK$_{BH+}$ of 8·HCl in CD$_3$CN
	Using ^{13}C NMR
Experiment 1	24.42
Experiment 2	24.45
Experiment 3	24.50
Average	**24.45**

General synthetic procedure for UiO-67-bpdc-az and UiO-67-bpdc-ip

UiO-67-bpdc-az[5]. Zirconium chloride (1.3 g, 5.6 mmol) was added to the mixture DMF (65 mL) and distilled water (0.602 mL) at room temperature on a stirring plate. Then, benzoic acid (4.1 g, 33.6 mmol) was added to the solution and stirred until dissolved. This solution was poured to round bottomed flask containing 1,4-bezenedicarboxylic acid (H_2bpdc) (0.675 g, 2.8 mmol) and 2-(azidomethyl)-[1,1'-biphenyl]-4,4'-dicarboxylic acid (H_2bpdc-az, 0.8 g, 2.8 mmol). This solution was heated at 130 °C, overnight with stirring and water condenser. Thus, obtained powder was filtered and washed with hot DMF (~80 °C) and afterwards acetone, followed by drying at 120 °C, overnight. The white solid MOF was obtained in 89% yield (1.6 g, 0.83 mmol).

The UiO-67-bpdc-az was further used for performing Staudinger reaction. UiO-67-bpdc-az (1.6 g, 0.7 mmol) and tris(4-methoxyphenyl) phosphine (0.26 g, 0.7 mmol) were weighed in a pressure tube under Ar atmosphere. Dry diethyl ether (0.4 M, 3 mL) was added and the reaction was stirred at room temperature for 24 hours. After the reaction was complete, the MOF was collected by filtration. The MOF was further washed first with diethyl ether and later with acetone. Afterwards the white solid was dried under vacuum. Finally, the **UiO-67-bpdc-ip** was obtained in 92% yield (1.8 g, 0.65 mmol).

General procedure for the allylic alcohols 11a, 11b

For the racemic compounds the procedure to follow was as follows:
The corresponding enone (1 mmol, 1 equiv.) was dissolved in dry CH_2Cl_2 (2 mL) and DIBAL-H (1 M in hexane, 1.2 mmol, 1.2 mL, 1.2 equiv.) was added at 0 °C under argon atmosphere. The reaction was stirred for 1.5 h and quenched with NH_4Cl (aq) sat. and HCl (aq, 0.1 M). The mixture was extracted with CH_2Cl_2 (3 x 15 mL), dried with $MgSO_4$ and the solvent was removed under vacuum. Silica gel column chromatography was performed using pentane:EtOAc (9:1) as eluent.

The enantiomeric allylic alcohols have been synthesized following the procedure reported in 2012 by Cahard group (Bizet, V.; Pannecoucke, X.; Renaud , J.-L.; Cahard, D. *Angew. Chem. Int. Ed.* **2012**, 51, 6467.)[6]

The corresponding enone (5.31 mmol) and [RuCl-(*p*-cym){(*R*,*R*)-Tsdpen}] (33.8 mg, 0.05 mmol, 1 mol%) were placed in a pressure tube under an argon atmosphere. Then an azeotropic mixture of Et_3N/HCO_2H (5 mol:2 mol) was added and the reaction was stirred at room temperature for 24 h. The mixture was quenched with H_2O and extracted with EtOAc (3 x 15 mL). The combined organic layers were washed with brine and $NaHCO_3$ (aq) sat. and then dried over $MgSO_4$. After evaporation of the solvents, the crude was purified by silica gel column chromatography with pentane:EtOAc (9:1) as the eluent. The *ee* was determined by HPLC.

General procedure for the isomerization of allylic substrates using UiO-67-bpdc-ip:

The corresponding allylic substrate (0.1 mmol, 1 equiv.) and MOF UiO-67-bpdc-ip (0.1 mmol, 105 mg, 1 equiv.) were placed in a pressure tube. Toluene was added (1 mL) and the mixture

was allowed to react at 120 °C during 48 hours. The reaction was centrifuged in an Eppendorf and washed three times with toluene and another three times with acetone. The solvent was removed under reduced pressure to yield the product.
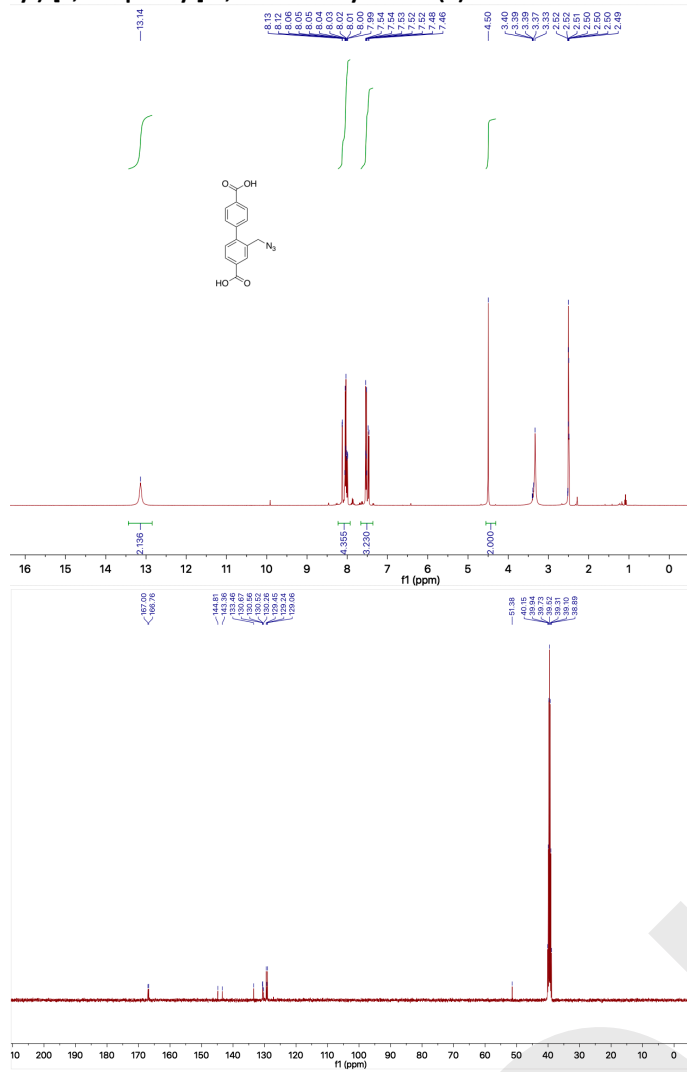
Dimethyl 2-methyl-[1,1'-biphenyl]-4,4'-dicarboxylate (4)
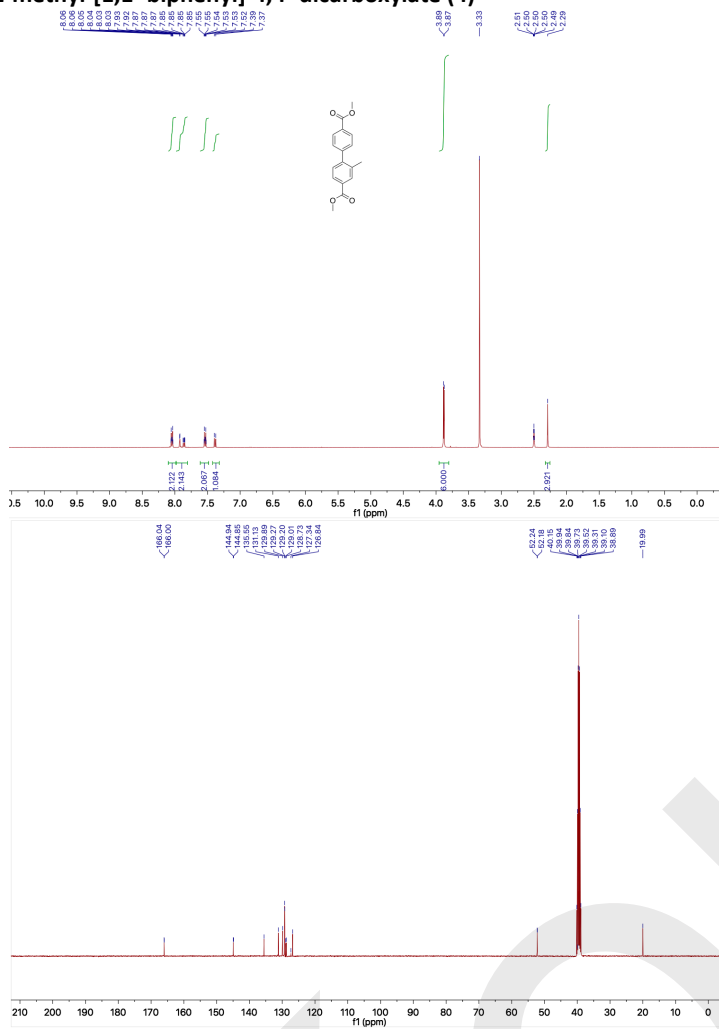
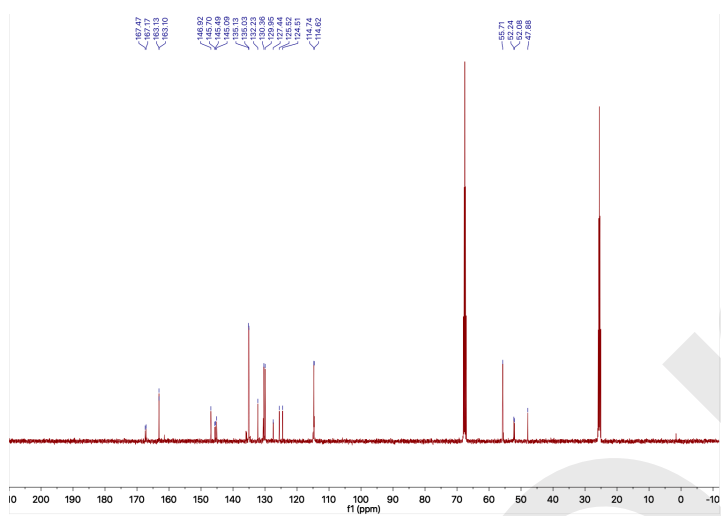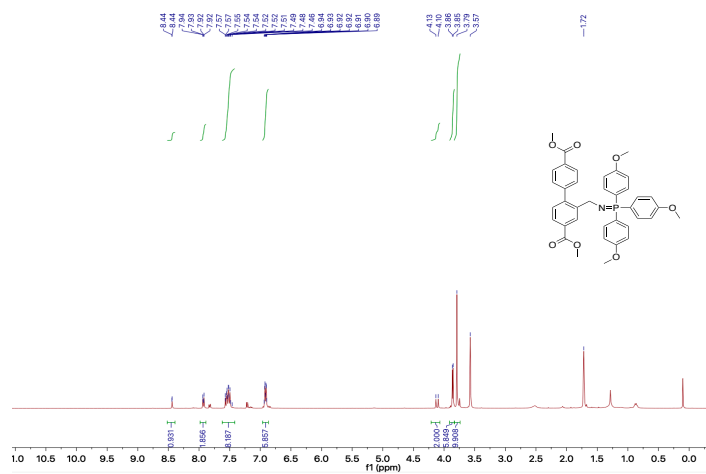**Dimethyl 2-(bromomethyl)-[1,1'-biphenyl]-4,4'-dicarboxylate (5)**

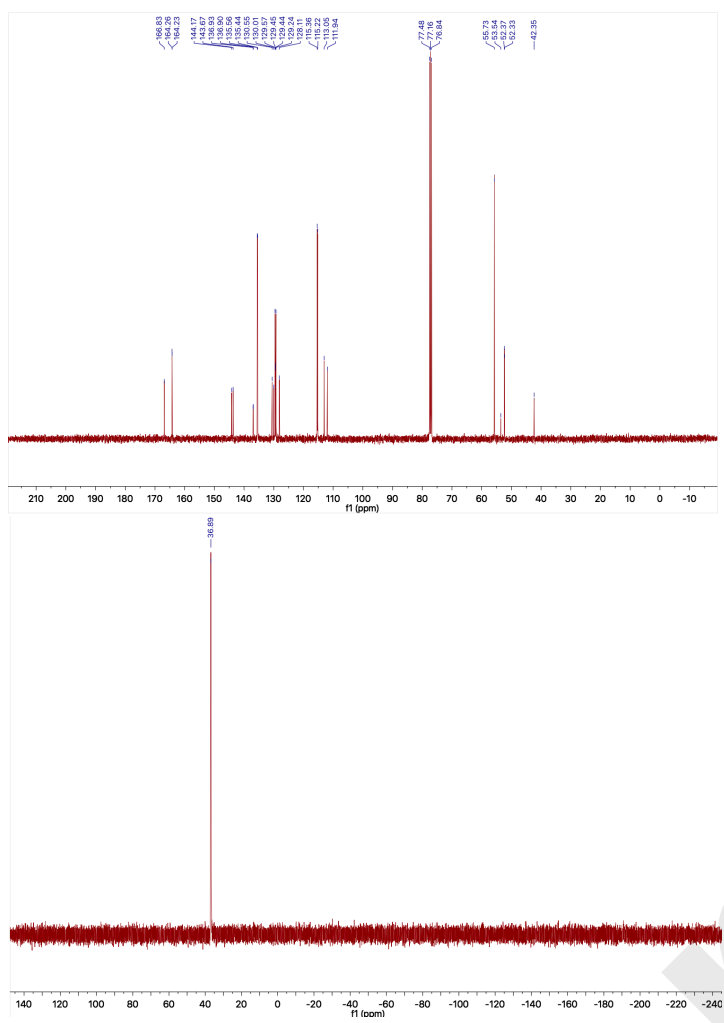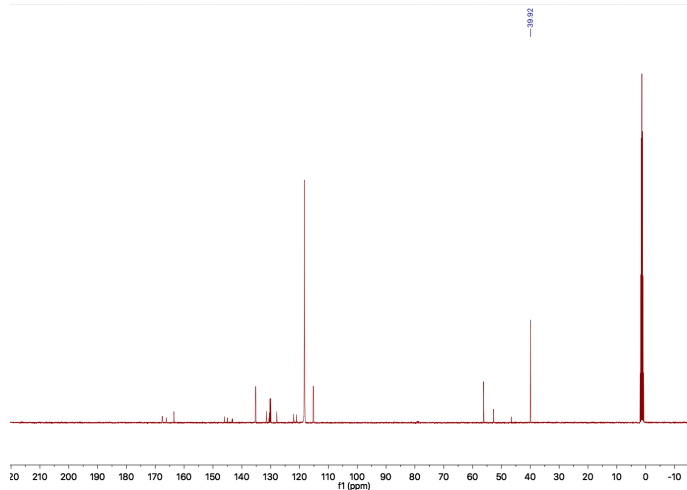**Dimethyl 2-(azidomethyl)-[1,1'-biphenyl]-4,4'-dicarboxylate (6)**
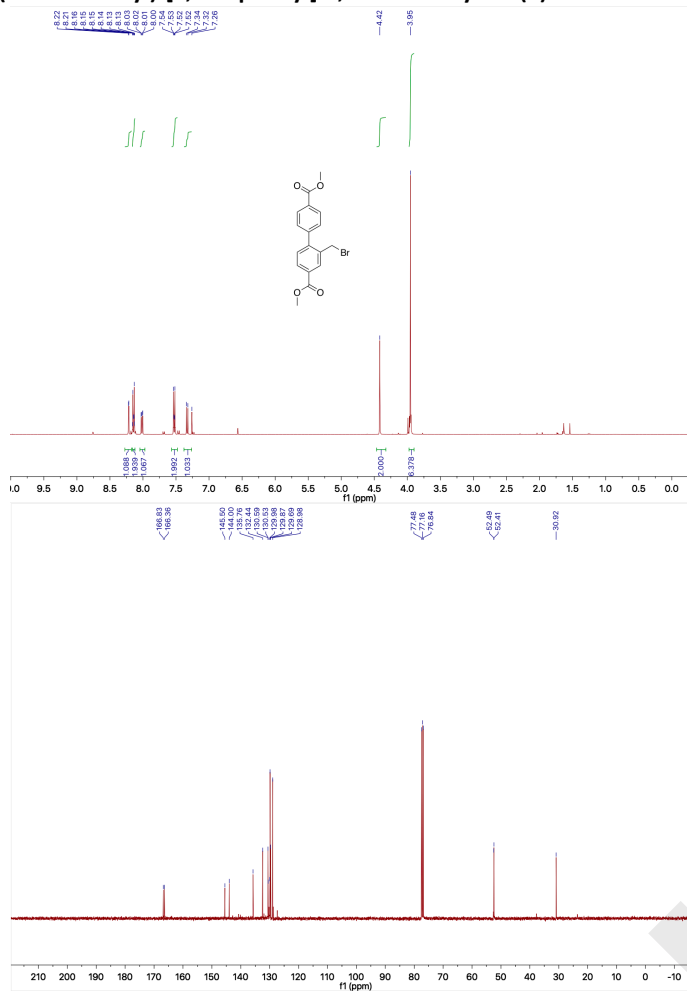
2-(Azidomethyl)-[1,1'-biphenyl]-4,4'-dicarboxylic acid (7)

Dimethyl-2-(((tris(4-methoxyphenyl)-l⁵-phosphaneyl dene)amino)methyl)-[1,1'-biphenyl]-4,4'-dicarboxylate (8)

Less than 5% impurity of unreacted triphenylphosphine

−6.10

Salt 8·HCl

pK$_{BH+}$ of salt 8·HCl

HPLC Chromatograms of allylic substrates 11a, 11b, 11c, 14 and recyclability study

(*R*,*E*)-4,4,4-Trifluoro-1,3-diphenyl-2-buten-1-ol (11a)
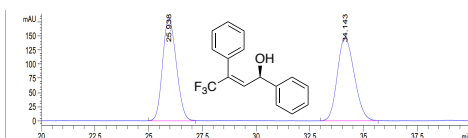
| Peak | RetTime | Type | Width | Area | Height | Area |
#	[min]		[min]	[mAU*s]	[mAU]	%
1	25.933	BV	0.6759	2.51684e4	567.01721	49.8332
2	34.133	VV	0.8110	2.53369e4	461.16422	50.1668
Totals :				5.05053e4	1028.18143	
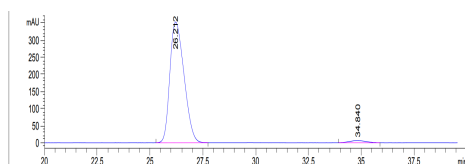
| Peak | RetTime | Type | Width | Area | Height | Area |
#	[min]		[min]	[mAU*s]	[mAU]	%
1	26.212	BV	0.6770	5.22322e4	1130.60364	97.9239
2	34.820	VV	0.6509	1107.39490	20.28606	2.0761
Totals :				5.33396e4	1150.88969	

(*R*,*E*)-4,4,4-trifluoro-1-phenyl-3-(4-(trifluoromethyl)phenyl)but-2-en-1-ol (11b)
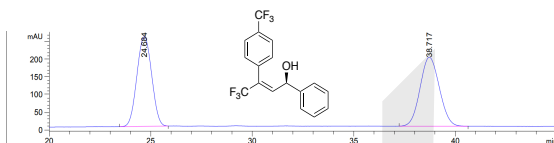
| Peak | RetTime | Type | Width | Area | Height | Area |
#	[min]		[min]	[mAU*s]	[mAU]	%
1	24.684	BV	0.7904	1.28465e4	254.73569	49.8674
2	38.717	VV	0.8786	1.29149e4	196.03011	50.1326
Totals :				2.57614e4	450.76579	
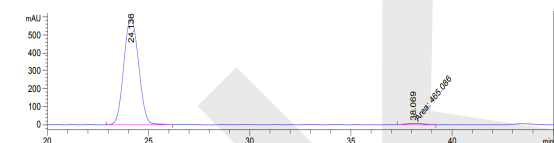
| Peak | RetTime | Type | Width | Area | Height | Area |
#	[min]		[min]	[mAU*s]	[mAU]	%
1	24.138	VV	0.8087	3.00661e4	591.86230	98.4767
2	38.069	MM	1.0817	465.08630	7.16608	1.5233
Totals :				3.05312e4	599.02838	

(*R*)-4,4,4-trifluoro-1-phenyl-3-(4-(trifluoromethyl)phenyl)butan-1-one (12a)
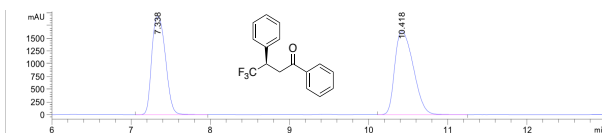
Peak #	RetTime [min]	Type	Width [min]	Area [mAU*s]	Height [mAU]	Area %
1	7.338	BV	0.1961	2.30998e4	1924.09827	46.5631
2	10.418	VB	0.2635	2.65098e4	1631.84265	53.4369
Totals :				4.96096e4	3555.94092	

DBU-catalyzed isomerization of **11a** to give **12a**:
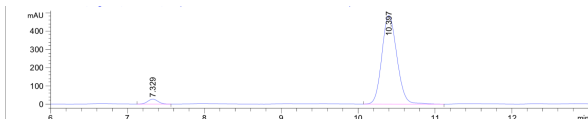
Peak #	RetTime [min]	Type	Width [min]	Area [mAU*s]	Height [mAU]	Area %
1	7.329	BB	0.1454	248.08594	26.96102	3.6399
2	10.397	BB	0.2101	6567.69092	484.62430	96.3601
Totals :				6815.77686	511.58532	

P$_4$-t-Bu catalyzed isomerization of **11a** to give **12a**:
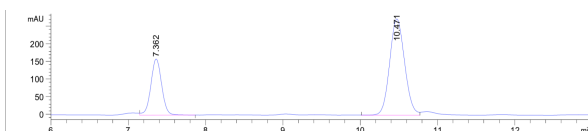
Peak #	RetTime [min]	Type	Width [min]	Area [mAU*s]	Height [mAU]	Area %
1	7.362	VB	0.1497	1551.78528	159.17252	29.7544
2	10.471	VV	0.2106	3663.53687	272.98050	70.2456
Totals :				5215.32214	432.15302	

(*R*)-4,4,4-trifluoro-1-phenyl-3-(4-(trifluoromethyl)phenyl)butan-1-one (12b)
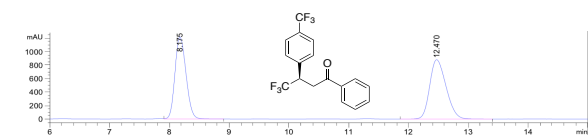
Peak #	RetTime [min]	Type	Width [min]	Area [mAU*s]	Height [mAU]	Area %
1	8.175	VB	0.2038	1.56466e4	1218.25061	48.3186
2	12.470	BV	0.2976	1.67356e4	881.25812	51.6814
Totals :				3.23822e4	2099.50873	

Phosphazene-PS (**13b**) catalyzed isomerization of **11b** to give **12b**:
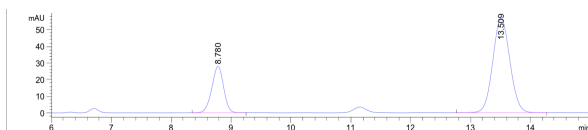
Peak #	RetTime [min]	Type	Width [min]	Area [mAU*s]	Height [mAU]	Area %
1	8.780	BB	0.2114	379.94098	27.81087	25.2124
2	13.509	BB	0.3111	1127.01807	56.88673	74.7876
Totals :				1506.95905	84.69760	

DBU-PS (**13c**) catalyzed isomerization of **11b** to give **12b**:
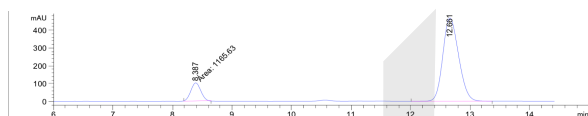
Peak #	RetTime [min]	Type	Width [min]	Area [mAU*s]	Height [mAU]	Area %
1	8.387	MM	0.1922	1165.63196	101.06386	11.9485
2	12.661	VV	0.2867	8589.83789	466.75305	88.0515
Totals :				9755.46985	567.81691	

Reciclability study of UiO-67-bpdc-ip for the isomerization of **11b** to gibe **12b**:
1st run:
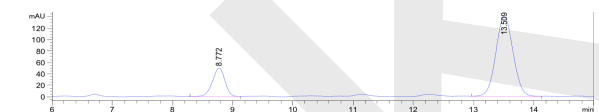
Peak #	RetTime [min]	Type	Width [min]	Area [mAU*s]	Height [mAU]	Area %
1	8.772	BB	0.2219	719.74329	50.01118	20.4814
2	13.509	VV	0.3098	2794.38696	140.65125	79.5186
Totals :				3514.13025	190.66242	

14

2nd run:

2nd run:

Peak #	RetTime [min]	Type	Width [min]	Area [mAU*s]	Height [mAU]	Area %
1	9.147	VV	0.2558	742.10364	45.61075	17.3452
2	14.304	VB	0.3325	3536.32617	166.01215	82.6548
Totals :				4278.42981	211.62289	

3rd run:

Peak #	RetTime [min]	Type	Width [min]	Area [mAU*s]	Height [mAU]	Area %
1	9.106	MM	0.2812	915.05829	54.23814	22.7036
2	14.116	MM	0.3529	3115.38745	147.14366	77.2964
Totals :				4030.44574	201.38180	

4th run:

Peak #	RetTime [min]	Type	Width [min]	Area [mAU*s]	Height [mAU]	Area %
1	9.158	VV	0.2666	3123.38574	179.86519	22.3880
2	14.119	VV	0.3314	1.08278e4	506.52316	77.6120
Totals :				1.39512e4	686.38835	

The materials were characterized as follows:

Powder x-ray diffraction (PXRD)

Samples were prepared using 20 mg of the sample on a silicon plate XRD sample holder by spreading it evenly and stabilizing with 2-3 drops of isopropanol. PXRD patterns (Cu Kα radiation, $\lambda = 1.5418$ Å, 2Ɵ range = 5-50 °) were collected in reflectance Bragg-Brentano geometry with a Panalytical PRO MPD diffractometer. The PXRD patterns (**Figure S1**) were compared to the theoretical diffraction pattern of UiO-67 (CCDC: 7033336). No significant differences were observed between UiO-67-bpdc-az, UiO-67-bpdc-ip and UiO-67. Thus, ensuring the purity of the phase obtained.
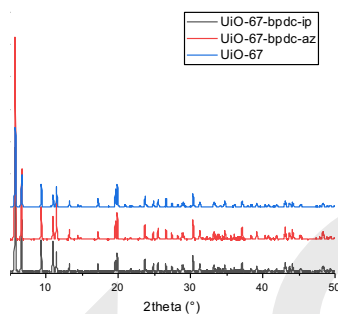

Figure S1. PXRD (4-50 def., in terms of 2Ɵ) UiO-67-bpdc-az (red) and UiO-67-bpdc-ip (blue) with the theoretical pattern (black, CIF in CCDC: 7033336).

Thermogravimetric analysis (TGA)

TGA demonstrated the weight losses for both MOFs synthesized in this work (**Figure S2**). Before applying 50 °C water from the surface of the graings is detached. Afterwards, in the range 50-150 ºC, internal water from pores is removed. UiO-67-bpdc-az showed a significant

15

decrease around 400 °C. UiO-67-bpdc-ip two main decompositions, first at 210 °C and the second one at 450 °C.
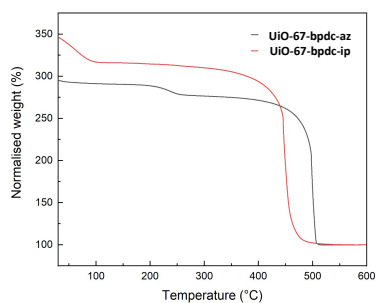

Figure S2. Thermogravimetric curves of UiO-67-bpdc-az and UiO-67-bpdc-ip in air from room temperature to 600 °C (5 °C/min).

Scanning electron microscopy (SEM)

The morphology of the new UiO-67 was analyzed under low acceleration voltages (5 kV) to avoid the damage of the polymer structure with the electron beam. Both MOFs crystallized in the shape of diamonds revealing the crystallization space group Fm-3m.
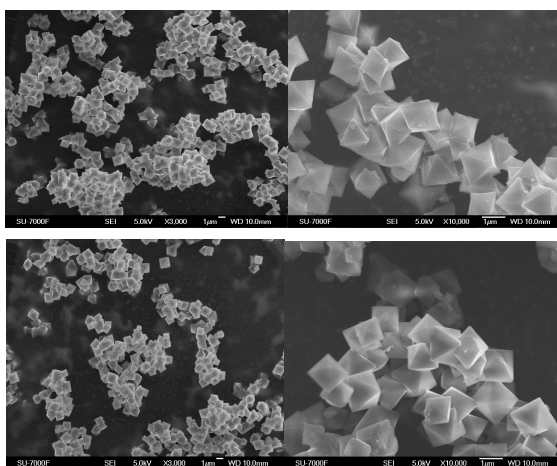
Figure S3. SEM images of UiO-67-bpdc-az (top) and UiO-67-bpdc-ip (bottom).

16

Elemental analysis

Table S1. Elemental analysis of UiO-67-bpdc-az and UiO-67-bpdc-ip synthesized in this work.

MOF		C	H	N	P	Zr
UiO-67-bpdc-az	Theoretical	54.48	2.97	5.84	-	12.52
	Experimental	44.02	2.58	3.90	<0.01	22.71
UiO-67-bpdc-ip	Theoretical	62.66	4.11	1.55	3.44	10.02
	Experimental	52.51	3.41	1.05	2.25	16.12

Nitrogen sorption isotherms, pore size and bet surface area

UiO-67-bpdc-az and UiO-67-bpdc-ip were analyzed by acquiring the whole nitrogen sorption isotherm at 77 K (**Figure S4**) with a BET surface area of 1846 m^2 g^{-1} for UiO-67-bpdc-az and 850 m^2 g^{-1} for UiO-67-bpdc-ip The pore size distribution of the MOF UiO-67-bpdc-ip was evaluated using Density Functional Theory model from experimental data, obtaining a median pore size of 7 Å and 10 Å for UiO-67-bpdc-ip, **Figure S5**.
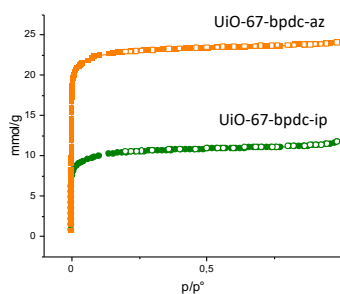

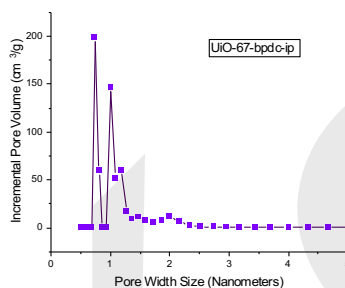**Figure S4.** Nitrogen sorption isotherms at 77 K of UiO-67-bpdc-az (left) and UiO-67-bpdc-ip (right).

Figure S5. Pore size distribution of MOF UiO-67-bpdc-ip.

Recyclability studies

In a pressure tube, *(E)*-4,4,4-trifluoro-1-phenyl-3-(4-(trifluoromethyl)phenyl)but-2-en-1-ol (**11b**, 1 mmol, 34 mg) and **UiO-67-bpdc-ip** (105 mg, 100 mol% based on the organic

counterpart) were mixed in toluene 0.1 M (1 mL). The tube was seaed with a Teflon lined cap and was purged with argon and stirred at 120 °C for 48 hours. After that, the crude was transferred to a propylene centrifuge tube, centrifuged and washed with toluene (3 x 1.5 mL) and acetone (3 x 1.5 mL). Supernantans were concentrated and analyzed by ^{1}H and ^{19}F NMR, *c.t.* was determined by HPLC and the cycle was repeated.

The yield and the chirality transfer are decreased after the first run (**Figure S6**). Therefore, crystallinity and morphology were studied by PXRD and SEM analysis. The PXRD pattern shown that the crystallinity of the material is maintained after the 4 runs (**Figure S7**). SEM images depict the octahedral shape of the crystals of the typical UiO-67 MOF, although there is partial decomposition of the material is observed by ^{1}H NMR, **Figure S8**.
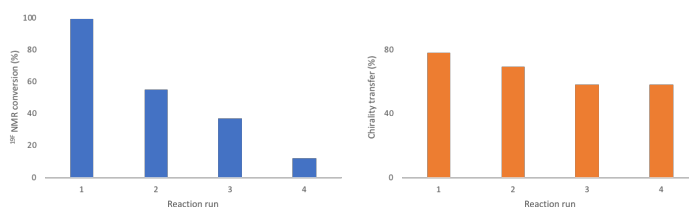

Figure S6. Study of recyclability of MOF UiO-67-bpdc-ip in the isomerization of electron-deficient allylic alcohols.
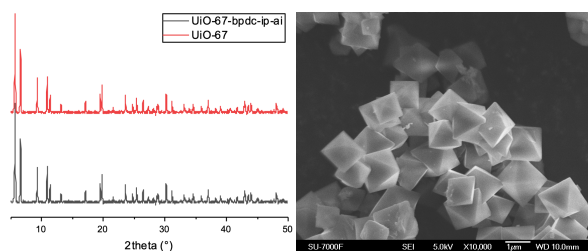

Figure S7. PXRD pattern (left) and SEM images (right) of the UiO-67-bpdc-ip after 4 runs.
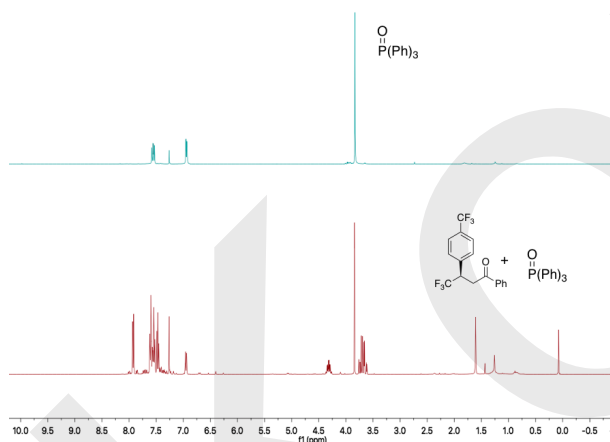

Figure S8. ^{1}H NMR of the decomposition of the iminophosphorane after recyclability studies.

18

References

1.   Burrows, A. D.; Frost, C. G.; Mahon, M. F.; Richardson, C., *Chem. Commun.* **2009**, 4218-4220.
2.   Núñez, M. G.; Farley, A. J. M.; Dixon, D. J., *J. Am. Chem. Soc.* **2013,** *135*, 16348-16351.
3.   Rodima, T.; Kaljurand, I.; Pihl, A.; Mäemets, V.; Leito, I.; Koppel, I. A., *J. Org. Chem.* **2002,** *67*, 1873-1881.
4.   Kanbara, T.; Suzuki, Y.; Yamamoto, T., *Eur. J. Org. Chem.* **2006,** *2006*, 3314-3316.
5.   Kaur, G.; Øien-Ødegaard, S.; Lazzarini, A.; Chavan, S. M.; Bordiga, S.; Lillerud, K. P.; Olsbye, U., *Cryst. Growth Des.* **2019,** *19*, 4246-4251.
6.   Bizet, V.; Pannecoucke, X.; Renaud, J.-L.; Cahard, D., *Angew. Chem. Int. Ed.* **2012,** *51*, 6467-6470.
7.   García-Vázquez, V.; Martínez-Pardo, P.; Postole, A.; Inge, A. K.; Martín-Matute, B., *Org. Lett.* **2022,** *24*, 3867-3871.